Pathogenic mycobacteria achieve cellular persistence via lipid-mediated inhibition of the Niemann-Pick disease type C pathway

Paul David Fineran

A thesis presented for the degree of
Doctor of Philosophy

Department of Pharmacology
Merton College
University of Oxford
Trinity Term 2014

Abstract

M.tuberculosis, the causative agent of human tuberculosis, is able to achieve long-term persistence within host organism macrophages. This persistence is achieved via the ability of the mycobacterium to prevent phagosomal-lysosomal fusion. The mechanisms by which fusion is inhibited remain incompletely understood. Here we provide evidence supporting a mechanistic link between infection with pathogenic mycobacteria and the cellular pathway defective in the rare lysosomal storage disorder Niemann-Pick disease type C (NPC). We observed that NPC phenotypes, including lipid storage and reduced lysosomal calcium release, can be induced in wild-type murine and human macrophages by infection with pathogenic mycobacteria. This phenotype induction did not occur following infection with the non-pathogenic *M.smegmatis*. Phenotype induction could be achieved in the absence of the mycobacteria using lipids from the mycobacterial cell walls. The importance of mycobacterial cell wall lipids to mycobacterial virulence has been well-documented. This lipid-mediated inhibition likely occurs through the NPC1 protein. Susceptibility to phenotype induction was inversely proportional to levels of functional NPC1, whilst a pre-existing dysfunction in the NPC pathway (either stemming from mutation or pharmacological inhibition) rendered cells less able to clear non-pathogenic mycobacteria. Finally, we demonstrate that therapies for NPC, particularly curcumin, are able to promote clearance of mycobacteria from infected macrophages. NPC therapies may hold promise for a new approach to the treatment of tuberculosis.

Acknowledgements

First and foremost I would like to thank Fran Platt for her patient mentorship and encouragement over the last four years, and to acknowledge her ability to return thesis chapters with near-superhuman speed. Many thanks also to all the members of the Platt lab, past and present, for making it such a pleasant environment in which to work. Special thanks to Nick (for assistance with manuscript writing and figure making, and for help with the human macrophage work), Dave (for his skills in mouse wrangling and for having an Aunt who enjoys baking), Danielle (for her excellent bonfire night parties and also for keeping us all in line and reasonably tidy), Allie (for the running, the conversations, and the conversations whilst running), Lauren (for selflessly acting as a buffer between us and the comedy of errors that is the BMS), Kerri (for her enthusiasm for after work drinks), Ralu (for providing tasty Romanian treats), Chris (for helping me with conference organisation), James (for his help with sphingosine quantification and for letting me steal his hot sauce), David (for help with HPLC and for his general expertise), Oscar (for assistance with anything related to antibodies), Nada (for her advice on thesis writing), Jo (for her bravery in subjecting herself to American working hours), Ian (for western blot expertise and providing numerous cups of tea), Pete (for his hard work using the synthetic mycolic acids and for patiently tolerating my supervision), Elias (for kindly offering to perform more western blots) and Emyr (for bringing me into the lab and for choosing his

other student when he needed an enormous pit digging). Within the department I would also like to thank Wendy (for the EM work and for being the nicest person in the building) and Lianne and Ant (for their calcium expertise and for being the nicest people in the building now that Wendy has retired). Thanks also to Nathan Lack for laying the groundwork for this project, and for his advice and encouragement throughout, and to Sridhar Vasudevan and Grant Churchill for allowing me access to their spectrophotometer.

Outside of the deparment I would like to thank all our collaborators who have assisted me over the last four years. In particular I would like to thank Raju Tatituri and Michael Brenner (for their provision of lipids), Dan Ory (for mass spec), Doris Höeglinder (for her work looking at the effect of purified mycolic acids), Frances Sharom (for looking at NPC1-lipid binding) and finally those at Public Health England for their assistance with work involving *Mtb* (with particular thanks to Dominic Kelly).

Thanks also to the National Institute of Health for funding the human cell work, and to the Medical Research Council for providing my salary.

Thank you to all my friends who have helped and supported me over the years. Thank you to Pauline for her love and support, and for doing her best to keep me sane. Last but certainly not least I would like to thank my parents and sister for their continued moral support, for their keen proofreading eye, and for keeping me fed, sheltered and watered for the last month of the write-up.

Contents

List of Figures

Abbreviations

ATRA	All-*trans*-retinoic acid
BAPTA	1,2–bis(o–aminophenoxy)ethane–N,N,N',N'–tetraacetic acid
BCG	Bacillus Calmette Guérin
BODIPY	Boron-dipyrromethene
BSA	Bovine serum albumin
C:M	Chloroform:methanol
CFU	Colony forming units
CNS	Central nervous system
CtxB	Cholera toxin subunit B
EE	Early endosome
EEA1	Early endosomal antigen 1
EGTA	Ethylene glycol tetraacetic acid
ER	Endoplasmic reticulum
FACS	Fluorescence activated cell sorting
FCS	Foetal calf serum
GA	Glutaraldehyde
GlcCer	Glucosylceramide
GMM	Glucose monomycolate
GPN	Glycyl-L-phenylalanine 2-naphthylamide
GSL	Glycosphingolipid
HBSS	Hank's balanced salt solution
HPβCD	Hydroxypropyl-β-cyclodextrin
LAMP	Lysosome associated membrane protein

LacCer	Lactosylceramide
LE/Lys	Late endosome/lysosome
LSD	Lysosomal storage disorder
mAGP	Mycolylarabinogalactan-peptidoglycan
MAMT	*S*-adenosylmethionine-dependent methyltransferases
Mtb	*Mycobacterium tuberculosis*
M-CSF	Macrophage colony-stimulating factor
MDR-TB	Multi-drug resistant *Mtb*
MEFL	Mean equivalents of fluorescence
MOI	Multiplicity of infection
Mtb	*Mycobacterium tuberculosis*
MTC	*Mycobacterium tuberculosis* complex
NAADP	Nicotinic acid adenine dinucleotide phosphate
NB-DNJ	N-butyl-deoxynojirimycin
NB-DGJ	N-butyldeoxygalactonojirimycin
NP/RP-HPLC	Normal/reverse phase high-perfomance liquid chromatography
NPA/B/C	Niemann-Pick Disease Type A/B/C
P/S	Penicillin/streptomycin
PFA	Paraformaldehyde
PI	Propidium iodide
PM	Plasma membrane
RND	Resistance nodulation division
rVSVs	Vesicular stomatitis Indiana virus expressing recombinant glycoproteins
SERCA	Sacro/endoplasmic reticulum Ca^{2+}-ATPase
SNARE	Soluble N-ethylmaleimide-sensitive factor-attachment protein receptor
TB	Tuberculosis
TDM	Trehalose dimycolate
TFEB	Transcription factor EB

TLC	Thin layer chromatography
TMM	Trehalose monomycolate
TPC	Two-pore channel
V-ATPase	Vacuolar-type H^+-ATPase
XDR-TB	Extensively-drug resistant *Mtb*

1 Introduction

1.1 Niemann-Pick Disease Type C

1.1.1 Lysosomal Storage Disorders

The lysosomal storage disorder (LSD) family encompasses over 60 different diseases, occurring at a collective frequency of 1 in 5000 live births [1] [2]. They are characterized by the accumulation of metabolites/ macromolecules in the lysosome as a consequence of a defect in lysosomal function [3]. Niemann-Pick Disease Type C (NPC) is a pan-ethnic autosomal recessive LSD estimated to occur at a frequency of 1 in 120000 live births [4].

1.1.2 Clinical Phenotypes

NPC has a broad clinical spectrum, and can present at any age; from immediately before birth to after 60 years of life [4] [5]. The classical NPC disease phenotype manifests in mid-to-late childhood and is characterised by splenomegaly, ataxia, dystonia and progressive cognitive impairment, with the patient typically succumbing to death via aspiration pneumonia in their late teens/early twenties [4]. The disease can also present in neonates (where it can be rapidly fatal due to hepatic failure) and in late-teens/adulthood. The latter form of the disease also involves neurological deterioration, although this occurs at a slower rate than in the classical disease phenotype [6].

1.1.3 Genetics

The majority of LSDs result from inherited deficiencies in genes encoding lysosomal enzymes. For example, Gaucher disease, the most common LSD, is caused by deficiencies in glucocerebrosidase, which leads to the lysosomal accumulation of glucosylceramide (GlcCer) [7]. This is also true for Niemann-Pick Disease Type A and B (NPA/B), which are characterized by decreased acid sphingomyelinase activity (stemming from mutations in *SMPD1*) and the subsequent build-up of sphingomyelin [8].

NPC shares with NPA/B an accumulation of sphingomyelin. However, NPC is not caused by an enzymatic defect. Rather, it results from mutations in either the *NPC1* or *NPC2* gene. These mutations account for, respectively, 95% and 5% of clinical cases [6]. *NPC2* encodes a small (132 amino acid) soluble glycoprotein of the lysosomal lumen (**Fig 1.1B**) [9]. The NPC2 protein has been crystallized and its structure solved [10]. By contrast, *NPC1* is located on chromosome 18q11-12 and encodes a large (1278 amino acids) integral multiple pass membrane glycoprotein of the limiting membrane of the late endosome/lysosome (henceforth referred to as the acidic compartment due to the pH of the organelle) (**Fig 1.1A**) [11] [12]. The NPC1 protein has a predicted topology of 13 trans-membrane domains, a small cytoplasmic tail and three lysosomal lumenal loops [13]. It has partial homology (residues 615-797) to the sterol-sensing domain present in other membrane proteins, and a similar membrane topology to prokaryotic resistance nodulation division (RND) permeases (with the addition of an N-terminal cholesterol binding loop which binds cholesterol with high affinity) [14]. More detail on the structure and evolutionary function of NPC1 can be found in Section 5.1.1. Mutations in *NPC1* & *2* give an identical clinical phenotype, indicating that they likely function in a common pathway (henceforth referred to as the NPC pathway) [15].

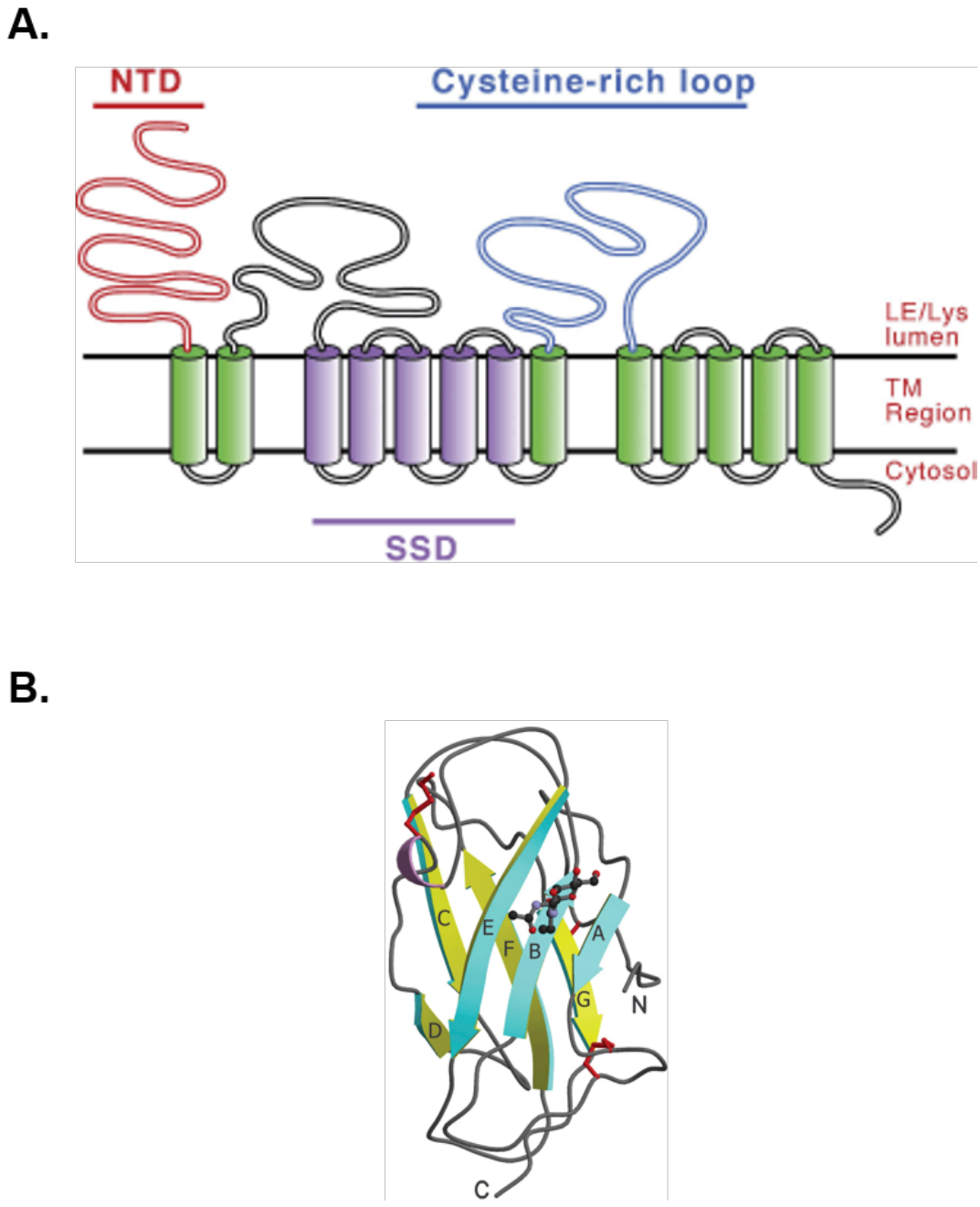

Figure 1.1: **Structure of NPC1 and NPC2. A.)** Predicted topology of NPC1. NTD = N-terminal domain, SSD = Sterol Sensing Domain. Taken from [11]. **B.)** Ribbon representation of NPC2. Adapted from [16].

1.2 NPC Cellular Phenotypes

Cells from NPC patients exhibit a range of phenotypes. Whilst the majority of LSDs are characterised by the accumulation of one type of storage material, NPC tissues accumulate lipids from multiple classes [11] [17] [18]. NPC cells are also defined by reduced endocytic trafficking, with profound defects in fusion at the level of the late-endosome/lysosome [19]. This is likely related to the reduced release of lysosomal calcium observed in NPC cells [11]. These phenotypes (and how they arise from mutations in *NPC1/2*) will be discussed in greater detail below, but it is key to appreciate that it is the combination of these phenotypes that define a NPC cell. Of the various cellular phenotypes associated with NPC cells, only sphingosine accumulation and reduced lysosomal calcium are unique to NPC [20]. For example, whilst lysosomal accumulation of cholesterol is regarded as a hallmark of NPC cells (see Section 1.2.1 below) it has also been observed in cells lacking the lysosome associated membrane protein (LAMP)-1/2 [21].

1.2.1 Lipid Accumulation

Mutations in *NPC1* or *NPC2* are associated with elevations in four lipid types: cholesterol, glycosphingolipids (GSLs), sphingomyelin and sphingosine [11]. The extent of elevation, relative to wild-type, differs between tissues. For example, all four show elevation in the NPC periphery [22] [23]. In the *Npc1*$^{-/-}$ mouse liver GSLs show a 2-fold elevation, with cholesterol and sphingomyelin increasing 4-fold and sphingosine levels 12 times higher than in wild-types (although the absolute levels of sphingosine remain low) [11]. No accumulation of cholesterol or sphingomyelin has been reported in the central nervous system (CNS) of *Npc1*$^{-/-}$ mice, whilst GSLs and sphingosine are increased 3 and 4-fold respectively [17] [20] [22]. In the CNS of NPC patients there is also no significant accumulation of cholesterol and sphingomyelin, but around a 3-fold increase in sphingosine levels

and a large increase in GSLs (around 10-20 fold for the GSL species GM2 and GM3) [4]. All four lipid types accumulate in the liver and spleen of NPC patients [4].

Cholesterol

In terms of absolute mass, cholesterol is the most abundant storage lipid in peripheral tissues of *Npc1*$^{-/-}$ mice [11]. Cholesterol can be synthesized in the host cell endoplasmic reticulum (ER) or be obtained from an exogenous source [24]. Exogenous cholesterol enters the cell in the form of low density lipoprotein, wherein it is trafficked along the endocytic pathway to the lysosome [25]. Here the low density lipoprotein undergoes de-esterification, resulting in the production of free cholesterol (**Fig 1.2**).

Cholesterol can also be synthesized *de novo* by the cell [24]. Post synthesis (in the ER) endogenously synthesised cholesterol is trafficked to the plasma membrane (PM), where it resides in cholesterol-rich microdomains (lipid rafts) [24]. From here it enters the endocytic pathway, and hence must pass through the lysosome [24]. In wild-type cells this cholesterol (along with that obtained through the de-esterification of low density lipoprotein) is trafficked out of the lysosome. From here it may be trafficked to the PM or the ER (with re-esterification of the sterol occurring in the latter organelle) [26]. In NPC cells cholesterol remains trapped in the acidic compartment [24]. The lysosomal accumulation of unesterified cholesterol can be studied via microscopy by staining with the fluorescent antibiotic filipin [4]. Increased filipin staining is a hallmark of the classical NPC cellular phenotype. Indeed, for many years filipin staining of patient fibroblasts has been used as the basis for clinical diagnosis of NPC [4].

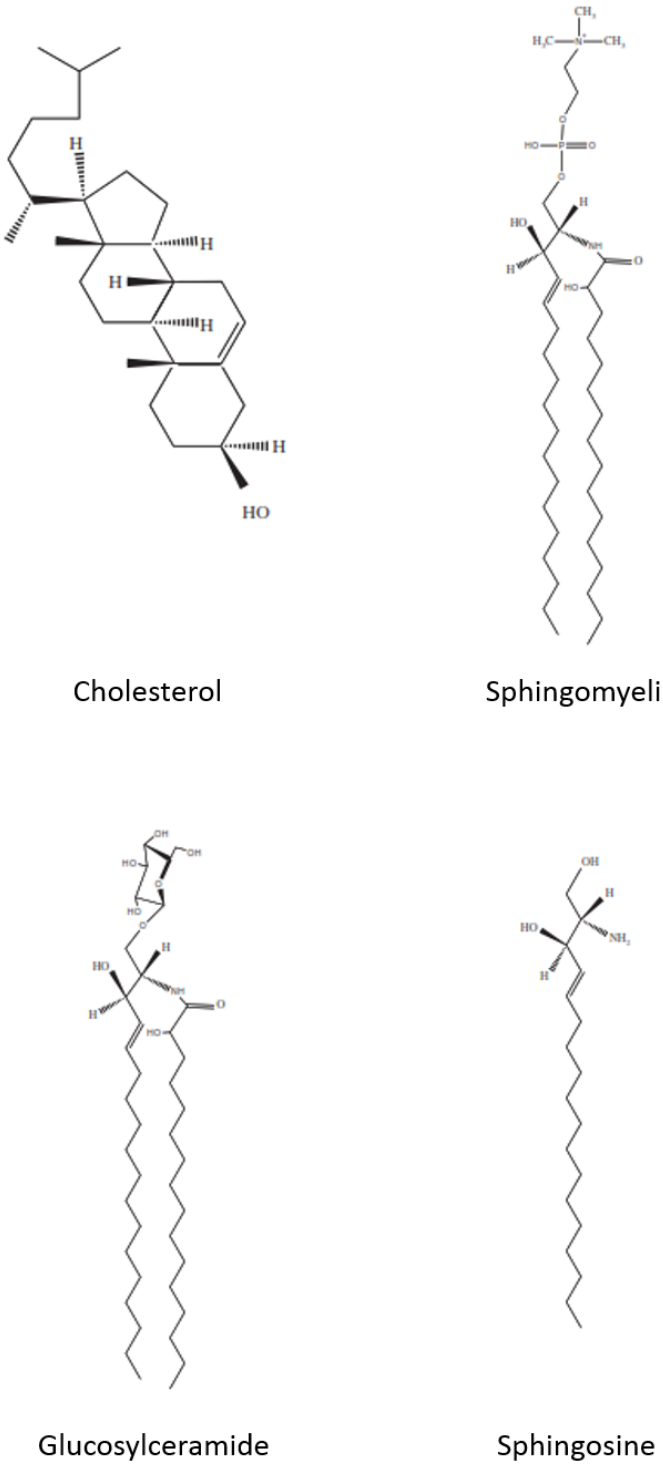

Figure 1.2: **Structure of NPC storage lipids.** Adapted from [11].

Glycosphingolipids

Glycosphingolipids are a complex and diverse group of sphingolipids. They all share a general structure consisting of a sphingolipid (fatty acid linked to a sphingosine group to form ceramide) attached, via a β-glycosidic bond, to a monohexoside [27]. Linkage to glucose or galactose results in GlcCer or galactosylceramide (GalCer) respectively [27]. These are the two simplest GSL species, and can be further modified (via addition of oligosaccharides and sulphate groups) to create a wide range of complex GSLs [27]. There is also significant variation in acyl chain length in the ceramide moiety [28]. To date, over 300 GSL structures have been identified, with the majority of these stemming from the modification of GlcCer (**Fig 1.3**). GalCer and its sulphated derivatives are generally restricted to myelin and the kidney. Those GlcCer-derived GSLs in which the head group contains sialic acid are termed gangliosides, and are important components of the mammalian nervous system [2]. The most common gangliosides in the mammalian brain are shown (highlighted in red) (**Fig 1.3**).

A number of genetic diseases arise from defects in GSL metabolism. A small number of these, such as GM2 and GM3 synthase deficiency, result from inborn defects in the GSL biosynthetic pathway [29] [30]. The vast majority of GSL metabolism defects are due to failures in catabolism. The main site of GSL catabolism is the acidic compartment. Here, the complex GSLs are broken down to their constituent parts (either to very basic building blocks such as monosaccharides or fatty acids, or to intermediate by-products such as lactosylceramide (LacCer)) before being exported from the organelle and utilised for further biosynthesis [31]. Diseases in which these catabolic processes go awry are collectively referred to as sphingolipid storage disorders [2]. They include Gaucher disease, in which glucocerebrosidase deficiency leads to accumulation of GlcCer [7], and Fabry disease, where Gb3 accumulates due to defective α-

galactosidase [32]. Such diseases, in which a defect in a catabolic enzyme leads directly to the accumulation of a metabolite, are designated primary sphingolipid storage disorders [2].

In contrast to the primary sphingolipid storage disorders, NPC involves accumulation of all GSL species, with major accumulation of LacCer, GlcCer (**Fig 1.2**), and GM2/3 gangliosides [33]. The apparent non-species specific nature of GSL accumulation occurring in NPC suggests that it is due to the defect in late-endosomal/lysosomal fusion in NPC cells (see below) as opposed to defects in catabolism as observed in the primary sphingolipid storage disorders [11] [20].

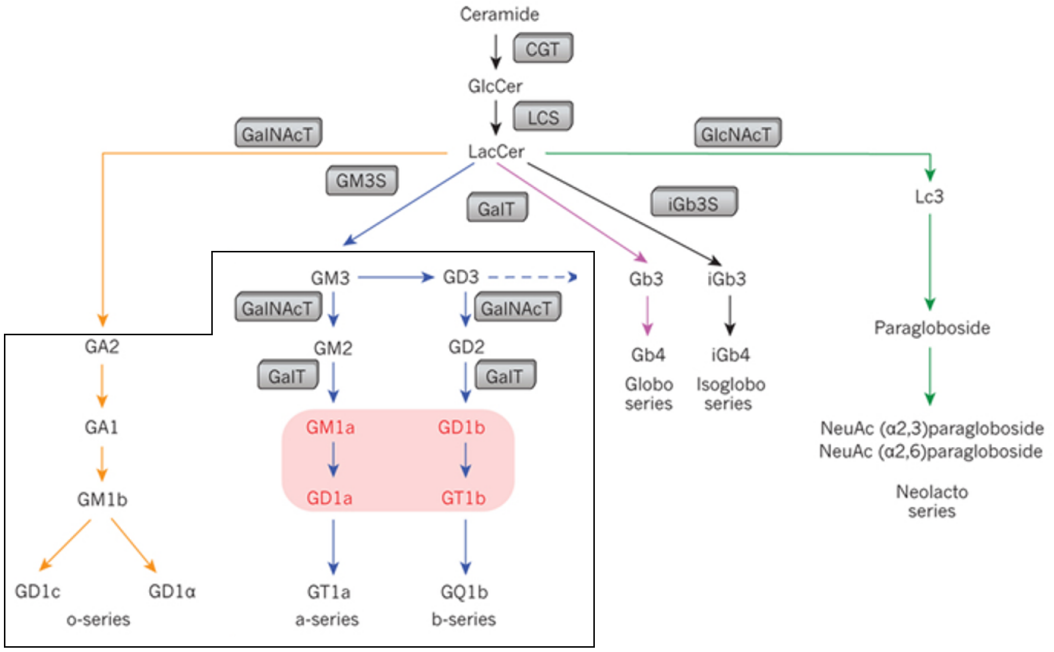

Figure 1.3: **Synthesis of glucosylceramide-derived glycosphingolipids.** Ceramide glucosyltransferase (CGT), galactosyltransferase (GaIT), N-acetylglucosamine transferase (GlcNAcT), GM3 synthase (GM3S), iGb3 synthase (iGb3S) and lactosylceramide synthase (LCS). GSL species enclosed in box are gangliosides, with those highlighted in red major species in the mammalian brain. Adapted from [2].

Sphingomyelin

Sphingomyelin is the most common sphingolipid in animal cells, accounting for up to 30% of the total lipid content of some tissues [27]. It consists of a ceramide (made up of sphingosine and a fatty acid) and a phosphocholine head group (**Fig 1.2**) [27]. It is primarily synthesized in the ER and is trafficked to the PM via the Golgi [34]. In a wild-type cell the majority of sphingomyelin is located in the PM [35]. Breakdown of sphingomyelin to ceramide and phosphocholine occurs in the lysosome and is catalysed by acid sphingomyelinase [36]. As in NPA & B, NPC cells show decreased activity of acid sphingomyelinase, and the subsequent lysosomal accumulation of sphingomyelin [8] [36]. As with cholesterol, sphingomyelin has not been observed to accumulate in the CNS [11]. Sphingomyelin and cholesterol are known to have a close biophysical relationship, forming complexes in the membrane [36] [37].

Sphingosine

Sphingosine is an amino alcohol which forms the backbone of sphingolipids (**Fig 1.2**). Sphingosine is produced in the lysosome via the degradation of ceramide obtained from the catabolism of GSLs and sphingomyelin. Efflux of lysosomal sphingosine is required for synthesis of GSLs via the salvage pathway [31]. Sphingosine is protonated at lysosomal pH (pKa of between 6.7 and 8.4 [38]), meaning that a protein transporter would be required for its lysosomal egress. The identity of this transporter is as yet unknown. It has been suggested that the NPC1 protein plays a role in lysosomal sphingosine egress, and that sphingosine accumulation in NPC is a direct downstream consequence of NPC1 dysfunction, with this accumulation the cause of the other NPC cellular phenotypes (see Section 1.2.4) [20]. Accumulation of sphingosine has been observed in both the CNS and periphery of NPC patients and NPC mice [4] [11].

1.2.2 Lysosomal Calcium

As well as the storage of various lipid species, NPC cells are characterised by reduced levels of lysosomal calcium [20]. The lysosome acts as a regulated store of cellular calcium, with an estimated concentration of between 400 and 600 µM [39]. The amount of calcium stored in the lysosome is relatively small when compared to the ER (a much larger organelle which is estimated to contain calcium in the millimolar range [40]), yet is of great physiological importance.

The route by which calcium is loaded into the lysosome is as yet unknown. A small amount may be taken up via endocytosis, with a drastic reduction in extracellular [Ca^{2+}] leading to a small reduction in lysosomal [Ca^{2+}] [39]. Release of this calcium is required for endocytosis. Mobilisation of the lysosomal calcium store occurs in response to the second messenger nicotinic acid adenine dinucleotide phosphate (NAADP). The receptor for NAADP has not been definitively proven, but the current best candidate is TPC2, a member of the transmembrane voltage-gated two-pore channel (TPC) family. There are 3 members of the TPC family in mammalian cells — TPC1-3 — all of which are localised to the endolysosomal system [41]. TPC2 is found in the late-endosome and lysosome, and experiments in which levels of the protein were altered support its role in NAADP-mediated calcium release [41].

Release of calcium from the acidic compartment is required for fusion of the late endosome (LE) with the lysosome. This fusion requires formation of a SNARE (soluble N-ethylmaleimide-sensitive factor-attachment protein receptor) protein complex [42] (see Section 1.2.3 below). The action of this complex is a calcium dependent process [43]. Release of lysosomal calcium is also required for fusion between the phagosome and lysosome [44]. The lysosome plays an important role in innate immunity, with fusion with the phagosome a key event in phagosomal maturation (the process in which the phagosomal environment

becomes increasingly hostile to the pathogen therein, leading to destruction of the pathogen - see Section 1.7) [45].

It is also hypothesized that the release of lysosomal calcium is able to trigger the release of calcium from ER and hence 'amplify' the size of the calcium response [46]. This trigger hypothesis would require the close apposition of the ER and lysosomal membranes. Such proximity has been observed at contact sites between the lysosome and the sarcoplasmic reticulum [47].

In NPC cells levels of lysosomal calcium release are reduced by 60-70%, with no corresponding change in ER calcium levels [20]. This reduced calcium release is unique to NPC amongst the LSDs (although many of the primary sphingolipidoses, such as Gaucher and Sandhoff disease, exhibit altered ER calcium homeostasis [48]).

1.2.3 Reduced Endocytic Trafficking

Endocytosis

A functional endocytic pathway is required for the proper regulation of the lipid and protein content of the PM (which in turn determines how a cell interacts with its environment) [49]. Following internalization macromolecules are trafficked through a series of morphologically distinct organelles of increasing acidity, wherein they may be degraded to their constituent parts or recycled back to the PM:

* **Early Endosome**: Early endosomes (EE) are located near the cell periphery, where they will receive macromolecules (often bound to their receptors) from the PM. The mildly acidic pH of the EE (pH 6) will cause dissociation of any receptor bound ligands [50]. The receptors can then be recycled back to the PM whilst the ligands are trafficked down the endocytic pathway to their eventual degradation [51]. Markers on the EE include the

Rab5 GTPase and Early Endosomal Antigen 1 (EEA1) [52] [53]. The Rab proteins are a family of Ras-like GTPases (with over 60 members in mammalian cells) involved in the sorting and regulation of traffic through the endocytic system [53]. Different organelles within the endocytic system will contain different members of the protein family.

* **Late Endosome**: LEs are also referred to as multivesicular bodies due to the presence of multiple intraluminal vesicles [54]. They have a spherical morphology, a pH of 5.5, and can be identified by the presence of Rab7/9 GTPases and the Mannose-6-phosphate receptor (M6PR) [55] [56]. In addition to receiving cargo from the EE they will also receive cargo from the phagosome or the *trans*-Golgi network [57] [58].

* **Lysosome**: The lysosome, an organelle discovered by Christian de Duve and named for its digestive properties, is the final organelle in the endocytic pathway and the principal site of hydrolytic breakdown within the cell [59]. They can be identified by the presence of LAMP1/2 and Rab9 [53] [60]. The organelles have a diameter of >1µm (with exact size depending on cell type) and have a pH of 4.5 [61] [62]. This acidic pH is principally maintained by the action of the Vacuolar-type H^+-ATPase (V-ATPase) which pumps H^+ into the organelle using energy obtained from ATP hydrolysis [62]. The acidic pH is required for the action of the degradative enzymes of the lysosome [61]. There are around 60 degradative enzymes present in the lysosome. The lysosome itself is not degraded (despite the presence of multiple degradative hydrolases) due to the presence of many heavily glycosylated integral membrane proteins (which make up the glycocalyx) [46]. In a wild-type cell macromolecules are degraded and the products of this degradation trafficked from the lysosome for further biosynthesis [31].

Trafficking along the endocytic pathway and the fusion of organelles requires the presence of SNAREs [42]. SNAREs can be classified as v-SNAREs or t-SNARES [42]. The former are found in the membrane of vesicles, the latter present in the target membrane. vSNAREs and tSNAREs will interact and form stable complexes (the *trans*-SNARE complex), and in doing so will bring the lipid bilayers of two membranes into apposition [42]. The final stage in the assembly of the SNARE complex is calcium dependent, with the fusion stimulating effect of calcium mediated through the Synaptotagmin-1 protein [43] [63] .

Endocytosis in NPC

NPC cells have a block in late-endosomal/lysosomal fusion [19]. Efficient trafficking in the endocytic system is dependent on the presence, and proper release, of lysosomal calcium [39]. NPC cells exhibit reduced calcium release and hence altered trafficking [20]. This reduced fusion may account for the lysosomal accumulation of lipids that are trafficked through the endocytic system [19]. Calcium chelation via Rhod-dextran (which reduces availability of lysosomal calcium) can induce NPC-like storage of cholesterol, sphingomyelin, and mistrafficking of boron-dipyrro-methene LacCer (BODIPY-LacCer) in wild-type cells [20].

1.2.4 NPC Pathogenesis

The mechanism by which mutations in *NPC1/2* lead to the aforementioned cellular phenotypes is contentious, as is the function of the wild-type NPC1 protein. NPC is classically regarded as a disease of cholesterol storage, with increased staining with filipin a hallmark of NPC disease cells, and the basis of the current diagnostic test for NPC [4] [25]. However, there are several strands of evidence that argue against the NPC1 protein playing a direct role in lysosomal cholesterol export, and that suggest that cholesterol accumulation is a downstream conse-

quence of NPC1 dysfunction. These include the observation of cholesterol egress from NPC1-null lysosomes [64] [65], and the lack of clinical benefit of lowering cholesterol (via pharmacological or dietary means) in NPC patients or murine and feline disease models [66] [67] [68]. There is also as of yet no evidence to show that the full-length NPC1 protein binds cholesterol (experiments demonstrating a NPC1-cholesterol interaction used an isolated N-terminal domain of NPC1 [69]). Crossing the *Npc1*$^{-/-}$ mouse with a mouse deficient in the low density lipoprotein receptor produces a mouse with reduced cholesterol storage in the liver. However this reduction is not accompanied by an improvement in function or an increase in lifespan, suggesting cholesterol is not a primary player in NPC pathogenesis [66].

More recent evidence argues that sphingosine is the primary disease metabolite in NPC. Lloyd-Evans *et al*. proposed a disease model in which NPC1 dysfunction directly led to accumulation of sphingosine [20]. Egress of lysosomal sphingosine would require the action of an as-yet-unidentified transport protein, due to its protonation at acidic pH [38]. Upon the treatment of wild-type cells with U18666A (a widely used pharmacological inducer of NPC phenotypes) the first measurable event was the accumulation of sphingosine [20] [70] [71]. This was followed by a reduction in lysosomal calcium levels and, hours later, the accumulation of cholesterol, GSLs and sphingomyelin. This accumulation of secondary storage lipids was proposed to be due to the defective endocytic trafficking occurring as a result of reduced lysosomal calcium (**Fig 1.4**) [20].

Accumulation of sphingosine as a direct consequence of NPC1/2 dysfunction may also account for the previously observed decreased acid sphingomyelinase activity in NPC cells [36]. Acid sphingomyelinase, which catalyses the breakdown of sphingomyelin to ceramide and phosphocholine, shows reduced activity in all Niemann-Pick disease subtypes (see Section 1.2.1). However, unlike in NPA/B,

NPC is not associated with mutations in *SMPD1*. Acid sphingomyelinase activity is modulated via phosphorylation, with activity increased by phosphorylation on Ser-508 [72]. This phosphorylation is performed by protein kinase C (PKC), the activity of which is decreased in response to increased levels of lysosomal sphingosine [73]. The accumulation of sphingomyelin in NPC cells may therefore be due to both the defect in endocytic trafficking and the reduced activity of acid sphingomyelinase. Due to the close biophysical relationship between sphingomyelin and cholesterol it has been suggested that the accumulation of sphingomyelin also promotes the accumulation of cholesterol [11] [36] [37] .

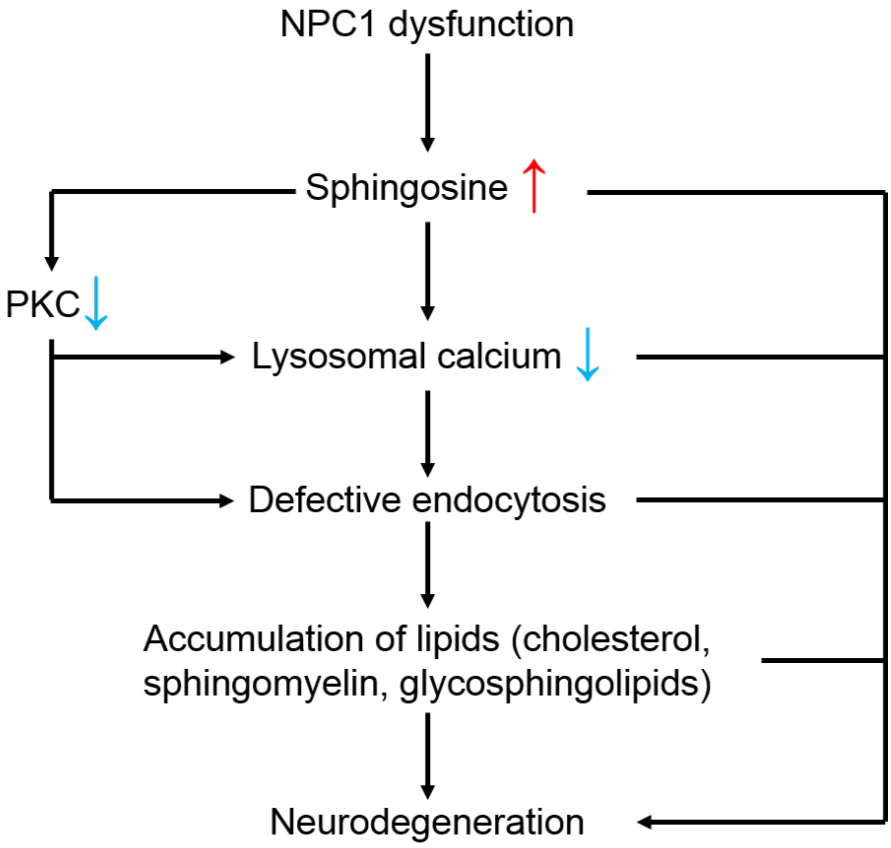

Figure 1.4: **Proposed order of cellular events following NPC1 dysfunction.** Protein kinase C (PKC). Adapted from [11].

1.3 NPC Therapies

Current therapeutic options for the treatment of NPC are limited. Whereas enzyme replacement therapy has been successfully used in the treatment of type 1 Gaucher disease (which involves dysfunction in the periphery) it is inappropriate for the treatment of NPC due to the inability of lysosomal enzymes to cross the blood-brain barrier and correct CNS defects [2]. Current therapies, and those which hold promise, are introduced below and discussed in more detail in Chapter 6.

Miglustat

Miglustat (tradename Zavesca) is currently the only licensed specific therapy for NPC [17]. It was developed to treat Type 1 Gaucher disease, which is characterized by accumulation of GlcCer [7]. It crosses the blood-brain-barrier and functions by inhibiting GlcCer synthase (the enzyme which catalyzes GlcCer formation, the first step in the GSL biosynthetic pathway (**Fig 1.3**)). This also leads to a downstream reduction in the levels of complex GSLs [17].

Curcumin

As detailed above, NPC cells show reduced lysosomal calcium levels and therefore reduced calcium release, which leads to reduced fusion along the endocytic pathway [20]. Lloyd-Evans *et al.* investigated whether it was possible to use antagonists of the sarco/endoplasmic reticulum Ca^{2+}-ATPase (SERCA), and the subsequent elevation of cytosolic calcium (due to decreased re-uptake into the ER), to compensate for the lack of lysosomal calcium release. They observed that curcumin was able to restore wild-type sphingolipid trafficking in *NPC1*$^{-/-}$ glial cells and improve the life span of treated *Npc1*$^{-/-}$ mice [20]. Curcumin is a curcuminoid, a group which also encompasses demethoxycurcumin and bis-

demethoxycurcumin [74].

Cyclodextrin

Cyclodextrins bind hydrophobic drugs and lipids, and are often used as drug carriers/excipients [75]. Hydroxypropyl-β-cyclodextrin (HPβCD), in the absence of any drug, prolongs the lifespan of *Npc1*$^{-/-}$ mice, as well as delaying onset of neurological symptoms [76]. HPβCD is currently undergoing phase 1 clinical trials at the NIH. It remains controversial as to whether HPβCD can cross the blood brain barrier of mice [77] [78]. Under the investigational new drug (IND) program the FDA has approved use of HPβCD in a small number of NPC patients prior to commencement of a clinical trial [77].

1.4 NPC and Tuberculosis - An Unexpected Link?

As detailed above, two well-characterized phenotypes of NPC cells are a reduction in endocytic trafficking (with reduced fusion at the level of the late endosome/lysosome) and the accumulation of cholesterol [19] [24]. Both cholesterol accumulation and defects in intracellular trafficking are also observed in wild-type macrophages infected with *Mycobacterium tuberculosis (Mtb)*, the causative agent of human tuberculosis [79] [80].

1.5 Tuberculosis: An Overview

Tuberculosis (TB) is a potentially deadly infectious disease arising following infection with pathogenic mycobacteria. In humans the vast majority of cases result from infection with *Mtb*, with the remainder of cases attributable to closely related members of the *Mycobacterium tuberculosis* complex (MTC) [81]. The MTC groups together those species, such as *Mycobacterium bovis* and *Mycobac-*

terium africanum, that are capable of causing TB in either humans or animals [81]. The majority (85%) of TB cases affect the lungs (pulmonary TB) with the remainder (extrapulmonary TB) affecting the nervous system, bones, lymph nodes, bladder and the reproductive system [82].

TB is an ancient disease, with an ancestor of *Mtb* hypothesized to have infected early hominids present in East Africa as much as 3 million years ago [83]. The emergence of *Mtb* is considered to be a much more recent event. Members of the MTC are believed to be descended from a single ancestor which had arisen from a genetic bottleneck occurring around 30,000 years ago [84]. The advent of TB as a major disease affecting humanity occurred around 10,000 years ago with the move away from a hunter-gatherer lifestyle and towards settlement in densely-populated agrarian societies [85]. Since then the disease has been a constant companion to humanity, with references to the disease dating back to the Old Testament and texts from classical antiquity [86] [87]. It was particularly prominent in 18th and 19th century Europe. At the turn of the 19th century TB was estimated to be responsible for a quarter of the total deaths in London [88].

Despite the existence of treatments for TB (see Section 1.8 below) it remains an enormous global health problem and the leading cause of death from infectious disease worldwide [89]. Whilst there has been a decrease in TB incidence over the last decade there were still 9 million new cases of TB in 2014, leading to 1.5 million deaths (with around a quarter of these deaths occurring in HIV-positive individuals) [89]. The majority of cases occurred in South-East Asia and Africa (58% and 25% of the total worlds cases respectively) [89].

TB is not currently a major health issue in the UK. In 2011 there were 8963 new cases of TB (14.4 people per 100000), with 95% of these cases occurring in individuals born outside of the UK (mostly in South Asia or Sub-Saharan Africa) [90]. 5.3% of these cases (436 people) lead to the death of the individual [90].

Levels of TB incidence in the UK have remained approximately constant since 2005 [90].

Not all individuals infected with *Mtb* become symptomatic [89]. Whilst the number of people developing active TB is large (8-10 million per year) it pales in comparison to the 2 billion people worldwide that harbour the mycobacterium [89]. This large discrepancy between the number of infections and number of active disease cases can be understood in light of the way in which *Mtb* interacts with the host immune system (see Section 1.7.2).

1.6 *Mycobacterium tuberculosis*

Mtb is one of around 100 members of the *Mycobacterium genus* and the most prominent member of the MTC [81]. It was identified in 1882 by Robert Koch [91]. *Mtb* is a slow-growing species with a generation time of approximately 24 hours [92]. In contrast *M.smegmatis*, a non-pathogenic species, has a generation time of around 3-4 hours [92].

Mtb is a rod-shaped mycobacteria around 2-4 µm long and 0.2-0.5µm wide [93]. One of the most noteworthy features of *Mtb* is the relatively complex and lipid-rich cell wall, with lipids accounting for around 60% of the cell wall [94]. The cell wall of *Mtb* will be discussed in more detail in Section 4.1. Although they are morphologically gram-positive bacteria, possessing a thick layer of peptidoglycan, mycobacteria cannot be stained using standard techniques such as gram staining [95] [96]. Staining for mycobacteria, including *Mtb*, uses the Ziehl-Neelsen (or acid-fast) stain [97]. Post-stain, mycobacteria will be stained red. Note that this stain is not specific for mycobacteria (with nocardia and schistosomes also stained) and is also relatively insensitive [97]. The presence of *Mtb* can also be ascertained via culture of the mycobacteria, although this process is slow due to the pathogen's long generation time [98].

1.7 Phagosomal Maturation

Macrophages are able to bind to and internalise microorganisms into phagosomes [80]. The phagosome will then undergo a maturation process in which the organelle environment becomes increasing hostile to microorganisms, leading to the microorganisms destruction [80]. Maturation involves a series of interactions with the endocytic system, with the phagosome fusing with sorting endosomes, late endosomes and finally the lysosome [80] [99] [100]. These fusion events lead to the transfer of constituents of the membranes and lumen of the endo-lysosomal system to the phagosome. Immediately post-internalisation the phagosome contains early endosomal markers such as EEA1 and Rab5 [99]. As maturation progresses these early endosomal markers will be lost, and replaced with late endosomal markers, and finally those of the lysosome (such as active cathepsin D and LAMPs) [99]. A pictorial representation of the maturation process and the accompanying changes in phagosomal composition is shown below (**Fig 1.5**). As in the endocytic system, this trafficking process is associated with increasing acidification [99] [101]. The end result of phagosomal maturation is the formation of a hybrid organelle, the phagolysosome, which possesses an extremely hostile luminal environment, including the presence of hydrolytic enzymes such as cathepsin D [99]. The pH of the phagolysosome ranges from 4.5-5.5, with the acidic pH due to the recruitment of the lysosomal V-ATPase to the phagosome membrane [101]. Formation of the phagolysosome is a key step in destruction of the pathogen [80] [99].

The role of calcium in phagosomal maturation is contentious. The initial ingestion of the pathogen appears to be a calcium-independent process [102]. Majeed *et al.* reported that the further internalisation of *Mtb* was accompanied by a spike in cytosolic [Ca^{2+}] [103]. Depletion of intracellular calcium (via culture in Ca^{2+}-depleted media) reduced the percentage of total bacteria killed by the host

cell [103]. This contrasted with previous reports in which phagosome:lysosome fusion appeared unaffected by a reduction in intracellular [Ca^{2+}] [104].

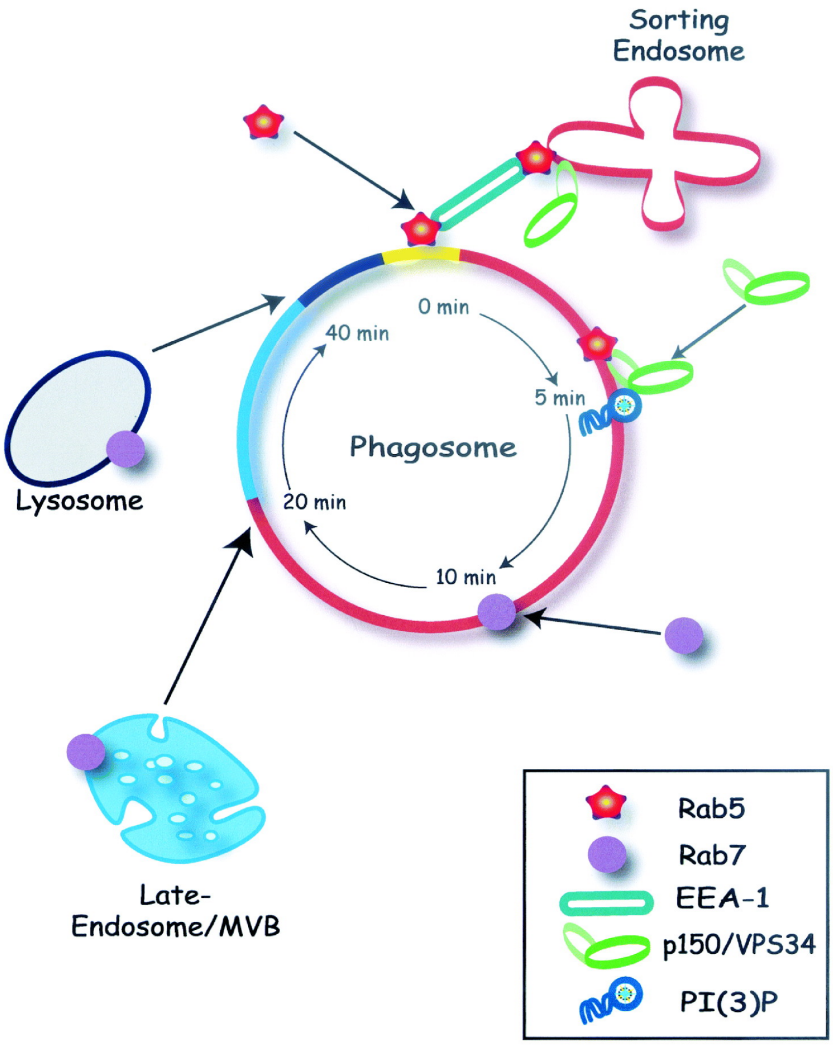

Figure 1.5: **Compositional changes of the phagosome during maturation.** Schematic illustrating some of the key events occurring during phagosomal maturation (and an approximate timecourse for the maturation process). Early endosomal antigen 1 (EEA-1), multivesicular bodies (MVB), phosphatidylinositol 3-phosphate (PI(3)P). Adapted from [99].

1.7.1 Intracellular Survival Strategies

There are a range of strategies by which pathogens attempt to avoid their phagocytosis and destruction. Species of the *Yersinia* genus are able to block their initial uptake by professional phagocytes, and will instead induce their uptake into host epithelial cells (wherein they replicate) [105] [106]. There are also a number of species, including *Shigella flexneri* and *Listeria monocytogenes*, that are able to escape from the phagosome via lysis of the organelle membrane [107] [108]. It is also possible for a pathogen to reside in the hostile environment of the phagolysosome without being destroyed. *Coxiella burnetti* is able to survive within the compartment, despite the acidic conditions and presence of hydrolytic enzymes [109]. Pathogenic mycobacteria employ a different survival strategy, with macrophages infected with pathogenic mycobacteria exhibiting incomplete phagosomal maturation.

1.7.2 Incomplete Phagosomal Maturation Leads to Intracellular Persistence of Pathogenic Mycobacteria

Infection with *Mtb* occurs via host-to-host transmission, with the mycobacteria carried in droplets exhaled by a person with an active TB infection [79]. Upon inhalation they are taken up by alveolar macrophages in the lung [79]. Here, the mycobacteria is able to subvert the process of phagosomal maturation which would otherwise have led to its destruction [110]. Phagosomes containing pathogenic mycobacteria do not fuse with the lysosome [80] [111]. The phagosome in *Mtb* infected cells remains at pH ~6.4, and retains the characteristics of the EE [110]. The lack of acidification of the *Mtb* phagosome is due to the absence of the V-ATPase from the organelle membrane, with inhibition of V-ATPase delivery to the phagosome attributed to the action of the secreted *Mtb* protein tyrosine phosphatase (PtpA) [112]. Inhibition of phagosomal maturation

is only observed following internalisation of pathogenic *Mycobacteria*, with non-pathogenic environmental bacteria such as *M.smegmatis* being cleared efficiently by host cells [113].

There is also evidence suggesting that calcium plays an important role in phagosomal maturation, and that defects in calcium homeostasis could account for the reduced phagosome:lysosome fusion observed following *Mtb* infection. It has previously been shown that the presence of calcium is required for phagosomal maturation to proceed as normal [103]. The pharmacological elevation of intracellular [Ca^{2+}] was also observed to promote maturation of phagosomes, and was associated with reduced survival of *Mtb* [114].

Regardless of the mechanism by which it is achieved, defective phagosomal maturation means that pathogenic mycobacteria cannot be destroyed and cleared from the host cell [80]. This failure in clearance ensures that *Mtb* can persist within a macrophage population for decades after the initial infection [115]. Because macrophages are unable to clear the mycobacteria they will instead use a granuloma structure to attempt to isolate the infection and prevent it from disseminating [116]. The TB granuloma consists of phagocytosing macrophages surrounded by foamy macrophages, monocytes and lymphocytes [79] (**Fig 1.6**). Granuloma formation is driven by the production of a range of pro-inflammatory chemokines and cytokines produced by the infected macrophages, including CCL2, IL-18 and TNF-α [117] [118]. These in turn serve to recruit leukocytes to the site of infection [116]. The granuloma is enclosed by fibroblasts, which form a fibrous barrier around the macrophage-containing centre [119]. Macrophages inside the TB granuloma have a characteristic foamy appearance due to defective low density lipoprotein efflux and the accumulation of lipids including cholesterol and LacCer [79] [119]. It is believed that inside the granuloma mycobacteria are present in a non-replicating, vegetative state [79] (although it has been argued

that mycobacterial division does occur, but is balanced by mycobacterial death, so that the infectious load remains unchanged [120]). A number of genes are upregulated in the TB granuloma. These include *NPC1* and *NPC2* as well as several genes whose products are involved in lipid metabolism [119].

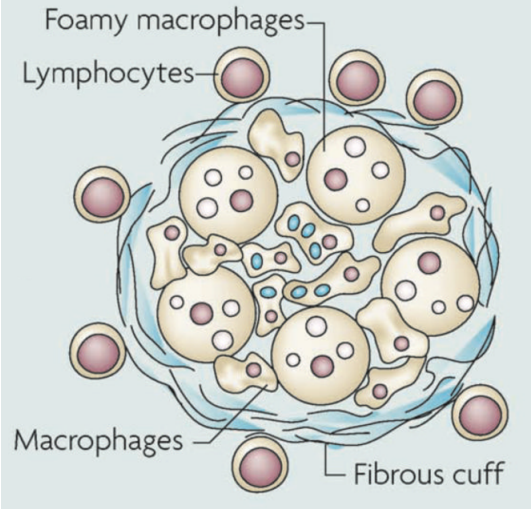

Figure 1.6: **Structure of the TB granuloma.** Adapted from [79].

The end result is effectively a stalemate between the host immune system and the mycobacteria - the infection is isolated inside the granuloma, so the host is asymptomatic and not contagious, but mycobacterial persistence means that a possibility remains of active disease developing at a later time point [79]. This persistence is responsible for the enormous number of people worldwide that harbour *Mtb* (individuals with a latent TB infection) [89]. Individuals with latent TB infections are not symptomatic or contagious. In healthy individuals the probability that latent TB will lead to the development of active TB is low - only 10% over the individuals lifespan (although this 10% still constitutes an enormous number of people) [121]. The transition to active TB involves the accumulation of necrotic material in the granuloma core, with the eventual collapse of the granuloma structure and the release of virulent mycobacteria into the airways [79]. The infected individual is now contagious and symptomatic. The factors

determining the progression of a latent infection to active disease are unclear. It has been shown that the probability of this 'reactivation' phenotype occurring is increased in the case of a pre-existing immunodeficiency. HIV positive individuals have a 30% chance of progressing to active disease (annual risk, 10%) [89] [122].

1.7.3 Cholesterol as a Food Source

The ability to metabolize host lipids is essential for the establishment of chronic *Mtb* infection. Pandey *et al.* used radiolabelled exogenous cholesterol to show that the mycobacteria are able to utilise cholesterol as a carbon source [123]. *Mce4* is an operon in the *Mtb* genome encoding a cholesterol importer system [123]. Mutations in this operon result in a mycobacteria that is able to establish an infection, but which is unable to achieve long-term persistence [123]. Electron microscopy has shown that the mycobacteria are located close to the large intracellular lipid stores, possibly using them as a nutrition source [121]. To obtain carbon from fatty acids requires gluconeogenesis, which in turn requires isocitrate lyase activity, an enzyme of the glyoxylate shunt. *Mtb* mutants lacking isocitrate lyase activity showed reduced viability during the chronic stage of infection [124]. The cholesterol accumulation seen in NPC cells would provide *Mtb* with a bountiful food supply.

1.8 Diagnosis and Treatment of TB

The only way in which TB can be definitively diagnosed is via the culture of mycobacteria from a patient [125]. An indication of TB infection can be achieved using a skin test, in which tuberculin (a glycerol extract of the mycobacteria) is injected [126]. In the Mantoux test, the current standard screening tool for TB, the tuberculin is injected intradermally. The size of the subsequent raised,

hardened area of skin indicates whether or not the individual has been previously exposed to TB (larger area means a more vigorous immune response, and hence a greater probability of prior infection). The size of the induration formed is also influenced by various medical risk factors, such as the presence/absence of HIV or end stage renal disease [126]. Chest X-rays are mainly used to rule out the presence of TB [125].

TB is a treatable disease, with the current treatment regimen being antibiotic-based. The standard short course of treatment for TB consists of treatment with isoniazid, rifampicin, pyrazinamide and ethambutol for two months, followed by 4 months with isoniazid and rifampicin alone [127]. This combination therapy (in theory) prevents the development of antibiotic resistant strains of the disease [128]. Treatment of latent TB requires 6-9 months treatment with isoniazid, with the aim of this treatment to prevent the disease progressing to its active form [129]. The efficacy of anti-*Mtb* agents is limited by the low permeability of the mycobacterial cell wall [130]. Mycobacteria have a thick (9-10nm) hydrophobic cell wall [113] (thickness due to the length of the cell wall fatty acids, the longest existing in nature [131]). In the absence of therapeutic intervention mortality in active TB cases is high - 70% of patients with active TB will die within 10 years [89].

The length of this 'short' course, and the fact that visible symptoms may cease after a few weeks of treatment, leads to issues with patient compliance. This has led to the development of multi-drug resistant (MDR) and extensively drug resistant (XDR) *Mtb* [89]. MDR-TB refers to mycobacteria that are resistant to isoniazid and rifampicin, and must be treated with second-line treatments (such as capreomycin, kanamycin and amikacin). XDR-TB are also resistant to isoniazid and rifampicin, and also resistant to any one second-line treatment [132]. In 2012 it was estimated that 450,000 of new TB cases involved MDR-TB

[89]. Over the last decade there has been a small but significant increase in the number of MDR-TB cases (from 0.9% of total cases in 2000 to 1.6% in 2011) [90]. The percentage of these cases that are XDR are estimated to range from 0.6% to 21.0%, depending on region [132]. Most worryingly, the last decade has seen cases of TB in patients in India, Italy and Iran resistant to all known anti-TB drugs – total drug resistant-TB [133] [134].

The only currently licensed TB vaccine is Bacillus Calmette-Guérin (BCG), an attenuated form of *Mycobacterium bovis* (the causative agent of bovine TB) [135]. It is reasonably effective at preventing extrapulmonary TB in children, but is less effective at preventing the development of pulmonary TB in adults [89]. There remains controversy as to the extent of protection afforded by the BCG vaccine. A metastudy estimated that receipt of the BCG vaccine resulted in a 50% reduction in the life time risk of contracting TB [136]. The duration of this protective effect is also under debate. Receipt of the BCG vaccine will also lead to difficulties in interpreting Mantoux skin test results, with vaccination leading to false positives [126]. Several novel TB vaccines are currently in development, with around a dozen currently undergoing clinical trials [137].

The rise of MDR and XDR-TB is concerning, particularly in light of the slow rate at which new anti-TB drugs are developed. Bedaquiline was approved for use in 2012, and was the first novel TB drug in 40 years [138]. It has been suggested that a new approach to drug development is needed, one in which instead of targeting the mycobacteria directly we attempt to modulate the way in which it interacts with the host cell, thus minimising the development of resistance.

1.9 Do Pathogenic Mycobacteria Target the NPC Pathway?

There are numerous phenotypic similarities between NPC cells and wild-type cells infected with pathogenic mycobacteria. Both have defects in intracellular trafficking, with the trafficking defect occurring at the level of the lysosome [19] [80]. Both also exhibit accumulation of cholesterol, with increased filipin staining (indicative of cholesterol accumulation) and the presence of foam cells hallmarks of NPC and the TB granuloma respectively [4] [79]. The TB granuloma exhibits upregulation of *NPC1* and *NPC2*, and also accumulation of the GSL LacCer [119]. On the basis of these observations we wished to investigate whether these similarities are simply superficial or whether they reflected an underlying mechanistic connection between pathogenic mycobacteria and the NPC pathway.

A key factor in the success of *Mtb* as a human pathogen is its ability to persist within host macrophages due to reduced phagosome:lysosome fusion [80] [99] [111]. The means by which pathogenic mycobacteria achieve this remain contentious. It has been suggested that calcium is a key modulator of the phagosomal maturation process, and that reduced calcium levels are responsible for the absence of phagosomal maturation in *Mtb*-infected macrophages [103] [114]. Altered calcium homeostasis is a hallmark of NPC cells, with reduced lysosomal calcium release thought to lead to reduced fusion along the endocytic pathway [20]. Inhibition of the wild-type NPC pathway, and the subsequent dysfunction in cellular calcium, could provide a means by which pathogenic mycobacteria prevent phagosome:lysosome fusion, and hence achieve long term cellular persistence.

The purpose of the work in this thesis will be to investigate a possible mechanistic link between infection with pathogenic mycobacteria and the NPC pathway

of the host cell. It would also be of great value to investigate whether therapies for NPC hold any promise in the future treatment of TB.

Aims

* Characterise the phenotypic similarities between NPC cells and wild type cells infected with pathogenic mycobacteria.

* Investigate the mechanism by which pathogenic mycobacteria, residing in the phagosome, may interact with the host NPC pathway.

* Assess the feasibility of therapies for NPC in the treatment of TB.

2 Induction of NPC Cellular Phenotypes in Wild-Type Murine Macrophages Following Infection with Pathogenic Mycobacteria

2.1 Introduction

As detailed in Chapter 1, mutations in *NPC1* or *NPC2* result in cells with a complex phenotype. NPC cells accumulate a range of lipids including cholesterol, GSLs and sphingosine, and show reduced calcium release from the lysosome due to impaired store filling. They also have reduced intracellular trafficking with defects in fusion at the level of the late-endosome/lysosome [11] [20].

Defective intracellular trafficking and accumulation of cholesterol and the GSL LacCer are well documented consequences of *Mtb* infection [99] [119] [121]. These infected cells show reduced fusion of the phagosome and lysosome, with this reduced fusion leading to long-term persistence of *Mtb* inside of host macrophages and the establishment of a latent TB infection. This latent infection may later develop into an active form of the disease, in which the host organism becomes symptomatic, contagious and susceptible to organ damage and death [89].

The majority of the work in this chapter (and thesis as a whole) will use Bacille-Calmette Guérin (BCG) in place of *Mtb*. BCG is an attenuated form of *Mycobacterium bovis* (*M.bovis*), the causative agent of TB in cattle. It was created by repeated *in vitro* passaging of *M.bovis*. BCG is used as a vaccine against TB [135]. Its genome has high (>99.95%) sequence homology to that of *Mtb* [139]. It also shares with *Mtb* an ability to persist within its host and to lead to a reactivation phenotype (as seen in the transition from latent to active TB) [140]. It is often used in place of *Mtb* in research due to safety considerations (with BCG and *Mtb* being containment level 2/3 microorganisms respectively).

In order to determine whether induction of NPC cellular phenotypes is a property unique to pathogenic mycobacteria we will also infect host macrophages with the non-pathogenic mycobacteria *M.smegmatis*. *M.smegmatis* is a fast-growing environmental mycobacterium [113]. *M.smegmatis* is rarely problematic for healthy individuals, although it has been noted to be responsible for lung infections and soft-tissue/skin lesions in immunocompetent individuals following cardiac surgery or trauma due to injury [141]. In patients with pre-existing IFN-γ deficiencies *M.smegmatis* infection has been reported as potentially fatal [142]. The mycobacterium lacks the ability to persist within host cells, and is cleared efficiently [113]. We are hypothesising that pathogenic mycobacteria achieve persistence through inhibition of the NPC pathway, and in doing so induce NPC cellular phenotypes. If so, then a non-persistent mycobacteria such as *M.smegmatis* would not induce NPC cellular phenotypes due to an inability to inhibit the NPC pathway.

We wished to investigate whether the cholesterol accumulation and defective intracellular trafficking in NPC cells and those infected with *Mtb* reflected only a superficial similarity between the two disparate diseases, or whether they were due to a mechanistic connection between the NPC cellular pathway and the

means by which pathogenic mycobacteria achieve cellular persistence. Therefore the specific aims of the work presented in this chapter are:

* Investigate whether other NPC cellular phenotypes, namely accumulation of sphingosine and glycosphingolipids and reduced lysosomal calcium, are also seen in murine macrophages infected with pathogenic mycobacteria.

* To study whether induced phenotypes are specific to pathogenic mycobacteria, and are not induced in response to infection with non-pathogenic mycobacteria.

2.2 Materials and Methods

2.2.1 Cell Lines and Bacterial Strains

RAW 264.7 macrophages were obtained from the European Cell Culture Collection (Porton Down, UK) and maintained in RPMI (Sigma-Aldrich) supplemented with 10% Foetal Calf Serum (FCS) (Biosera), 1% penicillin/streptomycin (P/S) (Gibco) and 1% glutamine (Gibco).

BCG (Pasteur strain) and *M.tuberculosis* (H37Rv strain) were kindly provided by Simon Clark (Public Health England, UK). Fluorescent *M.smegmatis* (mc^2155 strain expressing mCherry fluorescent protein) was kindly provided by Prof. David Russell (Cornell University, USA).

All work with *Mtb* was carried out under Category 3 conditions at Public Health England (Salisbury, UK).

2.2.2 Mycobacterial Culture

Thawed mycobacterial glycerol stocks were grown on 7H11 plates supplemented with Oleic Albumin Dextrose Catalase (Sigma-Aldrich) at 37°C/5% CO_2. Visible BCG colony formation occurred after 3-4 weeks, with *M.smegmatis* colonies visible within 48 hours. Single colonies were used to inoculate starter liquid cultures (15ml of 7H9 supplemented with Albumin Dextrose Catalase (Sigma-Aldrich)), which were incubated at 37°C with shaking (220rpm). Once starter cultures were well-developed additional pre-warmed media was added, to give a total volume of 50ml.

Culture growth was monitored spectrophotometrically via absorbance at 600nm. Sterile 7H9 media was used as a blank. An OD_{600nm} of 1.0 corresponded to 6 x 10^8 colony forming units (CFU) per ml culture. For experiments mid-exponential cultures of BCG were used (OD_{600nm}=0.6-1.0).

Media composition was as follows:

Media	Recipe
7H9 (liquid)	2.35g 7H9, 1.98g sodium pyruvate, 0.5ml Tween-80 (Sigma-Aldrich), 450ml mQ H_2O. The mixture was autoclaved for 15 minutes at 121°C. After cooling to 55°C media was supplemented with Albumin Dextrose Catalase and, if needed, 20µg/ml kanamycin.
7H11 (solid)	10.25g 7H11, 2.08g sodium pyruvate, 2.5ml glycerol (Sigma-Aldrich), 450ml mQ H_2O. The mixture was microwaved and brought to the boil prior to autoclaving for 15 minutes at 121°C. After cooling to 55°C media was supplemented with Oleic Albumin Dextrose Catalase and, if needed, 20µg/ml kanamycin.

2.2.3 Production of Mycobacterial Glycerol Stocks

Mycobacterial culture (0.5ml in exponential growth phase) was added to 0.5ml 80% glycerol in a cryovial. The cryovial was snap frozen in liquid nitrogen before transfer to -80°C for long term storage.

2.2.4 Production of Fluorescent mCherry-expressing BCG

The pV116 plasmid (containing genes for kanamycin resistance and production of mCherry fluorescent protein) was kindly provided by Prof. David Russell (Cornell University, USA).

Chemically competent *E.coli* were mixed with 100ng plasmid and kept on ice for 30 minutes prior to 60 seconds at 42°C and a further 60 seconds on ice. Liquid broth (0.5ml) was added, and the mixture shaken for one hour at 37°C. Culture

was plated out onto liquid broth agar plates supplemented with kanamycin and incubated overnight. The resulting colonies were used to establish liquid cultures of transformed cells. After 48 hours a DNA prep was used to recover large quantities of the plasmid.

BCG culture (100ml) was brought to log phase and centrifuged (2000g/15 min). The supernatant was discarded and the pellet washed with equal volume sterile 10% glycerol prior to second centrifugation (2000g/15min). This was repeated twice and the resulting pellet was resuspended in 1ml 10% glycerol. BCG (200µl) was mixed with 250ng plasmid and incubated at room temperature for 10 minutes. The mixture was transferred to a 0.2cm cuvette and electroporated (Bio-Rad Gene Pulser, 2500mV, 1000Ω, 25µF). 7H9 media (1ml) was added and the mixture transferred to falcon tube and incubated for 48hrs at 37°C/5% CO_2 (to allow expression of kanamycin resistance gene) prior to plating out onto 7H11 plates supplemented with 20µg/ml kanamycin and incubation at 37°C/5% CO_2. Visible colonies were present after 3 weeks. Red colonies (expressing mCherry) were selected for further work.

2.2.5 Infection of Host Cells

Host cells were plated out onto coverslips or in wells/flasks approximately 18hr prior to infection. Cells were washed with complete media (excluding 1% P/S) to remove non-adherent cells. Mycobacterial culture in exponential growth phase was spun down (3000rpm/10min) and resuspended in appropriate media before addition to host cells. Unless otherwise stated all infections used a multiplicity of infection (MOI) of 12.5.

2.2.6 Determination of Sample Protein Levels

Protein levels were determined using a BCA protein assay (Sigma-Aldrich) according to manufacturers instructions.

2.2.7 Sphingoid Base Extraction and Labelling

Lipids were extracted as previously described [143], with the following modifications. Post-addition of 2ml 1:1 chloroform:methanol (C:M) samples were spiked with 1µl 1mM C_{20} sphingosine standard (Avanti Polar Lipids). Solvent A was replaced with 1:1 MeOH:H_2O and RP18 SPE 1ml columns (Supelco) were used for solid-phase extraction. Post sample addition, columns were washed with 2x1ml 1:1 MeOH:H_2O and 4x1ml 3:1 MeOH:H_2O w/0.1% acetic acid, and the sample was eluted in 4x1ml 9:1 MeOH-10mM KH_2PO_4. The elutant was dried under N_2 and resuspended in 1ml HPLC-grade EtOH, prior to drying down and resuspension in 50µl warm EtOH. Extracted sphingoid bases were labelled with 50µl orthophthaldehyde reagent (12.5mg orthophthaldehyde (Sigma-Aldrich), 12.5µl 2-mercaptoethanol (Sigma-Aldrich), 0.25ml EtOH, 24.75ml 3% boric acid pH 10.5) and incubated for 5 min at room temperature.

2.2.8 Reverse Phase High Performance Liquid Chromatography (RP-HPLC)

RP-HPLC was carried out using a system consisting of a VWR Hitachi Organizer module, L-2200 Autosampler, L-2130 Pump, L-2485 FL Detector and BetaBasic-18 column (3µm, 100x4.6mm). Chromatography was carried out using a mobile phase of 85% acetonitrile/15% H_2O at a flow rate of 1.0ml/min. The orthophthaldehyde-labelled derivatives were monitored at an excitation wavelength of 340nm and an emission wavelength of 450nm. Quantification of trace

peak area was carried out using EZChrom Elite Software.

2.2.9 Quantification of Lysosomal Calcium

Measurements of lysosomal [Ca^{2+}] were performed by Dr. Lianne Davis.

Cells were infected 24hr prior to measurement. Cells were loaded with 2µM fura 2-AM (Teflabs) in the presence of 0.03% Pluronic F127 (Invitrogen) in a buffer containing :((mM) 121 NaCl, 5.4 KCl, 0.8 $MgCl_2$, 1.8 $CaCl_2$, 6 $NaHCO_3$, 25 HEPES, 10 Glucose) for 45 min at room temperature, followed by a 15 min de-esterification. Cells were washed once with Ca^{2+}-free buffer supplemented with 1 mM ethylene glycol tetraacetic acid (EGTA) and twice with Ca^{2+}-free buffer containing 100µM EGTA. Subsequent steps were conducted in the latter buffer. Cells were mounted on the stage of an Olympus IX71 microscope equipped with a 40x UApo/340 objective (1.35 NA) and a 12-bit Photometrics Coolsnap HQ2 CCD camera. Cells were excited alternately by 350- and 380-nm light using a Cairn monochromator; emission data were collected at 480-540 nm using a bandpass filter. Experiments were conducted at room temperature with an image collected every 2-3 seconds.

Lysosomal Ca^{2+} content was assessed upon addition of 200µM GPN (Glycyl-L-phenylalanine 2-naphthylamide) (Santa Cruz Biotechnology) which lyses cathepsin C-containing acidic intracellular Ca^{2+} stores. At the end of each run autofluorescence was determined by addition of 1µM ionomycin (Calbiochem) with 4 mM $MnCl_2$, which quenches fura-2. Images were analysed using custom-written Magipix software (R. Jacob, Kings College London, London, UK) on a single-cell basis. The autofluorescence signal was subtracted and the data expressed as the maximal peak fluorescence changes (Δ350/380).

2.2.10 Determination of Cathepsin C activity

Cathepsin C activity was assayed by Dr. Lianne Davis.

Cells were infected 24hr prior to measurement. The lysosomes of RAW 264.7 macrophages were labelled with LysoTracker Green DND-26 (Life Technologies) (100nM for 5 min at room temperature) in a buffer containing (mM): 121 NaCl, 5.4 KCl, 0.8 $MgCl_2$, 1.8 $CaCl_2$, 6 $NaHCO_3$, 25 HEPES, 10 Glucose. The cells were washed once in the same buffer but without Ca^{2+} (Ca^{2+}-free buffer) and supplemented with 1mM EGTA. The cells were then washed twice with Ca^{2+}-free buffer containing 100µM EGTA, with subsequent experiments conducted in this buffer. The cells were mounted on the stage of a Zeiss LSM510 Meta confocal laser-scanning microscope equipped with a 40x objective; excitation/emission (nm): green (488/505-530), red (543/>560). Experiments were conducted at room temperature with images collected every second. The activity of cathepsin C was inferred from the release of LysoTracker (and the resultant decrease in fluorescence) from lysosomes upon the addition of the lysosome-disrupting cathepsin C substrate GPN (200µM). Images were analysed using custom-written Magipix software (R. Jacob, Kings College London, London, UK) on a single-cell basis. Data are presented as the mean ± SEM of the initial rate (units of LysoTracker fluorescence per second normalised to the basal fluorescence) or by the rate constant calculated from an exponential curve fit.

2.2.11 Determination of Lysosomal pH

Lysosomal pH measurements were carried out by Dr. Lianne Davis.

Cells were infected 24hr prior to measurement. Lysosomal pH was measured as described with minor modifications [144]. Fluorescein-dextran and Rhodamine-dextran (Sigma-Aldrich) were loaded at 0.25mg/ml for 12hr into cells at 37°C followed by 12hr chase at 37°C to label lysosomes. Image analysis and quantifi-

cation of fluorescence was performed using SimplePCI software.

2.2.12 Quantification of Lysosomal Calcium by Rhod-dextran

Direct quantification of lysosomal calcium via Rhod-dextran was conducted by Dr. Emyr Lloyd-Evans and Dr. Nathan Lack, and performed as described [20]. Briefly, control/infected cells were loaded with low-affinity Rhod dextran (calcium sensitive) (0.25mg/ml) and Alexa Fluor 488 dextran (calcium sensitive) (0.1mg/ml) for 12hr, followed by a 12hr chase.

2.2.13 Preparation of Coverslips for Microscopy

Coverslips were washed in concentrated nitric acid overnight, prior to washing five times with distilled water and five times with mQ H_2O. Water was decanted and coverslips stored in EtOH. Coverslips were air dried in a sterile environment prior to use.

2.2.14 Fixation of Cells

Coverslips were washed with 2x1ml PBS prior to addition of 150µl 4% paraformaldehyde (PFA) (TAAB). After 15 minutes incubation at room temperature cells were washed with 1x3ml PBS.

2.2.15 Microscopy

Coverslips were mounted onto slides using Mowiol (Calbiochem). Mowiol was supplemented with anti-fade reagents 1, 4 Diazobicyclo-(2,2,2) octane (DABCO) (Sigma-Aldrich) (5%) and n-propyl gallate (n-PG) (Sigma-Aldrich)(2.5%). Unless otherwise stated all imaging was carried out using an Axio Imager A1 microscope in conjunction with an Axiocam High-Resolution Camera and Axiovision

software ver. 4.8.

2.2.16 Localisation of Cellular Cholesterol via Filipin Staining

Fixed cells were incubated with 1ml filipin working solution (0.05mg/ml in PBS with 0.2% Triton X100) for 1hr at room temperature, before being washed with 3 x 1ml PBS.

2.2.17 GSL Extraction and Labelling

GSLs were extracted from cellular homogenates (approx. 200µg protein) in 4 volumes of C:M (1:2 v/v) overnight at room temperature. The mixture was centrifuged (3000rpm/10min) before addition of 0.5ml chloroform and 0.5ml PBS to supernatant and repetition of centrifugation (3000rpm/10min). The resulting lower phase was dried under N_2, re-suspended in 50µl C:M 1:3 and recombined with the upper phase. GSLs were recovered using 25mg C18 Isolute columns (Biotage) pre-equilibrated with 4x1ml MeOH and 2x1ml H_2O. Sample was eluted via 1ml C:M 98:2, 2x1ml C:M 1:3, 1ml MeOH. Column elutant was dried under N_2, re-suspended in 100µl C:M 2:1, before being dried down and re-suspended in ceramide glycanase (CGase) buffer. CGase (50mU) was added, and samples were incubated at 37^{o}C for 16hr. Released oligosaccharides were anthranilic acid (2-AA) labelled as previously described [145]. Labelled oligosaccharides were purified via mixing with 1ml Acetonitrile:H_2O 97:3 and addition to Discovery DPA-6S columns (pre-equilibrated with 1ml acetonitrile, 2x1ml H_2O and 2x1ml acetonitrile). Column was washed with 2x1ml Acetonitrile:H_2O 95:5. Purified GSLs were then eluted into 2x0.75ml H_2O.

2.2.18 Normal Phase High Performance Liquid Chromatography (NP-HPLC)

NP-HPLC was carried out as previously described [145] with the following modifications. Solvent A was pure acetonitrile. Solvent B was mQ H_2O water. Solvent C was 100mM NH_4OH (pH 3.85) in mQ H_2O.

2.2.19 Statistical Analysis

Statistical analysis was performed using GraphPad Prism (ver 6.0). The specific test used is indicated in the figure legend.

2.3 Results

2.3.1 Quantification of Sphingosine Levels via HPLC

Accumulation of sphingosine has been previously shown to be a direct consequence of NPC1 dysfunction [20]. Infection of wild-type RAW 264.7 murine macrophages with the pathogenic mycobacteria BCG was associated with a significant increase in sphingosine levels 48hr post infection, as quantified via RP-HPLC **(Figure 2.1, p - 0.0329)**. Sphingosine levels in infected macrophages were around 2-fold higher than in uninfected controls.

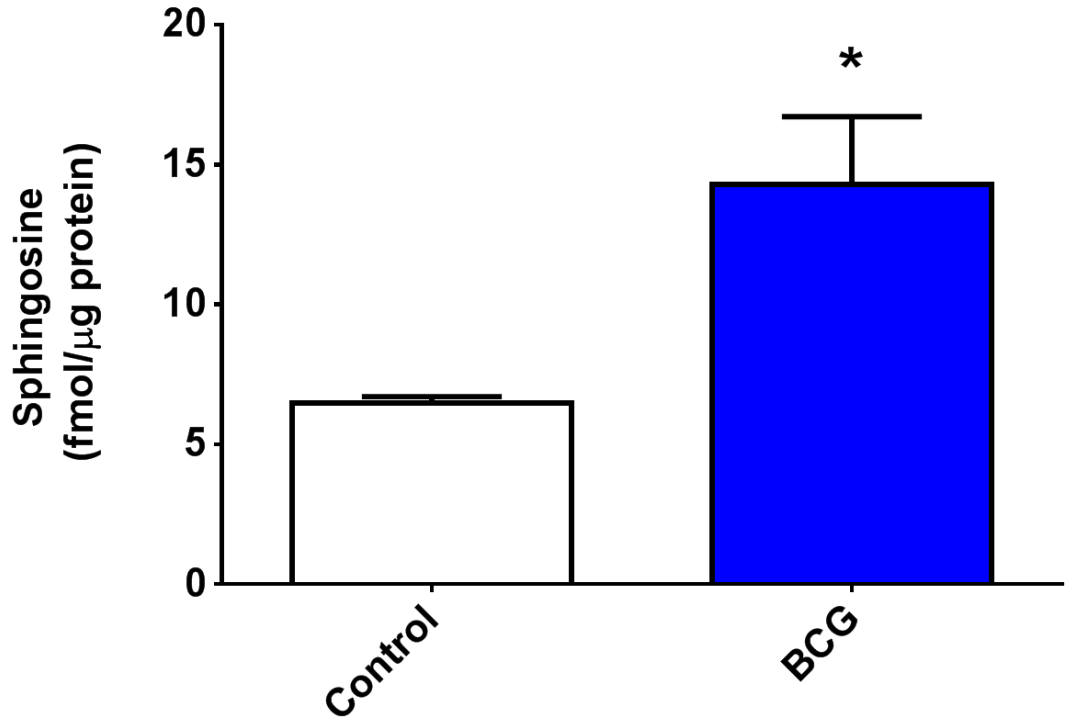

Figure 2.1: **Effect of BCG infection on sphingosine levels in RAW 264.7 cells.** 48hr infection, MOI 12.5. Values adjusted for sample protein concentration. Mean ± SEM of 5 biological replicates. * $p<0.05$ versus control (via t test).

2.3.2 Quantification of Lysosomal Calcium Release post-GPN Addition

Lysosomal [Ca^{2+}] was first quantified indirectly by using GPN. Upon being taken up into the acidic compartment GPN is hydrolysed by cathepsin C into free amino acids. The accumulation of these amino acids results in osmotic lysis of the lysosome and the subsequent release of the Ca^{2+} contained therein [20] [146]. Prior to addition of GPN, cells were loaded with fura-2, a ratiometric fluorescent dye that binds to free intracellular Ca^{2+}. The fluorescence of cells following excitation at 350nm and 380nm, specifically the ratio of these two values (350/380), acts as a measure of intracellular calcium. Ca^{2+} responses from single representative cells are shown (**Figure 2.2A**). The point at which GPN was added is indicated by the arrow. Following GPN addition there was an increase in intracellular Ca^{2+} indicative of the release of Ca^{2+} from the lysosome. This maximal Ca^{2+} response was reduced in macrophages infected with BCG (24hr). No such reduction was seen in cells infected with the non-pathogenic *M.smegmatis*.

A measurement of lysosomal calcium content can be attained by calculating Δ350/380 - the change in cytosolic Ca^{2+} levels upon addition of GPN. The basal Ca^{2+} level (prior to GPN) was subtracted from the maximal Ca^{2+} levels following lysosomal lysis. A summary of maximum Ca^{2+} changes in control and infected macrophages is shown (**Figure 2.2B**). The size of reponse is given as percentage change relative to uninfected controls. BCG-infected macrophages showed a significant reduction in GPN-induced Ca^{2+} release, with responses approximately 65% of that seen in control cells (**$p<0.001$**). No change was observed in cells infected with *M.smegmatis*.

Infection of macrophages was associated with a small (˜7%) but significant decrease in basal [Ca^{2+}] (**Figure 2.2C, p - 0.0067 (BCG)/ 0.0005 (Smeg)**

versus control). However, this decrease was not related to the pathogenicity of the mycobacteria, being observed following infection with both BCG and *M.smegmatis*. The change in basal [Ca^{2+}] was also far too minor to account for any changes in maximal Ca^{2+} between control macrophages and those infected with BCG.

The use of GPN to quantify lysosomal [Ca^{2+}] requires cathepsin C to catabolise GPN and cause lysosomal lysis. For it to be used in the comparison betwen control and mycobacterial-infected cells it was necessary to check that cathepsin C activity was not altered by BCG infection. To quantify cathepsin C activity cells were loaded with LysoTracker Green, a fluorescent dye which is selective for acidic organelles such as the lysosome [147]. Upon addition of GPN, and the osmotic lysis of the lysosome, this LysoTracker fluorescence will be lost. The rate at which LysoTracker fluorescence is lost is indicative of the rate of osmotic lysis and hence the activity of cathepsin C. A representative trace from a single cell is shown (**Fig 2.3B**). Quantification of the rate of fluorescence loss showed no significant difference between the control and BCG-infected cells, either when looking at the linear regression of the initial rate of loss (**Fig 2.3C, p - 0.936**) or by looking at an exponential fit of the whole post-GPN period (**Fig 2.3D, p - 0.273**).

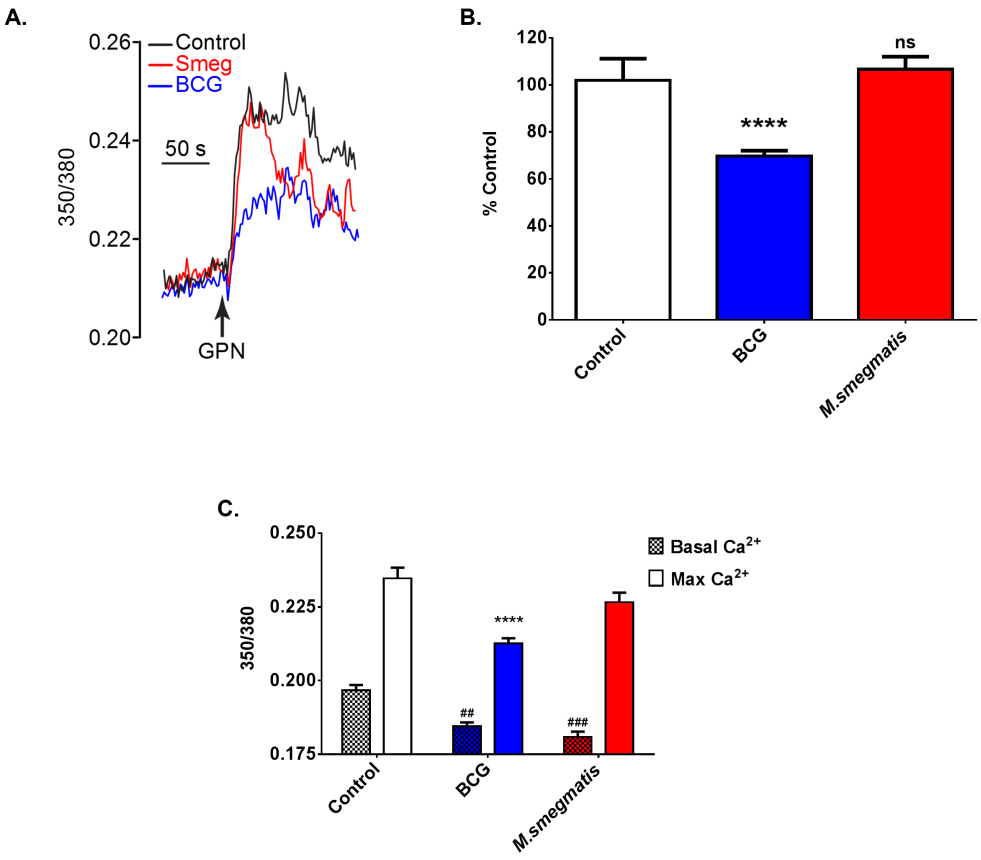

Figure 2.2: **Effect of mycobacterial infection on lysosomal Ca^{2+} levels in RAW 264.7 macrophages, as quantified by GPN-induced release of lysosomal Ca^{2+}.** 24hr infection, MOI 12.5 **A.)** Ca^{2+} responses from representative single fura-2 loaded RAW 264.7 cells upon addition of GPN (point of addition indicated by arrow). At the end of each run all cells responded to 1µM ionomycin. **B.)** Maximal Ca^{2+} responses upon addition of GPN as determined by the difference between basal and maximum fura-2 ratio (Δ350/380). Changes given as percentage difference relative to Δ350/380 in uninfected control. Mean ± SEM of n=167-311 individual cells per group. **** $p<0.001$ versus control (via 1-way ANOVA). **C.)** Basal [Ca^{2+}] (prior to addition of GPN) and maximum Ca^{2+} release upon lysosomal lysis. Mean ± SEM of n=167-311 cells per group. ****/### $p<0.001$ versus control (via 1-way ANOVA).

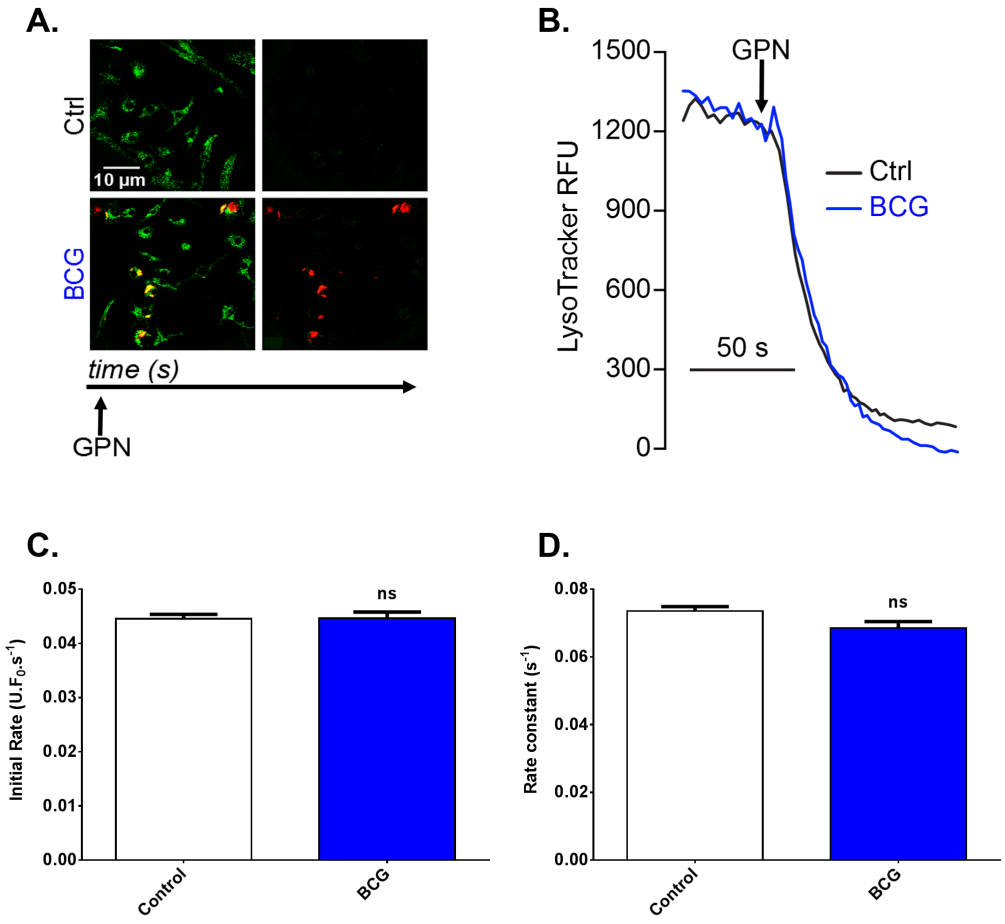

Figure 2.3: **Assessment of lysosomal cathepsin C activity in RAW 264.7 macrophages.** 24hr infection, MOI 12.5. **A.)** LysoTracker fluorescence (green) in RAW 264.7 macrophages in presence or absence of BCG infection (red). **B.)** Changes in LysoTracker fluorescence in representative single RAW 264.7 cells upon addition of 200µM GPN (point of addition indicated by arrow). **C/D.)** Rate of release of LysoTracker from lysosomes upon GPN-induced hydrolysis. Quantified by linear regression of the initial rate (**C**) or by an exponential fit of the entire post-GPN period (**D**). Mean ± SEM of n=190-227 individual cells per group. Analysis via t-test.

2.3.3 Quantification of Lysosomal Calcium via Rhod-Dextran

Direct quantification of lysosomal calcium was carried out using a calcium sensitive low-affinity Rhod- dextran in combination with a calcium-insensitive cascade-blue dextran. Both dextran molecules were loaded into the lysosome. By measuring the ratio between the fluorescence of the two probes the intralysosomal [Ca^{2+}] can be calculated. In agreement with the indirect calcium quantification performed above, macrophages infected with BCG (18hr) had significantly lower levels of lysosomal Ca^{2+} (with infected cells showing a 45% reduction relative to controls) (**Figure 2.4, p<0.0001**).

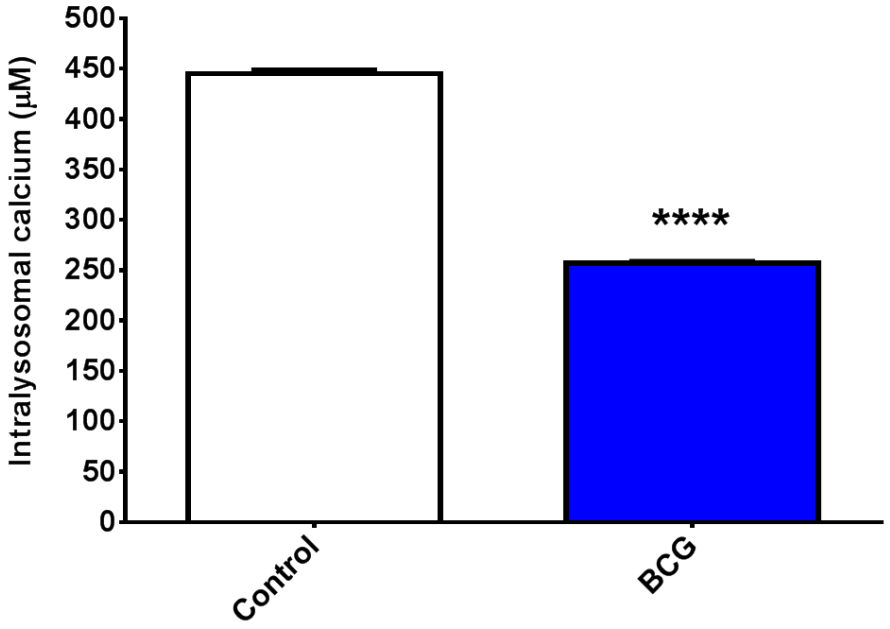

Figure 2.4: **Effect of BCG infection on lysosomal [Ca^{2+}] in RAW 264.7 macrophages, as assessed using calcium sensitive low-affinity Rhod-dextran.** 18hr infection, MOI 12.5. Mean ± SEM of n=90 individual cells/group. **** p<0.001 versus control (via t-test).

The use of Rhod-dextran to compare lysosomal Ca^{2+} levels in control and BCG infected cells requires lysosomal pH to be unaffected by mycobacterial infection. Assessment of lysosomal pH revealed no significant difference between control and BCG-infected cells (**Figure 2.5**).

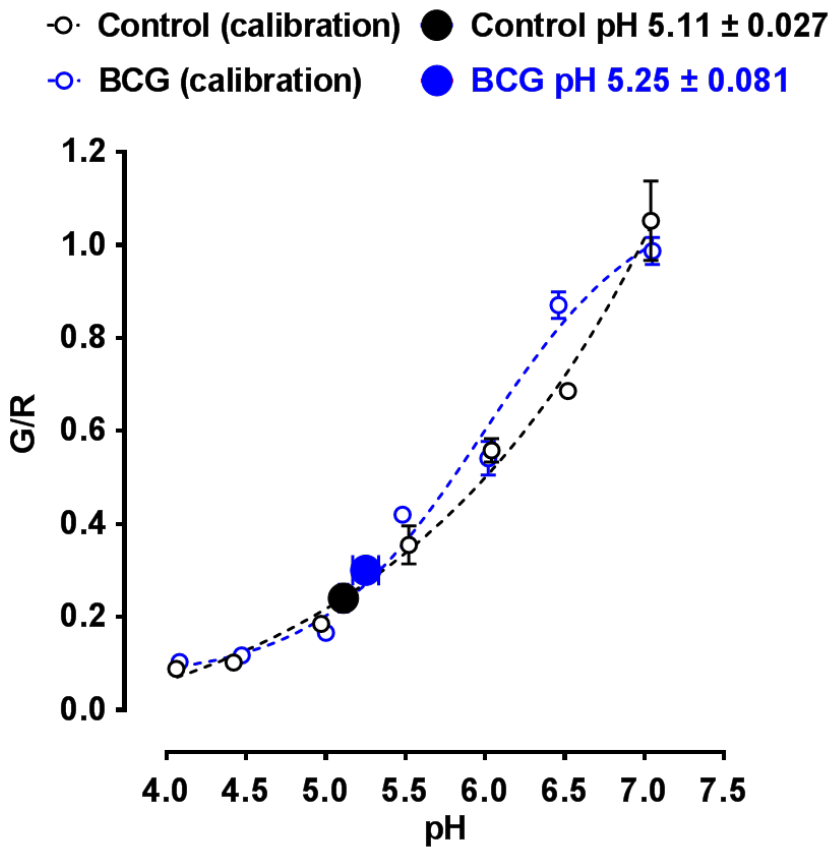

Figure 2.5: **Lysosomal pH in control and BCG-infected RAW 264.7 macrophages.** 24hr infection, MOI 12.5. Calibration curve constructed as detailed above. Endolysosomal pH of cells calculated from ratio between fluorescence of Fluorescein (G) and Texas-Red (R). Mean ± SEM of n=28-36 individual cells per group.

2.3.4 Quantification of GSL Levels via HPLC

Wild-type RAW 264.7 cells infected with BCG showed an increase in GSL levels, with this increase becoming significant (relative to uninfected controls) at 48-hours post infection (**Figure 2.6, p<0.0135**). At 48 hours infected cells showed an approximate 2-fold increase in GSL levels.

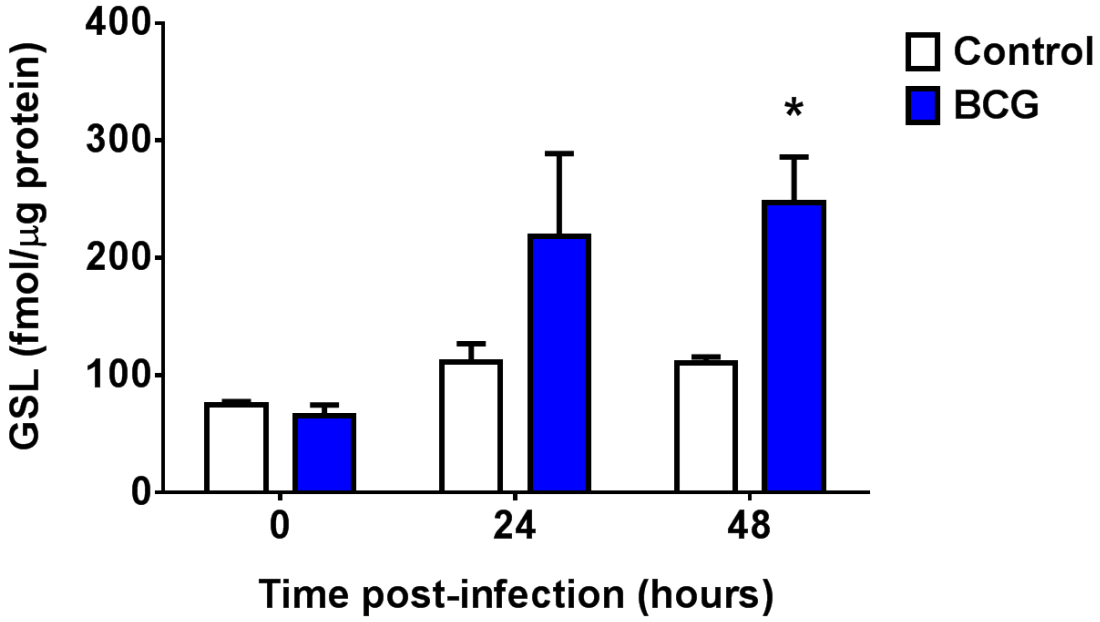

Figure 2.6: **Effect of BCG infection on glycosphingolipid levels in RAW264.7 macrophages.** MOI 12.5. Values adjusted for sample protein concentration. Mean ± SEM of 5 biological replicates. * $p<0.05$ versus control (via t-test).

2.3.5 Quantification of LacCer Levels via HPLC

RAW 264.7 cells that have undergone a longer-term infection with BCG (1 week) showed a significant increase in LacCer levels relative to uninfected controls **(Figure 2.7, p - 0.0044)**. LacCer levels in infected cells were approximately doubled.

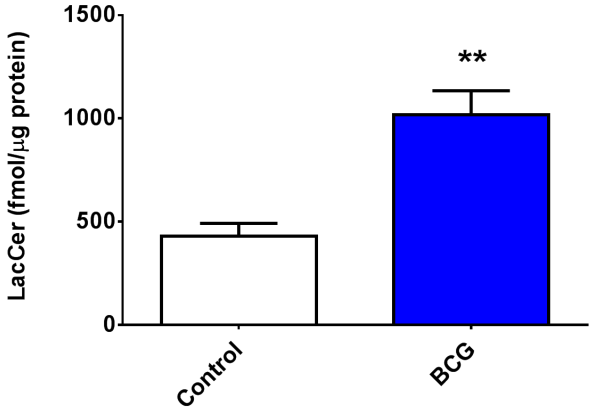

Figure 2.7: **Effect of BCG infection on lactosylceramide levels in RAW 264.7 macrophages.** 1 week infection, MOI 12.5. Values adjusted for sample protein concentration. Mean ± SEM of 4 biological replicates. * $p<0.05$ versus control (via t-test).

2.3.6 Cholesterol distribution

A 24 hour infection with BCG was associated with a redistribution of intracellular cholesterol (**Figure 2.8**). Staining with filipin (a fluorescent marker for unesterified cholesterol [4]) was brighter and more punctate in the BCG-infected cells, relative to uninfected controls, indicative of lysosomal accumulation of free cholesterol. No such accumulation was observed in cells infected with the non-pathogenic *M.smegmatis*.

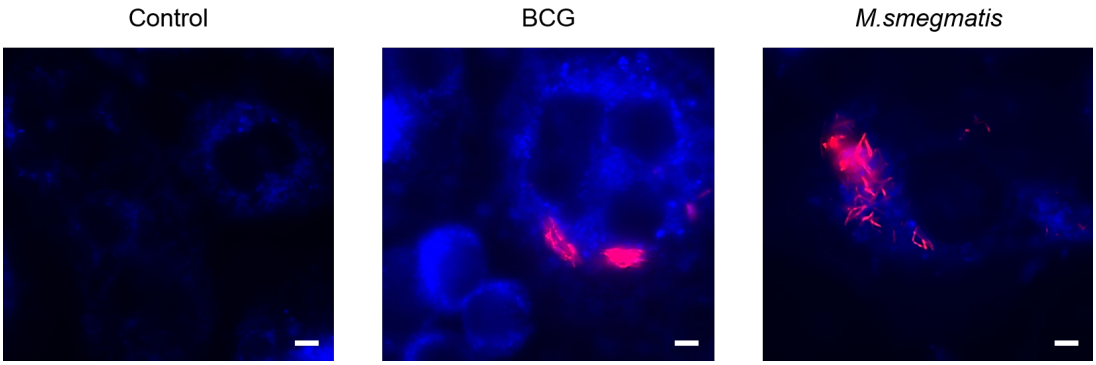

Figure 2.8: **Effect of mycobacterial infection on cholesterol distribution in RAW 264.7 macrophages.** 24hr infection, MOI 12.5. Images shown are representative. Blue - filipin (cholesterol), red - mCherry-expressing mycobacteria. Scale bar - 5μm.

2.3.7 Quantification of GSL Levels via HPLC post *Mtb* Infection

In order to verify the significance of the above effect with regards to the human pathogen we infected wild-type RAW 264.7 murine macrophages with live *Mtb* (H37rv strain). The infection was carried out under Category 3 conditions at Public Health England (Salisbury, UK). Representative HPLC traces from control and infected macrophages are shown, with major GSL species indicated (**Figure 2.9A**). 48hr post-infection, total GSL levels were significantly higher in infected cells (with levels approximately double that in uninfected controls) (**Figure 2.9B, p - 0.0237**). This increase was observed in all individual GSL species (**Figure 2.9C**), with all species exhibiting a significant or close to significant rise (**Gb3/GM3 p - 0.06; GM1a p - 0.07; GA1 p - 0.0036; GM1b 0.0242; GD1a 0.06**).

2.3.8 Quantification of LacCer Levels via HPLC post *Mtb* Infection

A 48hr infection with *Mtb* was not sufficient to induce LacCer accumulation in RAW 264.7 macrophages (**Figure 2.10, p - 0.6695**). When using BCG a longer term infection was required to induce storage, with accumulation significant after 1 week of infection (**Figure 2.7, p - 0.0044**). A longer-term infection with *Mtb* may yield similar results.

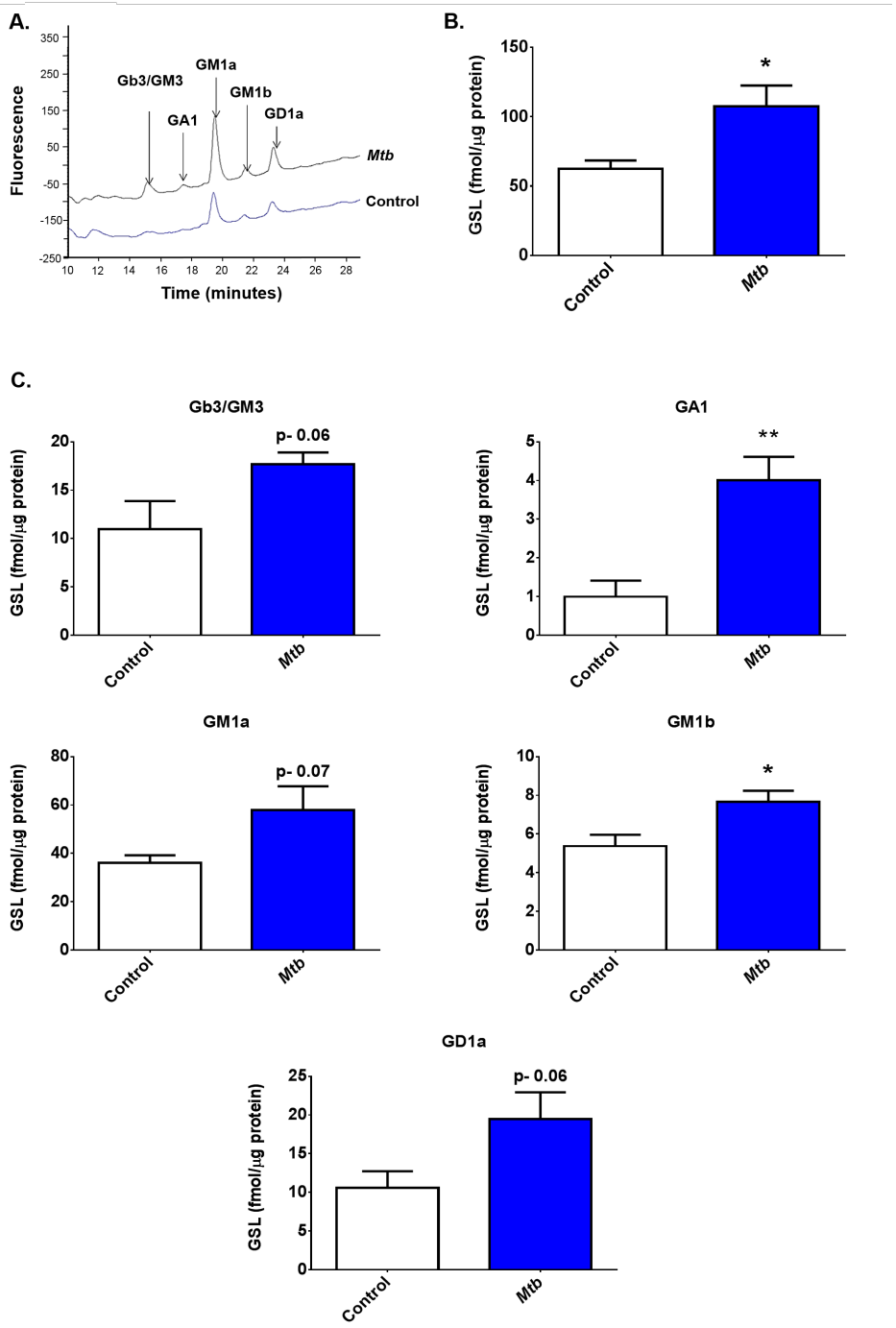

Figure 2.9: **Effect of *Mtb* infection on glycosphingolipid levels in RAW 264.7 macrophages.** 48hr infection, MOI 12.5. **A.)** Representative HPLC traces of control and *Mtb*-infected RAW 264.7 macrophages. Major GSL species are indicated. **B.)** Total GSL levels in RAW 264.7 macrophages with or without *Mtb*. Values adjusted for sample protein concentration. Mean ± SEM of 5 biological replicates. * $p<0.05$ versus control (via t-test). **C.)** Levels of individual GSL species in RAW 264.7 macrophages with or without *Mtb*. Values adjusted for sample protein concentration. Mean ± SEM of 5 biological replicates. * $p<0.05$, ** $p<0.01$ versus control (via t-test).

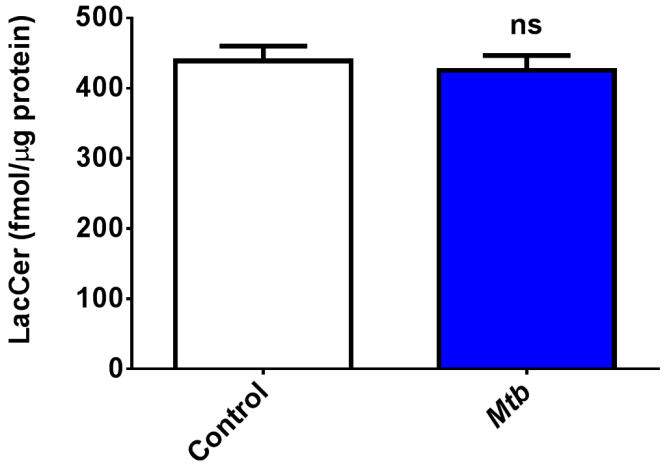

Figure 2.10: **Effect of *Mtb* infection on lactosylceramide levels in RAW 264.7 macrophages**. 48hr infection, MOI 12.5. Values adjusted for sample protein concentration. Mean ± SEM of 5 biological replicates. Analysis via t-test.

2.4 Discussion

As discussed in Section 1.2 NPC cells are defined by a combination of phenotypes, including accumulation of several classes of lipid, defects in endocytic trafficking and reduced lysosomal calcium release [20]. Here we show that infection with pathogenic mycobacteria is able to replicate several of these NPC phenotypes in wild-type cells, including accumulation of cholesterol (**Figure 2.8**), storage of GSLs (including LacCer) (**Figure 2.6/2.7**), reduced lysosomal calcium release (**Figure 2.2/2.4**) and storage of sphingosine **(Figure 2.1)**. The latter two phenotypes are unique to NPC amongst the LSDs [11]. Importantly, NPC cellular phenotypes could not be induced by the non-pathogenic mycobacteria *M.smegmatis*.

A key aspect of pathogenic mycobacteria (most notably *Mtb*) is its ability to avoid destruction and clearance and therefore persist inside host macrophages for extended periods of time [80]. They are able to persist due to their ability to subvert the process of phagosomal maturation in which the phagosome and lysosome fuse leading to the pathogen's destruction. The role that calcium plays in the process of phagosomal maturation is contentious [103] [104]. It has been reported that fusion requires a transient rise in cytosolic calcium [103]. In *Mtb*-infected cells this elevation does not occur. If calcium is required for mycobacterial clearance then the NPC pathway would be an attractive target for pathogens, with inhibition of the pathway having been demonstrated to lead to defects in intracellular calcium homeostasis [20]. In NPC cells the reduced lysosomal calcium leads to defects in endocytic trafficking due to reduced fusion [39]. We propose that NPC pathway dysfunction also leads to reduced fusion between the phagosome and the lysosome. Our work in this chapter supports previously published studies showing that phagosome:lysosome fusion is a calcium-dependent process [103].

The non-pathogenic mycobacteria *M.smegmatis* is unable to subvert the phagosomal maturation process and is hence easily cleared by host macrophages [148]. We observed here that it is also unable to induce NPC cellular phenotypes, suggesting that this is a property unique to pathogenic mycobacteria.

The majority of the work in this chapter utilised BCG, an attenuated form of *Mycobacterium bovis*. Genetically it is very similar to *Mtb*, and shares with it an ability to persist within host macrophages [139] [140]. However, some studies were also performed with *Mtb*. We found that like BCG, *Mtb* was able to induce GSL storage in murine macrophages (**Figure 2.9**). Accumulation occurred over a similar timespan when using either pathogenic mycobacteria. As in NPC, this GSL accumulation was non-species specific (**Figure 2.9C**).

An interaction between pathogenic mycobacteria and the NPC pathway (and the pathway´s subsequent inhibition) would provide a mechanistic explanation for the failure in phagosomal maturation observed in infected cells. It would also account for other phenotypes associated with *Mtb* infection, including the accumulation of cholesterol and LacCer in patient granulomas and the defects in calcium homeostasis [103] [119] [121].

Summary

Wild-type murine macrophages infected with pathogenic mycobacteria exhibit a range of NPC cellular phenotypes, including accumulation of several lipid species and a reduction in lysosomal calcium. This is consistent with a model in which pathogenic mycobacteria inhibit the NPC pathway. This phenotype induction was restricted to pathogenic mycobacteria.

3 Induction of NPC Cellular Phenotypes in Wild-Type Primary Human Macrophages Following Infection with Pathogenic Mycobacteria

3.1 Introduction

Work in Chapter 2 was carried out using a mouse macrophage cell line, and demonstrated that it was possible to induce NPC cellular phenotypes in wild-type cells via infection with pathogenic mycobacteria. Mice are the most popular animal model for the study of TB [149]. A large part of this is due to practical considerations: experiments in mice are relatively inexpensive, and researchers have access to a large number of inbred strains (with genetic standardization within a strain leading to decreased individual variation). There also exist an enormous range of immunological reagents geared towards mouse experimentation [150]. The mouse model of TB has to date been used to obtain large amounts of information regarding the immunological response to *Mtb* infection, with this

information proving applicable to humans [149]. Despite this, the mouse model of TB is regarded as imperfect, with a number of reservations stemming from the difference in the structure of the granulomas formed following infection in mice and humans.

3.1.1 Granulomas

One of the initial responses to inhalation of *Mtb*-containing aerosols is the formation of granulomas. The phagocytosing macrophages will activate a pro-inflammatory response, invade the nearby epithelium and recruit mononuclear cells (which will be recruited from nearby blood vessels) [79]. Formation of the TB granuloma is a TNF-α dependent process, with the cytokine being required for recruitment of immune cells.

The characteristic TB granulomas in human infection consist of a necrotic core surrounded by T lymphocytes and foamy macrophages (along with aggregates of B cells associated with CD3+ T cells). The granuloma is enclosed by fibroblasts, which form a fibrous barrier around the macrophage-containing centre [119]. Within the human TB granuloma there exist hypoxic microenvironments (mostly surrounding the necrotic core) [151]. It is possible to use the hypoxia marker pimonidazole hydrochloride to stain for hypoxic regions. Pimonidazole hydrochloride is activated by mammalian nitroreductases at very low oxygen concentrations, and subsequently binds to thiol groups and can be detected via antibody. The low oxygen concentration in these micro-environments is believed to be key in inducing a state of non-replicative persistence in the bacteria. Whilst in this state they are less susceptible to many TB therapies [152]. Electron microscopy data shows that they are located (in the macrophage) close to the large intracellular lipid stores, possibly using them as a nutrition source [121]. Hypoxic microenvironments have also been observed in TB granulomas in guinea

pigs, rabbits and nonhuman primates [151].

Granulomas can either effectively contain the infection (which occurs in most cases), or the granuloma core may undergo necrosis and cavitation, allowing free mycobacteria to spill out into the bloodstream [79] [153]. The path which the infection takes appears to be determined at the level of the granuloma [79].

3.1.2 Mouse Models for TB: Potential Issues

The mouse model for TB is generally regarded as problematic, with several apparent structural and histopathological differences between the granulomas formed in mice and humans. Murine TB granulomas lack the necrotic core and hypoxic microenvironments seen in humans [151] [154]. The spatial organisation of macrophages and T cells also differs between the two species [116]. It is worth noting however, that the work leading to the above conclusions was carried out in only two inbred mouse strains : C57BL/6 and BALB/c [150]. In humans and mice there is a great deal of evidence that genetics affect susceptibility to TB infection [155]. It has been observed that TB granulomas in the C3HeB/FeJ mouse strain show the presence of hypoxic lesions [156].

We therefore wished to investigate whether the NPC cellular phenotypes induced as a result of BCG infection in RAW 264.7 murine macrophages are also induced in human macrophages. Primary human macrophages were obtained from the differentiation of monocytes purified from human blood. Due to the effect of genetic variation on susceptibility to *Mtb* infection these investigations were carried out using cells derived from a number of independent healthy donors. The specific aims of the work presented in this chapter were:

* Investigate whether NPC phenotypes are induced in primary human macrophages in response to infection with BCG.

* To study whether this phenotype induction is unique to pathogenic mycobacteria, and does not occur post-infection with non-pathogenic *M.smegmatis*.

3.2 Materials and Methods

3.2.1 Mycobacterial Culture

Production, culture and long-term storage of mCherry-expressing mycobacteria was as detailed in Sections 2.2.1, 2.2.2, 2.2.3 and 2.2.4.

3.2.2 Isolation of Monocytes From Human Blood

A leukocyte cone was flushed through with RPMI and the elutant was slowly layered over lymphoprep to filter cells by density, before centrifugation (2000rpm/ 30minutes/ acceleration 5/ deceleration 1). The leukocyte (middle) layer was collected and topped up to 50ml with RPMI. The mixture was centrifuged (1200rpm/15min), resuspended in 50ml RPMI, centrifuged (1200rpm/10min) and the pellet resuspended in 2ml MACS buffer (10% FCS, 2mM EDTA in PBS) (Miltenyi Biosciences). CD14 beads (200 µl) were added and gently mixed prior to 15 minutes at 4°C. The cell mixture was topped up to 50ml with MACS buffer and centrifuged (1500rpm/5min). The supernatant was decanted and the pellet resuspended in 3ml MACS buffer. A LS column (Miltenyi Biosciences) was affixed to a MACS magnet and prewashed with 3ml MACS buffer. The cell suspension was added to the column and the column washed twice with MACS buffer before removal of the column from the magnet and elution of the positive fraction with 5ml MACS buffer. The column elutant was topped up to 50ml with RPMI and cells counted before centrifugation (1500rpm/5min) and resuspension at 0.5-1x10^6 cells/ml in X-vivo media (supplemented with 2% human serum, 1% P/S, 1% glutamine, 500U/ml IL-4 amd 800U/ml granulocyte macrophage colony-stimulating factor (GM-CSF) (Peprotech)). Immature dendritic cells were visible after around 4 days.

3.2.3 Differentiation of Monocytes into Macrophages

Monocytes were cultured in X-vivo media (Lonza) containing 10% FCS and 100ng/ml macrophage colony-stimulating factor (M-CSF) (Peprotech). The differentiation of monocytes to macrophages was established after 6 days. The macrophages were maintained in X-vivo with 10% FCS and 50ng/ml M-CSF prior to use.

3.2.4 Infection of Host Cells

As detailed in Section 2.2.5

3.2.5 Determination of Sample Protein Levels

As detailed in Section 2.2.6

3.2.6 Quantification of GSL and Sphingosine Levels via HPLC

As detailed in Sections 2.2.17, 2.2.18, 2.2.7 and 2.2.8.

3.2.7 Lysosomal Calcium Quantification

As detailed in Section 2.2.9.

3.2.8 Fixation of Cells

As detailed in Section 2.2.14

3.2.9 Microscopy

As detailed in Sections 2.2.13 and 2.2.15.

3.2.10 Localisation of Cellular Cholesterol via Filipin Staining

As detailed in Section 2.2.16.

3.2.11 Distribution and Intracellular Transport of GM1 Ganglioside

Fluorescently labelled Cholera Toxin B subunit 596 (CtxB) (Invitrogen) specifically binds GM1 ganglioside [157]. Coverslips containing live cells were washed twice with cold RPMI (to prevent internalization) prior to addition of 2µg/ml CtxB in RPMI for 30min at room temperature (enabling toxin/PM GM1 interaction). Coverslips were then incubated in RPMI for 2hr at 37°C/5% CO_2 (to internalize the toxin). Post-incubation coverslips were washed with 3x1ml 1% bovine serum albumin (BSA) (Sigma-Aldrich) in RPMI to remove non-internalized toxin (10 minutes/wash).

3.2.12 Nuclear Staining

Nuclei were stained via 5 minutes incubation with 0.33µg/ml Hoechst nuclear stain (Life Technologies) (in PBS) at room temperature. Coverslips were washed with 5x1ml PBS prior to mounting.

3.2.13 LysoTracker Staining

Live cells grown on coverslips were washed thrice with 1ml Hank's Balanced Salt Solution (HBSS) (Sigma-Aldrich) prior to addition of 200nM LysoTracker Green solution (diluted in HBSS). Coverslips were incubated at 37°C/5% CO_2 for 30 minutes prior to washing with 3x1ml HBSS and PFA fixation.

3.2.14 Trafficking of BODIPY-LacCer

Live cells grown on coverslips were washed with fresh media prior to addition of 100µl 5 µM BODIPY-LacCer (Life Technologies) for 45 minutes at room temperature. The coverslips were washed with 3x200µl cold media supplemented with 10% FCS and 1% BSA. This was followed by a 1hr chase in 1ml fresh media (37°C/5% CO_2). Post-chase period coverslips were washed with 3x1ml supplemented media prior to fixation and visualisation.

3.2.15 Electron Microscopy of Human Macrophages

Preparation of samples for electron microscopy, and subsequent visualization, was carried out by Patricia Tynan.

Cells were infected with BCG/*M.smegmatis* or treated with U18666A at 2µg/ml for 48 hrs prior to harvesting. Pelleted human macrophages in 1.5 ml PBS were slowly mixed with 2.5% glutaraldehyde (GA) to achieve a final concentration of 0.1%. The pellet was fixed for 30 minutes on ice. The fixative was withdrawn, pellets washed twice with cacodylate buffer on ice and the pellet fixed in a solution of 2% PFA, 2.5% GA in 0.1M cacodylate buffer on ice for 15 minutes, and at RT for 2hrs. Pellets were washed thrice with 0.1M cacodylate, then treated with a solution of 0.1M glycine for 45 minutes to remove any free aldehyde groups before post fixation in 1% osmium tetroxide for 2hrs, washing with cacodylate then maleate buffer, and further post fixation and staining with 1% uranyl acetate in maleate buffer for 1hr in the dark, washes in maleate buffer and dehydration through an ascending series of ice-cold ethanol up to 100% ethanol, then three changes at room temperature in dry ethanol, three changes of propylene oxide, and infiltration with 1:1 araldite:propylene oxide for 1.5hrs. Propylene oxide was blown off in the hood and pieces of the pellet transferred to the tops of resin filled capsules. These were allowed to sink overnight before capsules were transferred

to a 60°C oven for 3 days prior to sectioning.

For Kupffer cell analysis, *Npc1*$^{-/-}$ mice were PBS perfused for 10 minutes, followed by perfusion with a mixture containing 4% PFA, 15% picric acid, and 0.5% GA in 0.1M cacodylate buffer for 20 minutes. The liver was removed, sectioned, and fixed in a solution of 2% PFA, 2.5% GA, 2mM calcium chloride and 0.1% picric acid in 0.1M cacodylate buffer on ice for 2hrs, before overnight fixation in cold room. Samples were then fixed at room temperature for 6 hours, returned to the cold room overnight, washed with cacodylate buffer and transferred to antifreeze and allowed to sink overnight. Samples were cut into 1-2mm cubes in 0.1M cacodylate buffer with 2mM calcium chloride, washed thrice, and post-fixed for 90 minutes in 1% osmium tetroxide buffer. From this point the protocol used was as above.

3.2.16 Mass Spectrometry

Mass spectrometry and subsequent data analysis was performed by the laboratory of Dr. Dan Ory (University of Washington, St Louis, USA).

Cells were infected with mycobacteria for 48hr prior to harvesting. The samples were homogenized using a Bead Ruptor Homogenizer (OMNI) and a protein precipitation method was used to extract lipids from homogenized cell samples in the presence of deuterium labelled internal standards/C17 (MC 18:0-d35 30ng, DC 16:0-d3 100ng, GM1 18:0 d3 100ng, GM3 d3 100ng, Ceramide C17:0 30ng, Sphingomyelin C17 30ng, Sphingosine C17 3ng, S1P C17 3ng and Cholesterol D7 2µg). Sample analysis was performed with a Shimadzu HPLC system, Leap-PAL autosampler coupled to a triple quadrupole mass spectrometer (API 4000) operated in MRM mode under ESI (+/-).

Data processing was conducted with Analyst software (Applied Biosystems). Data are presented as peak area ratio of analyte to internal standard.

3.2.17 Statistical Analysis

Statistical analysis was performed using GraphPad Prism (ver 6.0). The specific test used is indicated in the figure legend.

3.3 Results

3.3.1 Quantification of Sphingosine Levels via HPLC

Infection of wild-type primary human macrophages with the pathogenic mycobacteria BCG was associated with a significant increase in sphingosine levels 48 hours post-infection, as quantified via RP-HPLC **(Figure 3.1, p - 0.036)**. No such increase was observed in macrophages infected with non-pathogenic *M.smegmatis* (**p - 0.9803**). Sphingosine levels in BCG-infected macrophages were around 2-fold higher than in uninfected controls, a similar fold increase to that observed following infection of RAW 264.7 murine macrophages (**Figure 2.1**).

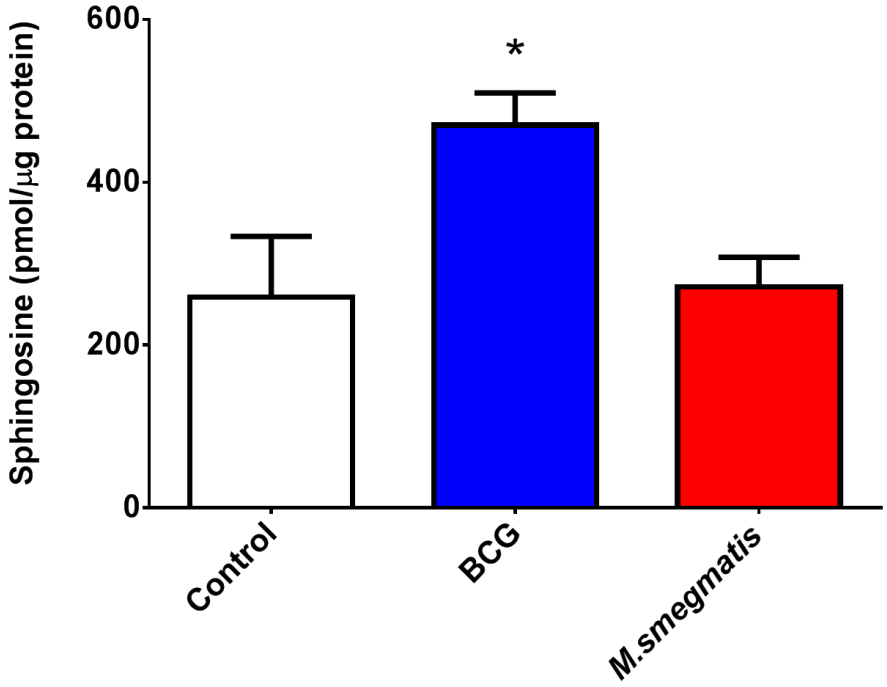

Figure 3.1: **Effect of mycobacterial infection on sphingosine levels in primary human macrophages.** 48hr infection, MOI 12.5. Macrophages obtained by differentiation of monocytes isolated from blood of donor number 4. Values adjusted for sample protein concentration. Mean ± SEM of 4 biological replicates per condition. * $p<0.05$ versus control (via 1 way ANOVA).

3.3.2 Lysosomal Calcium Quantification

Quantification of lysosomal [Ca^{2+}] was performed using GPN. Representative Ca^{2+} traces and a summary of maximum Ca^{2+} changes are shown (**Figure 3.2A/B** respectively). Size of reponse is given as percentage change relative to uninfected controls. BCG-infected macrophages showed a significant reduction in GPN-induced Ca^{2+} release, with responses approximately 40% of that seen in control cells (**Figure 3.2B, $p<0.001$**). No change was observed in cells infected with *M.smegmatis*. There were no significant differences in the level of basal Ca^{2+} (levels prior to addition of GPN) between control and infected macrophages (**Figure 3.2C**).

3.3.3 Cholesterol Distribution

Primary human macrophages infected with BCG showed increased staining with filipin, indicative of the lysosomal accumulation of free cholesterol (**Figure 3.3**). These experiments were replicated in primary human macrophages obtained by differentation of monocytes isolated from the blood of 6 independent healthy donors. All donor cells exhibited cholesterol accumulation post-24hr BCG infection. No such accumulation was observed in cells infected with the non-pathogenic *M.smegmatis*.

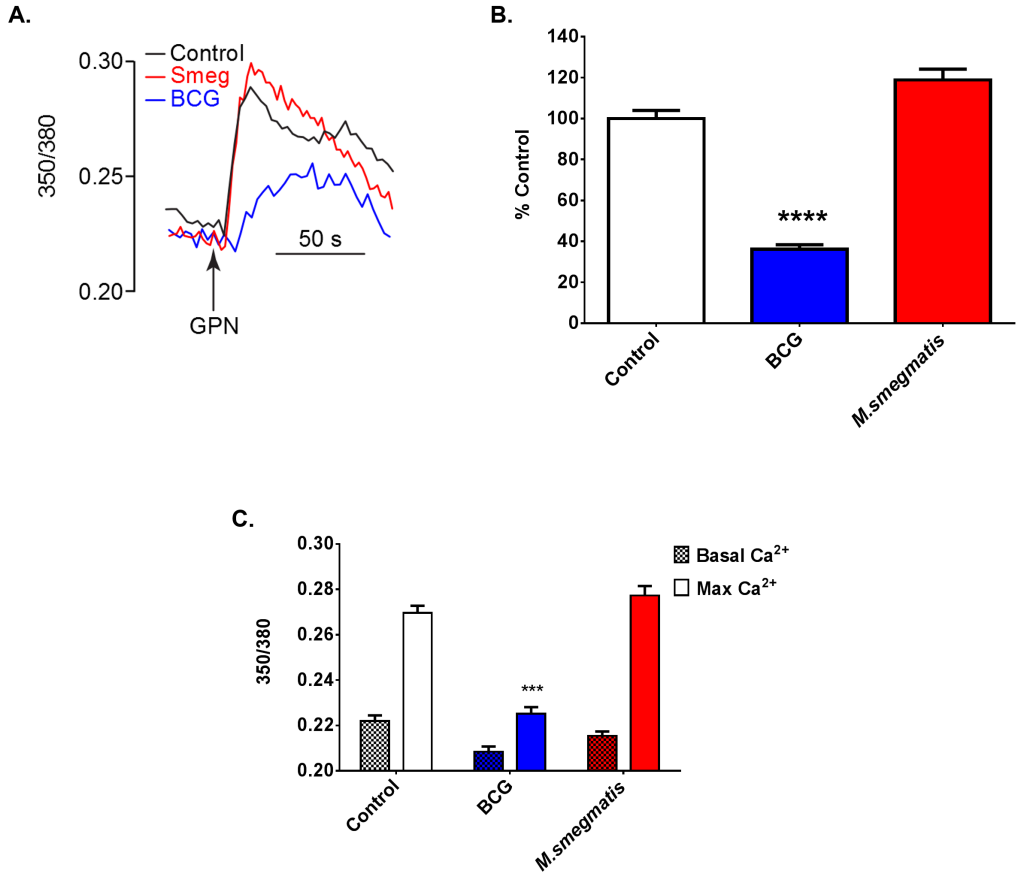

Figure 3.2: **Effect of mycobacterial infection on lysosomal Ca^{2+} levels in primary human macrophages, as quantified by GPN-induced release of lysosomal Ca^{2+}.** 24hr infection, MOI 12.5. Macrophages obtained by differentiation of monocytes isolated from blood of donor number 1. **A.)** Ca^{2+} responses from representative single fura-2 loaded primary human macrophages upon addition of GPN (point of addition indicated by arrow). At the end of each run all cells responded to 1 µM ionomycin. **B.)** Maximal Ca^{2+} responses upon addition of GPN as determined by the difference between basal and maximum fura-2 ratio (Δ350/380). Changes given as percentage difference relative to Δ350/380 in uninfected control. Mean ± SEM of n=71-173 individual cells per experimental group. **** $p<0.0001$ versus control (via 1-way ANOVA). **C.)** Basal Ca^{2+} (prior to addition of GPN) and maximum Ca^{2+} release upon lysosomal lysis. Mean ± SEM of n=71-173 individual cells per group. **** $p<0.0001$ versus control (via 1-way ANOVA).

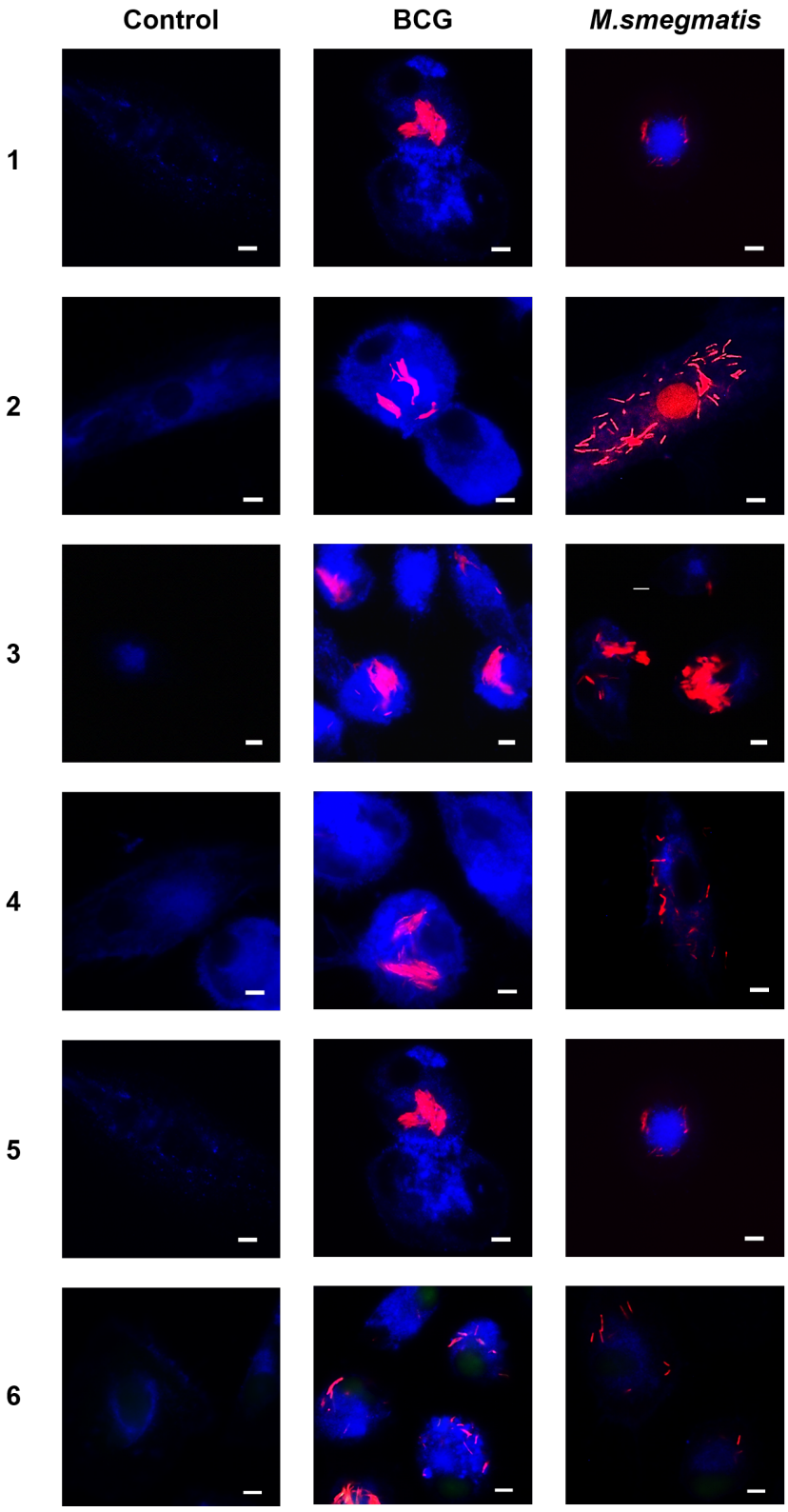

Figure 3.3: **Effect of mycobacterial infection on cholesterol distribution in primary human macrophages.** 24hr infection, MOI 12.5. Images shown are representative. Macrophages obtained by differentiation of monocytes isolated from the blood of 6 independent healthy donors. Blue - filipin (cholesterol), red - mCherry-expressing mycobacteria. Scale bar - 5µm.

3.3.4 LysoTracker Microscopy

LysoTracker is a fluorescent dye which accumulates in acidic organelles such as the lysosome. An increase in LysoTracker staining (observed in NPC) is indicative of expansion of the lysosomal compartment [147]. An increase in LysoTracker staining was observed in human macrophages infected with BCG (but not in those infected with *M.smegmatis*) (**Figure 3.4**).

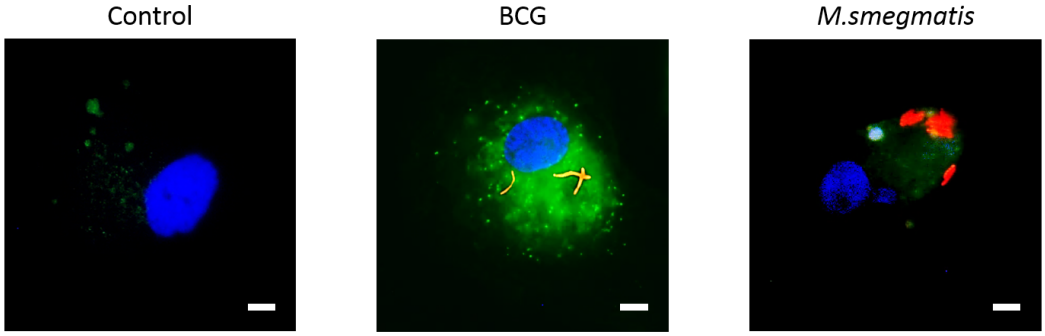

Figure 3.4: **Effect of mycobacterial infection on LysoTracker staining in human primary macrophages.** 24hr infection, MOI 12.5. Images shown are representative. Macrophages obtained by differentiation of monocytes isolated from blood of donor number 3. Green - LysoTracker (lysosomes) , red - mCherry-expressing mycobacteria, blue - Hoescht (nucleus). Scale bar - 5µm.

3.3.5 Trafficking of GM1 Ganglioside

Primary human macrophages infected with BCG exhibited altered trafficking of GM1 ganglioside (**Figure 3.5**). BCG-infected cells have lost the Golgi localization seen in wild-type cells. GM1 instead shows a punctate, lysosomal storage pattern. These experiments were replicated in primary human macrophages obtained by differentation of monocytes isolated from the blood of 6 independent healthy donors. All donor cells exhibited mislocalisation of GM1 ganglioside post-BCG infection. Localisation of GM1 ganglioside was not affected by infection with *M.smegmatis*.

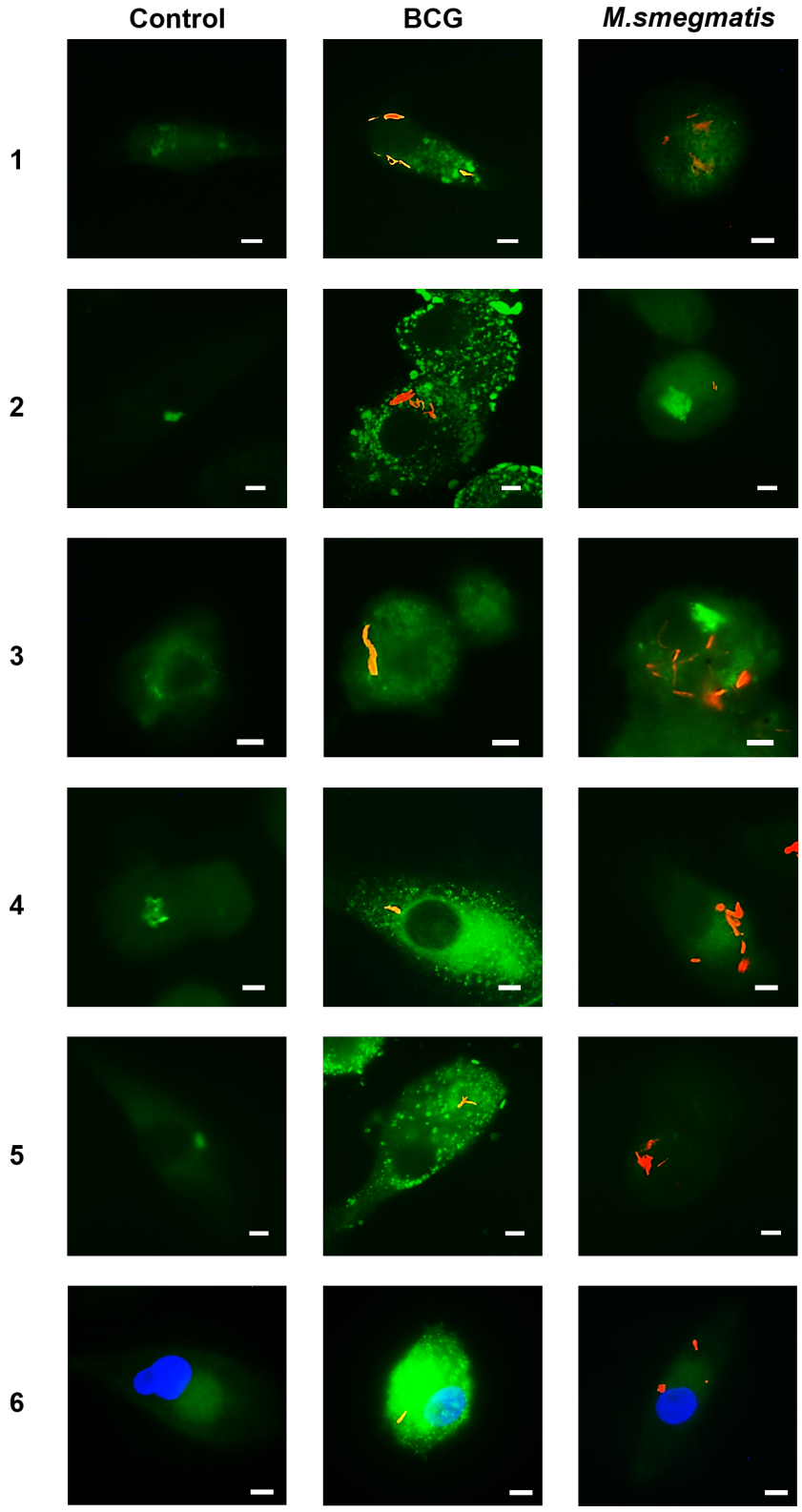

Figure 3.5: **Effect of mycobacterial infection on GM1 ganglioside trafficking in primary human macrophages.** 24hr infection, MOI 12.5. Images shown are representative. Macrophages obtained by differentiation of monocytes isolated from the blood of 6 independent healthy donors. Green - CtxB (GM1 ganglioside), red - mCherry-expressing mycobacteria. Scale bar - 5µm.

3.3.6 Trafficking of BODIPY-LacCer

Endocytic trafficking can also be investigated using LacCer fluorescently labelled with boron-dipyrromethene (BODIPY). Cells infected with BCG showed mislocalization of BODIPY-LacCer indicative of lysosomal storage (**Figure 3.6**). This mislocalisation did not occur in cells infected with *M.smegmatis*.

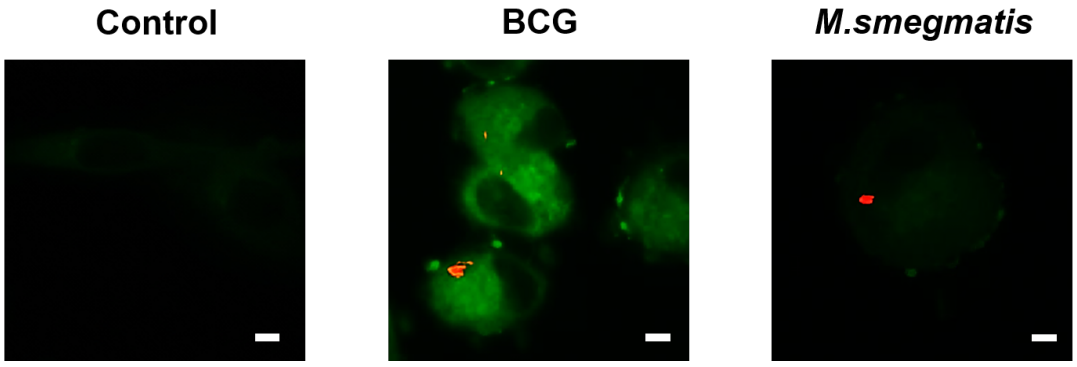

Figure 3.6: **Effect of mycobacterial infection on BODIPY-LacCer trafficking in primary human macrophages.** 24hr infection, MOI 12.5. Images shown are representative. Macrophages obtained by differentiation of monocytes isolated from blood of donor number 1. Green - BODIPY-LacCer, red - mCherry-expressing mycobacteria. Scale bar - 5µm.

3.3.7 Electron Microscopy of Infected Human Macrophages

Electron microscopy was carried out on primary macrophages infected with BCG and *M.smegmatis*, and also on cells treated with U18666A. U18666A is able to pharmacologically induce NPC phenotypes in wild-type cells [20]. Cells infected with BCG or treated with U18666A showed the presence of storage bodies similar to those found in NPC cells (indicated by white arrow) (**Figure 3.7**). A Kupffer cell from a *Npc1*$^{-/-}$ mouse liver is provided for reference. No such storage bodies were observed in cells infected with *M.smegmatis*.

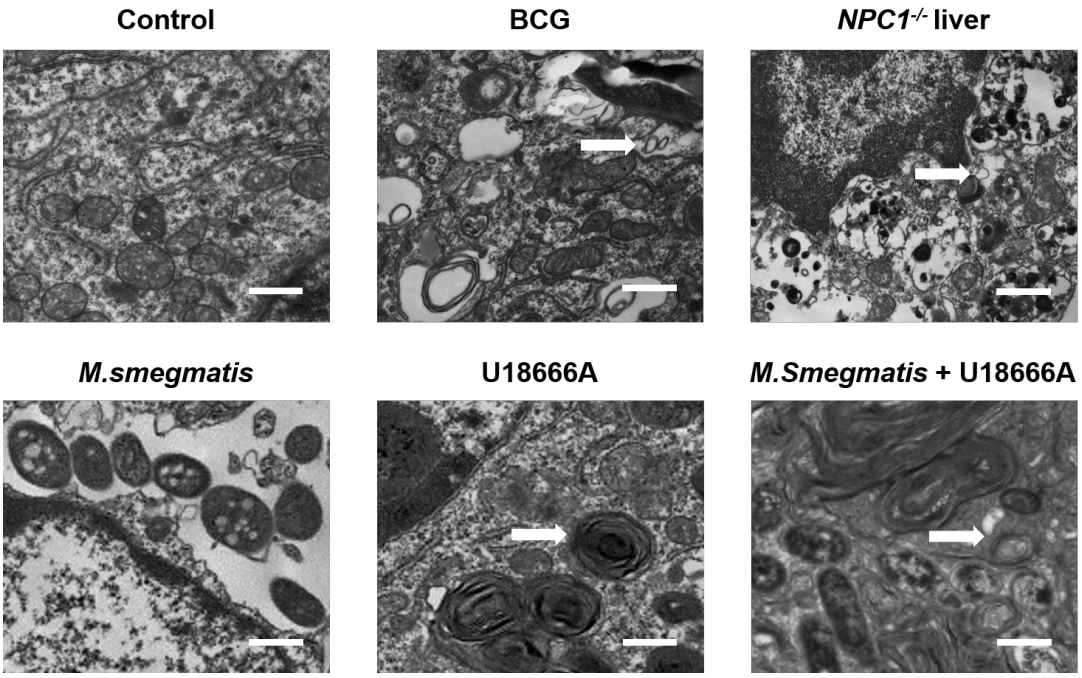

Figure 3.7: **Electron microscopy of primary human macrophages.** Macrophages obtained by differentiation of monocytes isolated from blood of donor number 3. Where indicated, cells were infected with mycobacteria (MOI 12.5) and/or treated with 2µg/ml U18666A. Treatments and infections were for 48 hours. A *Npc1*$^{-/-}$ liver Kupffer cell is provided for reference. Storage bodies are indicated by the white arrow. Scale bar - 500nm

3.3.8 Quantification of GSL Levels via HPLC

A comparison of representative GSL HPLC profiles from RAW 264.7 and primary human macrophages showed that there are fewer major GSL species in the human cells (**Figure 3.8**). The GSL profile from human macrophages was dominated by LacCer. Human macrophages infected with BCG showed a significant increase in GSL levels, with this approximately two-fold increase principally due to increases in the level of LacCer (**Figure 3.9, p - 0.0019**). No such increase was observed following infection with *M.smegmatis* (**p - 0.5552**).

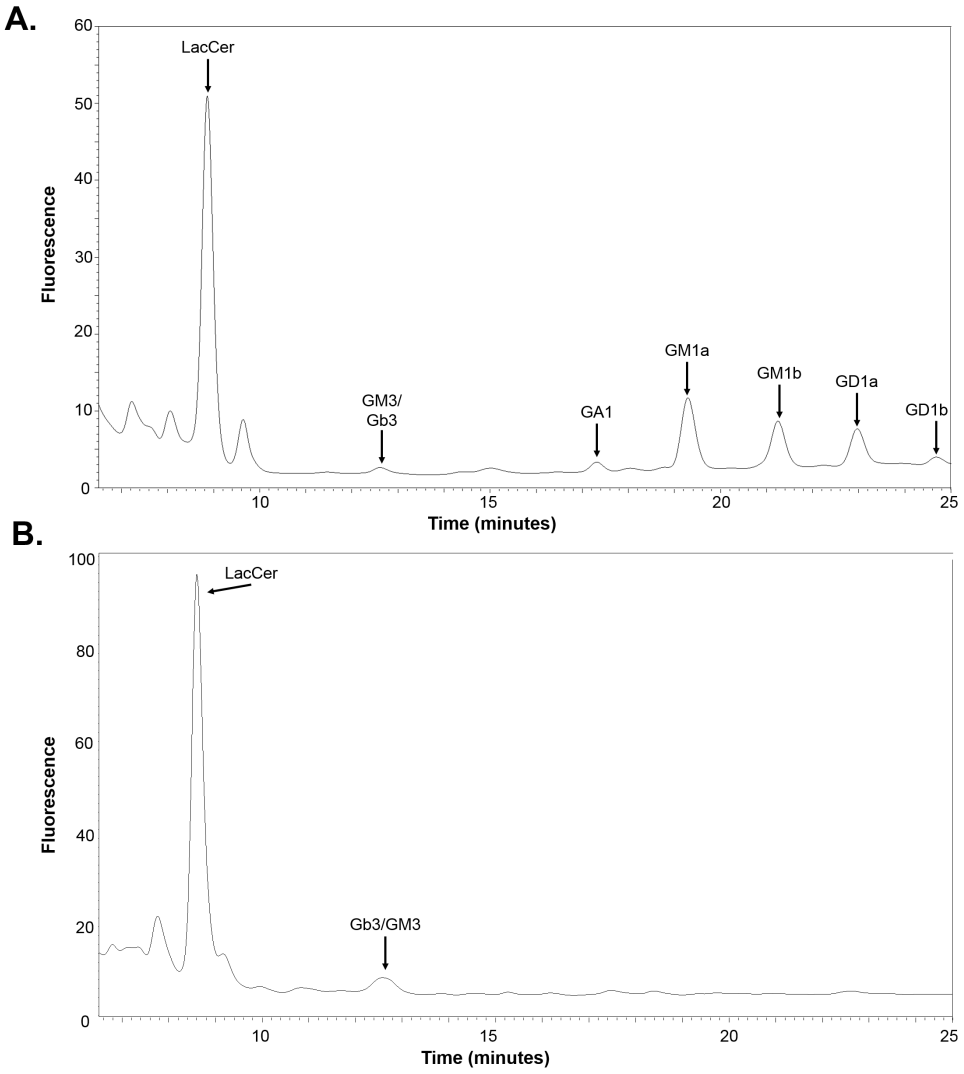

Figure 3.8: **Representative GSL HPLC traces from uninfected RAW 264.7 (A) and primary human macrophages (B).** Primary human macrophages obtained by differentiation of monocytes isolated from blood of donor number 3. Major GSL species are indicated.

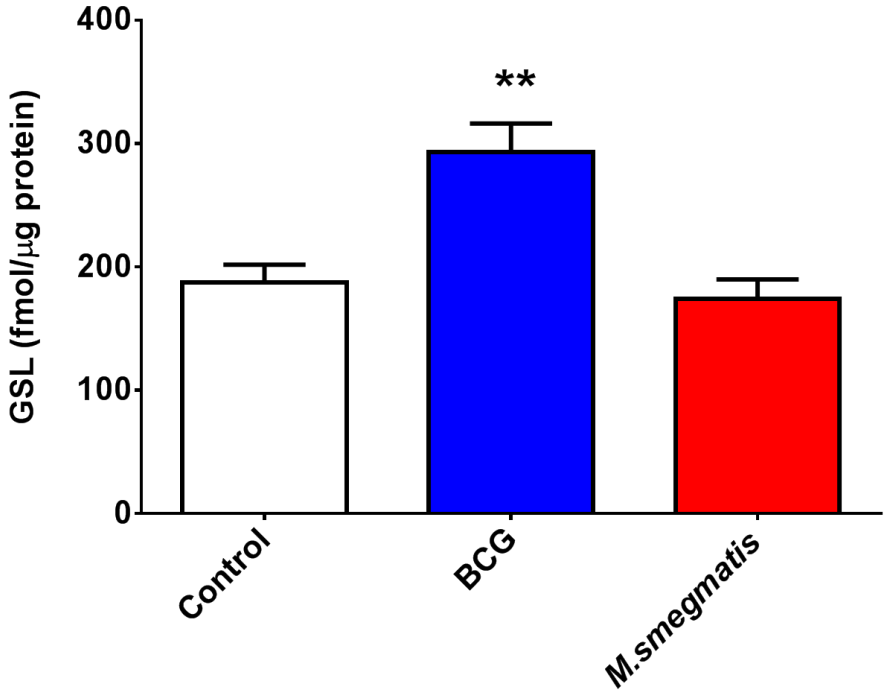

Figure 3.9: **Effect of BCG infection on glycosphingolipid levels in primary human macrophages.** 48hr infection, MOI 12.5. Primary human macrophages obtained by differentiation of monocytes isolated from blood of donor number 3. Values adjusted for sample protein concentration. Mean ± SEM of 4 biological replicates. ** $p<0.01$ versus control (via 1-way ANOVA).

3.3.9 Quantification of Lipids via Mass Spectrometry

We attempted to quantify lipid levels in control and BCG-infected primary human macrophages using mass spectrometry. This analysis revealed no significant increases in lipids in the infected cells. Selected data from this analysis (for cholesterol and sphingosine) is shown (**Figure 3.10**). These findings contradict both the observed increase in sphingosine in BCG-infected cells **(Figure 3.1)** and the fact that cholesterol accumulation is a well-characterized consequence of infection with pathogenic mycobacteria [121].

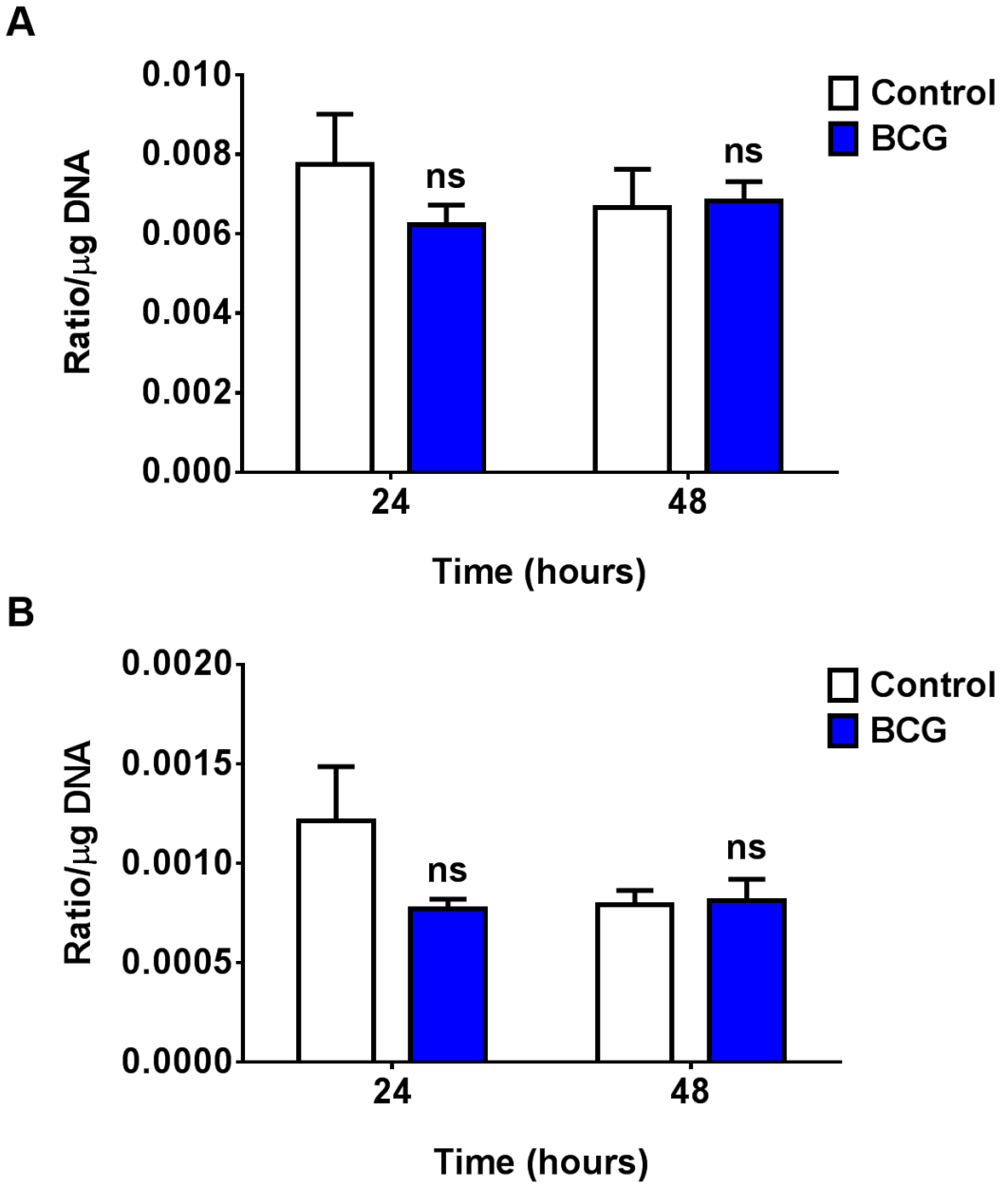

Figure 3.10: **Effect of BCG infection on lipid levels in primary human macrophages as quantified via mass spectrometry.** MOI 12.5. Macrophages obtained by differentiation of monocytes isolated from blood of donor number 5. Mean ± SEM of 4 biological replicates. Values given as ratio of peak area of analyte to internal standard. **A.)** Cholesterol. **B.)** Sphingosine. Statistical analysis via t-test.

3.4 Discussion

Work in this chapter was carried out using macrophages differentiated from $CD14^+$ monocytes isolated from the blood of 6 independent healthy donors. Due to limitations in cell number (with each donor giving approximately $1x10^8$ cells) not all assays could be carried out on cells from all donors. Those assays that required fewer cells, specifically staining with filipin or CtxB, were carried out on primary cells from all donors. Assays which required more cells required us to be more selective and were only carried out on cells from selected donors. A summary table showing all assays, and the donor cells in which they were performed, is shown below:

Phenotype	Donor Number					
	1	**2**	**3**	**4**	**5**	**6**
Cholesterol storage	*	*	*	*	*	*
GM1 mistrafficking	*	*	*	*	*	*
Sphingosine storage				*		
GSL storage			*			
Reduced LE/Lys Ca^{2+}	*					
BODIPY-LacCer mistrafficking	*					
Storage body formation via EM			*			
Increased LysoTracker staining			*			

Infection with the pathogenic mycobacteria BCG (but not the non-pathogenic *M.smegmatis*) was associated with the induction of several NPC cellular phenotypes in primary human macrophages. These included accumulation of sphingosine, cholesterol and GSLs **(Figure 3.1/3.3/3.9)**, a reduction in lysosomal calcium levels (**Figure 3.2**), and defects in intracellular trafficking (**Figure 3.5/3.6**).

These phenotypes were also observed in RAW 264.7 murine macrophages infected with pathogenic mycobacteria. Additionally, we also demonstrated the formation of storage bodies in BCG-infected cells similar to those seen in NPC (**Figure 3.7**), and observed increased LysoTracker staining indicative of lysosomal expansion (**Figure 3.4**). These results serve to replicate our observations from Chapter 2, and support a model in which infection with pathogenic mycobacteria leads to induction of NPC cellular phenotypes in wild-type macrophages (from both mice and humans).

One surprising observation in this chapter was that measurement of lipid levels via mass spectrometry showed no difference in the levels of sphingosine and cholesterol between uninfected control cells and those infected with BCG **(Figure 3.10)**. This conflicted with earlier observations which showed a clear accumulation of both lipids following infection with pathogenic mycobacteria **(Figure 3.1/3.3)**. It is also surprising because the accumulation of cholesterol is a well-characterised consequence of infection with pathogenic mycobacteria [121]. The lack of observable increases in lipid levels could be due to issues with the sensitivity of mass spectrometry. Due to the limited number of cells obtained from the blood of each donor it was necessary to be fairly parsimonious with the number of cells used for each assay. The levels of lipid reported by mass spectrometry were close to the baseline for detection (Dan Ory, personal communication). It is feasible that a lack of sensitivity prevented the detection of a change in lipid levels. It would be beneficial to repeat this assay with a greater cell number.

Summary

Primary human macrophages obtained from the blood of several healthy donors and subsequently infected with pathogenic mycobacteria exhibited a range of

NPC cellular phenotypes, including accumulation of several lipid species and a reduction in lysosomal calcium. This was in agreement with our previous experiments using murine macrophages. Together with work performed in Chapter 2 these experiments support a mechanistic link between the host NPC pathway and infection with pathogenic mycobacteria.

4 Induction of NPC Cellular Phenotypes by Lipids from the Cell Wall of Pathogenic Mycobacteria

4.1 Introduction

In Chapters 2 and 3 we demonstrated that NPC cellular phenotypes are induced in wild-type murine and human macrophages following infection with pathogenic mycobacteria. This supports a model in which pathogenic mycobacteria achieve cellular persistence by inhibiting the NPC pathway and consequently preventing phagosome:lysosome fusion. This would require the mycobacteria residing within the phagosome to have the ability to interact with the NPC pathway (in the late endosome/lysosome). It has been previously demonstrated that components of the mycobacterial cell wall are exported from the phagosome, and are subsequently found in the endocytic systems of both the host cell and that of neighbouring uninfected cells [79] [158]. In chapter 2 we observed that cells infected with pathogenic mycobacteria exhibited accumulation of free cholesterol (**Section 2.3.6**). However, this increased cholesterol was not restricted to those

cells that harboured pathogenic mycobacteria. Neighbouring uninfected cells showed comparable levels of cholesterol storage (**Figure 4.1**). This bystander effect could be accounted for by mycobacterial cell wall components being released from the cell wall and exported from the infected host cells, entering neighbouring uninfected cells and inhibiting their NPC pathway.

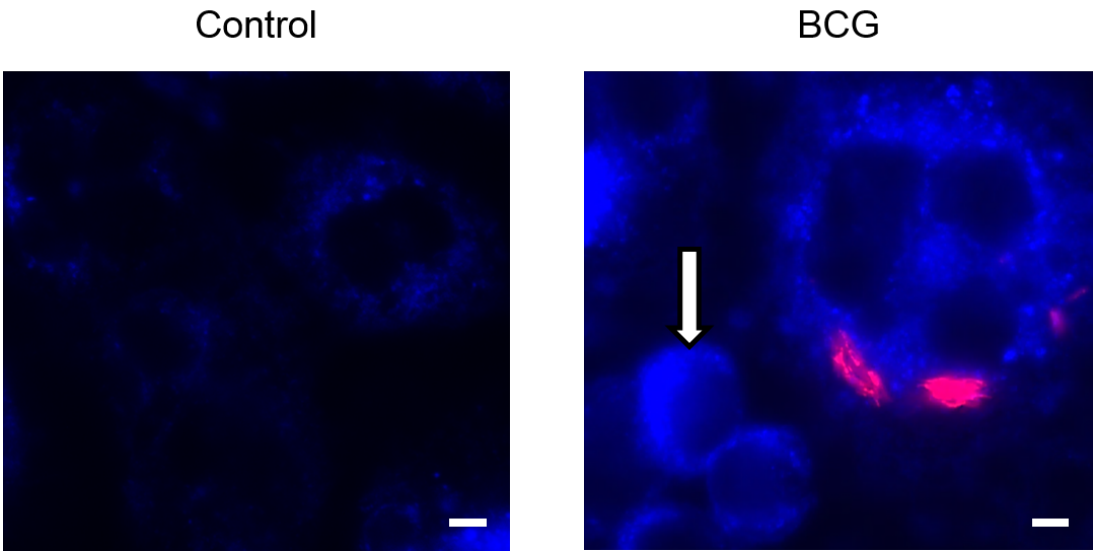

Figure 4.1: **Free cholesterol accumulates both in cells infected with BCG and their non-infected neighbours.** 24hr infection, MOI 12.5. Images shown are representative. Non-infected cells with accumulation of cholesterol are indicated by the arrow. Blue - filipin (cholesterol), red - mCherry-expressing mycobacteria. Scale bar - 5µm.

4.1.1 The Mycobacterial Cell Wall

One noteworthy morphological feature of *Mycobacteria* are their complex and lipid-rich cell walls. Around 60% of the dry weight of the cell wall is estimated to be due to lipids [94]. The structure of the cell wall can be divided into two sections. The inner section is referred to as the mycolylarabinogalactan-peptidoglycan (mAGP) core (**Figure 4.2**) [159]. The innermost part of this core is made up of peptidoglycan (PG) attached to the cell membrane [93]. PG is made up of glycan strands and peptides. In *Mtb* these glycan strands

consist of *N*-acetylglucosamine linked to muramic acid N-acylated to glycolic acid [96] [159]. PG is linked, via a phosphodiester bond, to arabinogalactan, a polysaccharide made up of arabinan and galactan [160] [161]. Arabinogalactan is in turn attached to a layer consisting of mycolic acids, a group of long chain β-hydroxy fatty acids (see Section 4.1.2 below) [162].

There are also a number of types of lipid either intercalated into the cell wall or present in the wall's outer section. These include lipomannan, lipoarabinomannan, the phosphatidylinositol mannosides, the phthiocerol-containing lipids and a number of glycomycolates (**Figure 4.2**) [159]. The last class of molecules will be described in more detail below (Section 4.1.2).

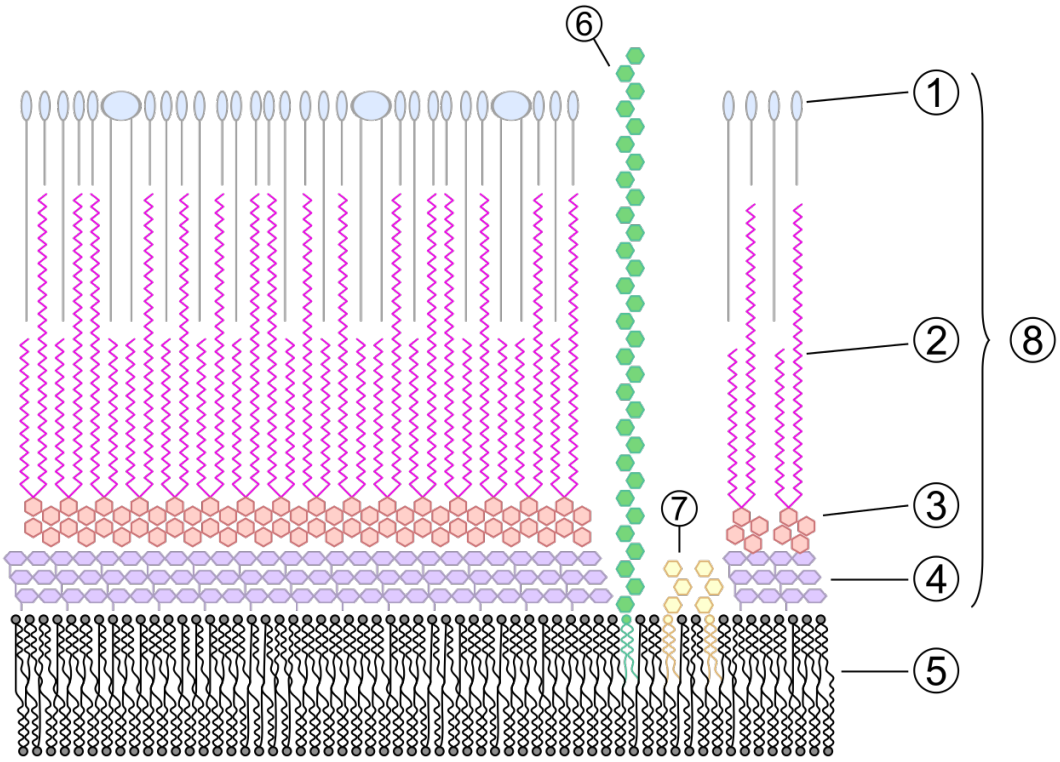

Figure 4.2: **Structure of the mycobacterial cell wall.** 1- outer lipids, 2- mycolic acids, 3- arabinogalactan, 4- peptidoglycan, 5- plasma membrane, 6- lipoarabinomannan, 7- phosphatidylinositol mannoside, 8- cell wall skeleton.

4.1.2 Mycolic Acids

A major lipid component of the mycobacterial cell wall are long chain β-hydroxy fatty acids known as mycolic acids [162]. Mycolic acids share a basic structure consisting of a mycolic motif (itself with an alkyl chain of variable length) and a meromycolate chain with a distal and proximal functional group (X and Y respectively) (**Figure 4.3A**) [162].

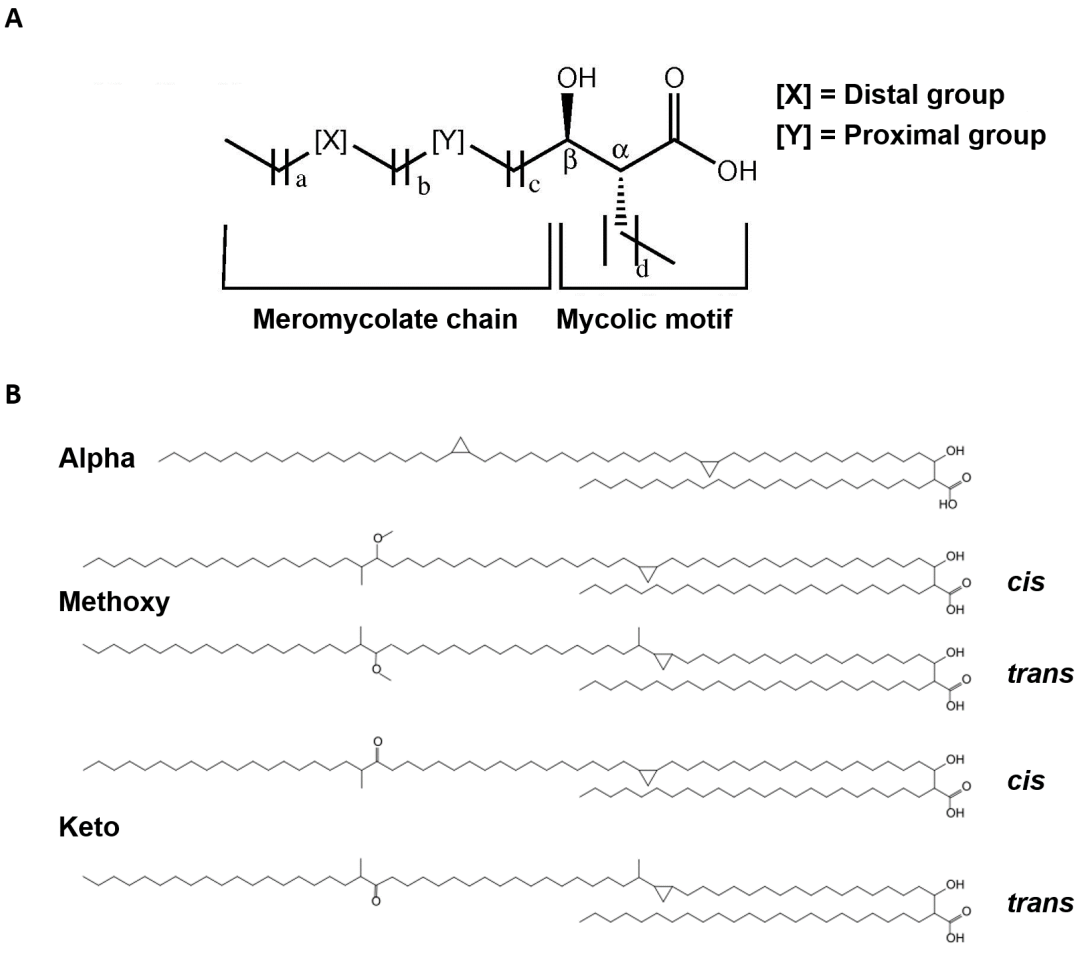

Figure 4.3: **General structure of mycolic acids. A.)** General structure of mycolic acids. Meromycolate chain and mycolic motif are indicated. [X]/[Y] distal/proximal functional group respectively. a-d indicate variable chain lengths. **B.)** Structure of mycolic acid classes found in the *Mtb* cell wall [162].

In addition to *Mycobacteria*, mycolic acids are found in the cell walls of *Nocardia*, *Rhodococcus* and *Corynebacterium* [163]. The mycolic acids from *Mycobacterium* have a relatively long alkyl chain (C_{60}-C_{90}) when compared to that of other genera, with *Corynebacterium* and *Rhodococcus* having alkyl chain lengths of C_{28}-C_{40} and C_{30}-C_{54} respectively [163] [164]. They are also more complex. Whereas mycolic acids from *Nocardia* are reasonably long (C_{42}-C_{66}) they have little variety in functional groups, with the most complex structure in the meromycolate chain a double bond [165]. In contrast, *Mycobacteria* mycolic acids may contain cyclopropane rings, double bonds and methoxy and keto groups [162]. Mycolic acids are classified into types on the basis of these functional groups. In *Mtb* there are 3 classes of mycolic acids [162]:

* Alpha mycolates (two cyclopropane rings)

* Keto mycolates (single cyclopropane ring and a ketone group)

* Methoxy mycolates (single cyclopropane ring and a methoxy group)

The keto and methoxy mycolic acids can also be subclassified as *cis* or *trans*, depending on the stereochemistry around the cyclopropane ring [162]. Their general structures are shown below (**Figure 4.3B**).

There is an enormous amount of structural diversity within mycolic acids, both in terms of the identity of the proximal and distal functional groups and the length of alkyl chains [162]. A full discussion of their structural diversity is beyond the scope of this thesis. It is however, essential to appreciate that different mycobacteria, and indeed different strains of the same species, differ in their mycolic acid composition [162] [166]. For example, mycolic acids in *Mtb* show a high degree of cyclopropanation, with alpha mycolic acids (with two cyclopropane rings) accounting for around 70% of the total mycolic acid content [167]. In contrast, mycolic acids from the cell wall of non-pathogenic

M.smegmatis are generally believed to have very low levels of cyclopropanation (although interestingly the degree of cyclopropanation has been reported to be increased at temperatures below that found in the body [168]). Additionally, the cell walls of non-pathogenic mycobacteria such as *M.smegmatis* do not contain oxygenated mycolic acids (i.e. those belonging to the methoxy and keto classes) [121]. The mycolic acids of *Mtb* also differ from that of BCG (despite both being pathogenic members of the *Mycobacteria* genera). Unlike that of *Mtb* (and indeed that of *M.bovis*), the BCG cell wall does not contain methoxymycolic acids [169] [170].

The presence of 'canonical' mycolic acids structures is essential for the functioning of different mycobacterial species. The majority of the evidence linking structure to function has been obtained via mutation of genes involved in mycolic acid biosynthesis. Modification of the basic mycolic acid structure is carried out by the *S*-adenosylmethionine-dependent methyltransferases (MAMT) [171]. There are 8 MAMTs present in *Mtb*, with 6 of these - *MmaA1-4*, *PcaA* and *CmaA2* - having been shown to play a role in mycolic acid modification [171]. The products of these genes play a role in addition of cyclopropane rings, ketone/methoxy groups and methyl branches to the basic mycolic acid structure. A summary of these genes and the function of their products is given below.

Mtb lacking all MAMTs due to genetic deletion remain viable [171]. Note, however, that the chemical inhibition of MAMTs remains lethal due to the rapid changes in mycolic acid composition and subsequent effect on membrane fluidity [171]. *Mtb* with genetic deletion of all MAMTs are unable to add cyclopropane rings or methoxy/keto groups to the basic mycolic acid structure, meaning that neither alpha, keto or methoxy mycolic acids can be manufactured [169] [172] [173] [174] [175]. Barkan *et al.* experimented with two mutant strains of *Mtb*. One had completely lost MAMT function, whilst one had mutations

in *mmaA1*, *mmaA2*, *pcaA* and *cmaA2* and therefore retained the ability to add methoxy and keto groups whilst being unable to perform cyclopropanation [171]. Both strains showed attenuated growth within mice [171]. Interestingly, cyclopropane-deficient *Mtb* showed attenuated growth within the first week of infection, whereas the strain completely lacking MAMTs was not attenuated until the second week [171].

Gene	**Function of gene product**
mmaA1	*trans*-cyclopropanation of oxygenated mycolic acids [172].
mmaA2	Addition of cyclopropane ring to distal position of alpha mycolic acids and *cis*-cyclopropanation of oxygenated mycolic acids [173] [172].
mmaA3	Addition of methyl group for production of methoxy mycolic acids [169].
mmaA4	*cis*-cyclopropanation of oxygenated mycolic acids [174].
pcaA	Addition of cyclopropane ring to proximal position of alpha mycolic acids [175].
cmaA2	*cis*-cyclopropanation of oxygenated mycolic acids [172].

Investigations have also been performed into the effect of the presence or absence of single MAMTs. *ΔpcaA* BCG was associated with greater levels of phagosomal maturation and reduced cellular persistence relative to the wild-type strain [175] [176]. It also been reported that transformation of *M.smegmatis* with the *Mtb mmaA4* gene (the product of which is required for formation of keto and methoxy mycolic acids) leads to the production of *M.smegmatis* with a significantly increased ability to induce foam cell formation [121] [174]. These findings support a link between the mycolic acid structures found in *Mtb* and the means by which the bacteria achieves long-term intracellular persistence.

When considering the relationship between the structure of a mycolic acid and its importance to mycobacterial function, an extra layer of complexity is introduced by the fact that in the cell wall mycolic acids may be present in a number of contexts [162]. They may form part of the insoluble mAGP core, being tightly bound to arabinogalactan, or be found more loosely associated with the outer cell wall. These loosely associated lipids may be present as free mycolic acids or esterified to sugar molecules to form glycomycolates [162].

Examples of glycomycolates include trehalose monomycolate (TMM) and trehalose dimycolate (TDM) (or cord factor), which consist of glucose/trehalose sugars bound to one or two mycolic acids respectively [177]. TDM and TMM occur in the cell walls of both pathogenic and non-pathogenic mycobacteria [178]. However, there is a great deal of variety with regards to the structure of the mycolic acid motifs of the glycolipid, even within a species. The use of MALDI-TOF mass spectrometry to determine the molecular mass of the mycolic acid in *Mtb* TMM revealed up to 38 significant components [179]. The mycolic acid portion of the *Mtb* TMM consisted of alpha (C_{75}-C_{85}), methoxy (C_{83}-C_{94}) and keto (C_{83}-C_{94}) mycolic acids. Similar experiments with BCG TMM revealed that it lacks methoxy mycolic acids, in line with previous observations [169] [170]. TDM is even more complex, due to the possible combinations of two different mycolic acids [180].

The immunological properties of mycolic acids, both in their free and glycolipid form, have been well documented. Peyron *et al.* demonstrated that the addition of oxygenated keto/methoxy-mycolic acids could induce formation of foamy macrophages [121]. These oxygenated mycolic acids are not found in the non-pathogenic *M.smegmatis*. Also, TDM has previously been shown to prevent phagosomal maturation and induce the formation of both caseating granulomas and foamy macrophages [181] [182] [183]. This did not require the presence of

intact mycobacteria. Modification of the TDM structure due to mutation in *MAMTs* altered its immunological properties. Whereas TDM from wild-type *Mtb* induced granuloma formation, TDM from *Δpca* mice showed a two-fold decrease in potency [184].

The importance of mycolic acids to mycobacterial persistence, their proven immunological properties, and the fact that mycobacterial cell wall lipids have been demonstrated to be trafficked from the host phagosome to the endocytic system of the host cell and that of neighbouring uninfected cells, makes them strong candidates for the means by which pathogenic mycobacteria inhibit the NPC pathway [79] [158]. If this is the case then it should be possible to induce NPC cellular phenotypes in wild-type cells, similar to those observed in chapters 2 and 3, in the absence of whole mycobacteria using the cell wall lipids only. As detailed above, the cell wall of mycobacteria is lipid-rich, with these lipids exhibiting great structural diversity [162]. The importance of canonical lipid structures to correct mycobacterial function has been previously well documented [121] [171] [174]. Therefore the aims of the work presented in this chapter are:

* Investigate whether cell wall lipids from pathogenic mycobacteria are sufficient for the induction of NPC cellular phenotypes in the absence of the mycobacteria itself.

* Attempt to identify the specific lipid species responsible for inhibition of the NPC pathway.

* Investigate the relationship between the structure of mycolic acids and their ability to induce NPC cellular phenotypes.

4.2 Materials and Methods

4.2.1 Cells

RAW 264.7 cells and primary human macrophages were obtained and cultured as described in Section 2.2.1 and 3.2.3 respectively.

4.2.2 Lipids

A general mycolic acid fraction and purified TDM (>97% purity) from the pathogenic *M.bovis* were obtained from Sigma-Aldrich and used at the indicated concentrations for the indicated duration. Purified glycomycolates were kindly provided by Prof. Michael Brenner and Dr. Raju Venkata V. Tatituri (Brigham and Women's Hospital, Harvard). The steps by which they were purified are detailed below (Section 4.2.9). Synthetic mycolic acids were kindly provided by Prof. Mark Baird (University of Bangor, UK). Work investigating the effect of these lipids on LysoTracker fluorescence and GSL levels in RAW 264.7 macrophages was performed by Peter Johnstone (under my supervision). Purified versions of alpha, methoxy cis and keto cis mycolic acid classes were obtained from Avanti Polar Lipids.

4.2.3 Fixation of Cells

As detailed in Section 2.2.14.

4.2.4 Microscopy

As detailed in Sections 2.2.13 and 2.2.15.

4.2.5 Localisation of Cellular Cholesterol via Filipin Staining

As detailed in Section 2.2.16.

4.2.6 Distribution and Intracellular Transport of GM1 Ganglioside

As detailed in Section 3.2.11.

4.2.7 Nuclear Staining

As detailed in Section 3.2.12.

4.2.8 LysoTracker Microscopy

As detailed in Section 3.2.13.

4.2.9 Purification of Glycomycolates from the *M.tuberculosis* Cell Wall

Lipid Extraction and Analysis

Crude non-polar lipids and polar lipids were initially extracted from *Mtb* as previously described [185]. Briefly, dried cells were stirred in 220ml of methanolic saline (20ml of 0.3% NaCl and 200ml of CH_3OH) and 220ml of petroleum ether for 2hr. The biomass was allowed to settle overnight and centrifuged (3000rpm/5 min). The resulting bi-phasic solution was separated and the upper layer containing non-polar lipids recovered. The lower layer was treated with petroleum ether, mixed and harvested as described above [185]. The two upper petroleum ether fractions were combined and dried under reduced pressure. To extract polar lipids, a mixture of $CHCl_3/CH_3OH$/NaCl was added to the

lower methanolic saline layer. The solution was stirred for 4hr and left to settle overnight. This mixture was filtered and the filter cake re-extracted twice with $CHCl_3/CH_3OH$/NaCl solution. Appropriate amounts of $CHCl_3$ and NaCl solution were added to the combined filtrates and the mixture stirred for 1hr and allowed to settle. The lower layer containing the polar lipids was recovered and dried under reduced pressure. The non-polar and polar lipid extracts were examined by 1D thin-layer chromatography (TLC) on aluminum TLC plates of silica gel 60 F254 (Merck EMD Millipore, Catalog no. 5554-7). Lipids were visualized by spraying plates either with 5% ethanolic molybdophosphoric acid and charring, α-naphthol/sulphuric acid followed by gentle charring of plates for glycolipids, a Dittmer and Lester reagent which is specific for phospholipids and glycophospholipids or using ninhydrin, an amino-specific reagent for detecting amino residues on extracted lipids [185].

Purification of Lipid Extract

After analysing the lipid profiles by TLC, purifications were performed using diethylaminoethyl (DEAE) cellulose chromatography. The crude polar lipid extract was dissolved in Solution A ($CHCl_3/CH_3OH$ (2:1, v/v)) and a few drops of H_2O added as necessary to dissolve the lipids. The polar lipid fraction was eluted using Solution A to remove all mycolates, their glycosylated forms and other zwitterionic lipids. Charged lipids were then eluted using ammonium acetate dissolved in Solution A in a stepwise gradient of increasing concentration of ammonium acetate in C:M ranging from 1mM to 300mM.

Further Purification of Mycolates

The glycolate mycolate fraction was further purified by either using silica gel packed into glass columns or by preparative TLC. In the silica gel procedure

the mycolate fraction was dissolved in 100% $CHCl_3$ and initially eluted with $CHCl_3/CH_3OH$ (80:1, v/v) and further eluted with decreasing concentration of $CHCl_3$ (with constant $[CH_3OH]$). The glycomycolate fractions were monitored by TLC on 10cm x 10cm aluminum-backed TLC plates of silica gel 60 F254 (Merck EMD Millipore) and plates developed in either $CHCl_3/CH_3OH$ (80:10, v/v) or $CHCl_3/CH_3OH/H_2O$ (65:25:4 v/v/v). The glycomycolates were visualized by spraying with α-naphthol/ sulphuric acid followed by gentle charring. In preparative 1D TLC the mycolate extract was loaded on 10cm x 20cm plastic-backed TLC plates of silica gel 60 F254 (Merck EMD Millipore) and ran in TLC solvent system $CHCl_3/(CH_3)_2CO/CH_3OH/H_2O$ (50:60:2.5:3 v/v/v/v). TLC plates were subsequently sprayed with either ethanolic Rhodamine 6G for detection of non-polar lipids or 1,6-diphenyl-1,3,5-hexatriene for polar lipids. The lipid bands were visualized, marked under UV light and the corresponding purified lipid spots were scraped from the plates, silica extracted and used for biological testing.

4.2.10 Quantification of LysoTracker Staining via Plate-reader

Purified glycomycolates were re-suspended in $CHCl_3$:EtOH (1:4 v/v) to a concentration of 1mg/ml prior to dilution into RPMI to 1ng/ml. A 96-well plate was seeded with RAW 264.7 cells ($5x10^4$ cells/well), which were allowed to adhere overnight. Glycomycolates were then added prior to 24hr incubation at 37°C/5% CO_2. Post-incubation, the cells were stained with LysoTracker as in Section 4.2.8. Fluorescence was quantified using a 96-well plate reader (ex/em 485/520nm) (FLUOstar OPTIMA).

4.2.11 Lysosomal Calcium Quantification

As detailed in Section 2.2.9.

4.2.12 Quantification of LysoTracker Levels via Fluorescence Activated Cell Sorting (FACS)

RAW 264.7 cells were grown in 6 well plates. For FACS analysis around 0.5-1 x 10^6 cells were harvested via scraping and centrifuged (1200rpm/10min). The media was removed and replaced with 2ml PBS and centrifuged again. The PBS wash and centrifugation was repeated before removal of PBS prior to resuspension of the cell pellet in 1ml LysoTracker Green working solution (200nM in PBS) prior to incubation for 10 minutes at 37°C/5% CO_2. Cells were centrifuged (3000rpm/5min) and the pellet resuspended in 250µl FACS buffer (100 µl 10% BSA, 100 µl 2M NaN_3 per 10ml PBS).

Immediately prior to analysis cells were co-stained with propidium iodide (PI) (Life Technologies) to assess cell viability. The cells were mixed with 250µl PI (4µg/ml in FACS buffer).

Samples were analysed using a BD FACSCanto II flow cytometer with BD Bioscience FACSDiva software, with 10000 cells observed per tube. Excitation source consists of three lasers: blue (488-nm, air-cooled, 20-mW solid state), red (633-nm, 17-mW HeNe), and violet (405-nm, 30-mW solid state). Compensation controls (unstained cells, and cells stained with either LysoTracker or PI only) were used to correct for any spectral overlap between the FITC and PE fluorescence channels. The LysoTracker Mean values were converted to mean equivalents of fluorescence (MEFL) values using Rainbow Calibration Particles (BD Biosciences). Samples were gated to exclude dead cells (those in the high PI staining population).

4.2.13 Quantification of Lactosylceramide Levels via HPLC

As detailed in Sections 2.2.17 and 2.2.18.

4.2.14 Localisation of Cellular Cholesterol via Laser Scanning Confocal Microscope

Performed by Doris Höeglinder (European Molecular Biology Laboratory, Germany). Filipin staining was carried out as in Section 2.2.16. Images were obtained using a laser scanning confocal microscope.

4.2.15 Statistical Analysis

Statistical analysis was performed using GraphPad Prism (ver 6.0). The specific test used is indicated in the figure legend.

4.3 Results

4.3.1 Effect of Mycolic Acids on Cholesterol Distribution in RAW 264.7 Macrophages

RAW 264.7 macrophages treated with a general mycolic acid fraction (from the cell wall of *M.bovis*) (Sigma) showed accumulation of free cholesterol (**Figure 4.4**). This accumulation was similar to that observed in macrophages infected with BCG (**Figure 2.8**).

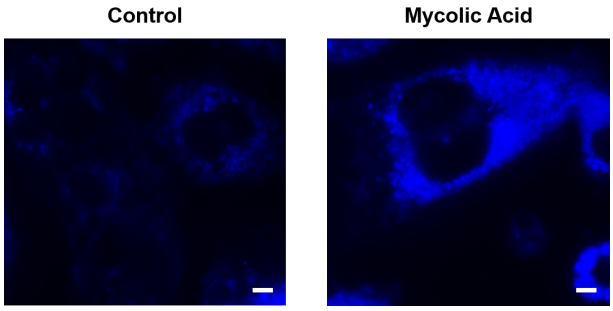

Figure 4.4: **Effect of mycolic acids on cholesterol distribution in RAW 264.7 cells.** 24hr treatment, 1µg/ml lipid. Images shown are representative. Blue - filipin (cholesterol). Scale bar - 5µm.

4.3.2 Effect of Mycolic Acids on Cholesterol Distribution in Primary Human Macrophages

Primary human macrophages treated with a general mycolic acid fraction (from the cell wall of *M.bovis*) (Sigma) demonstrated accumulation of free cholesterol (**Figure 4.5**), thereby replicating the effect seen upon the treatment of RAW 264.7 macrophages with lipids (**Figure 4.4**) and the infection of human macrophages with BCG (**Figure 3.3**). These experiments were replicated in primary human macrophages obtained by differentation of monocytes isolated from the blood of 6 independent healthy donors. Cells from all donors exhibited cholesterol accumulation post-lipid treatment.

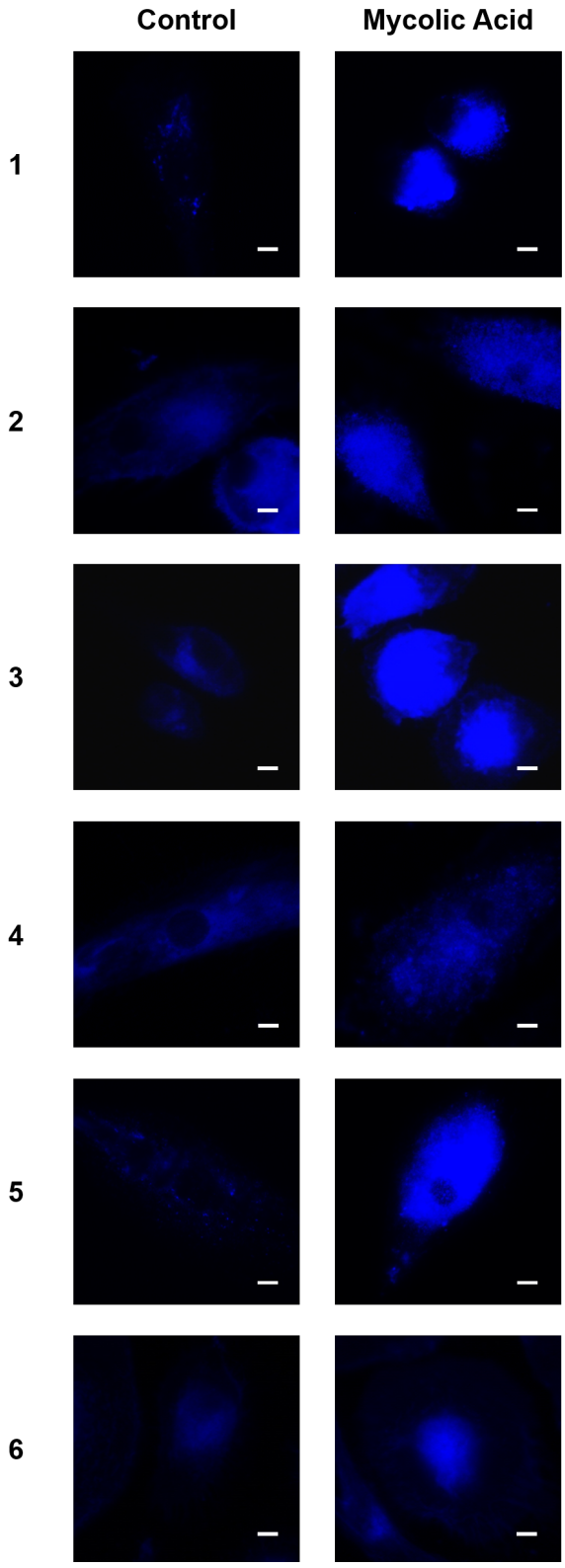

Figure 4.5: **Effect of mycolic acids on cholesterol distribution in primary human macrophages.** 24hr treatment, 1µg/ml lipid. Images shown are representative. Macrophages obtained by differentiation of monocytes isolated from the blood of 6 independent healthy donors. Blue - filipin (cholesterol). Scale bar - 5µm.

4.3.3 Effect of Mycolic Acids on LysoTracker Staining Levels

Primary human macrophages treated with a general mycolic fraction (from the cell wall of *M.bovis*) (Sigma) exhibited increased staining with LysoTracker, indicative of expansion of the lysosomal compartment (**Figure 4.6**). A similar increase in staining was observed in cells infected with BCG (**Figure 3.4**).

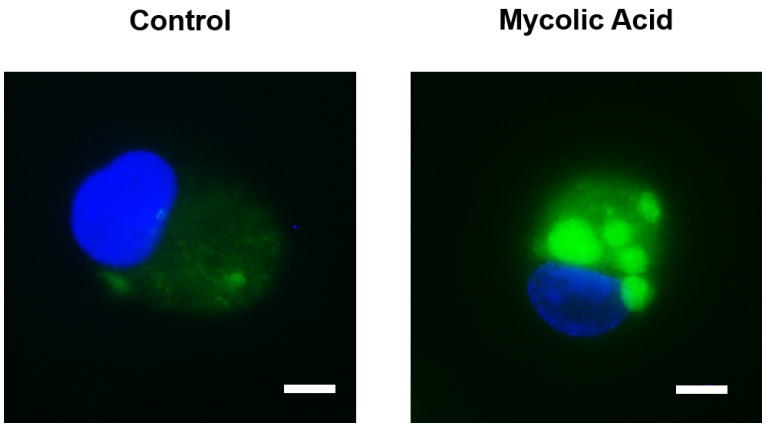

Figure 4.6: **Effect of mycolic acids on LysoTracker staining in primary human macrophages.** 24hr treatment, 1µg/ml lipid. Images shown are representative. Macrophages obtained by differentiation of monocytes isolated from blood of donor number 3. Green - LysoTracker green, blue - Hoescht (nucleus). Scale bar - 5µm.

4.3.4 Effect of Mycolic Acids on Trafficking of GM1 Ganglioside

Primary human macrophages treated with a general mycolic acid fraction (from the cell wall of *M.bovis*) (Sigma) exhibited mistrafficking of GM1 ganglioside (**Figure 4.7**) similar to that observed in cells infected with BCG (**Figure 3.5**). These experiments were replicated in primary human macrophages obtained by differentation of monocytes isolated from the blood of 6 independent healthy donors. All donor cells exhibited mistrafficking of GM1 ganglioside post-lipid treatment.

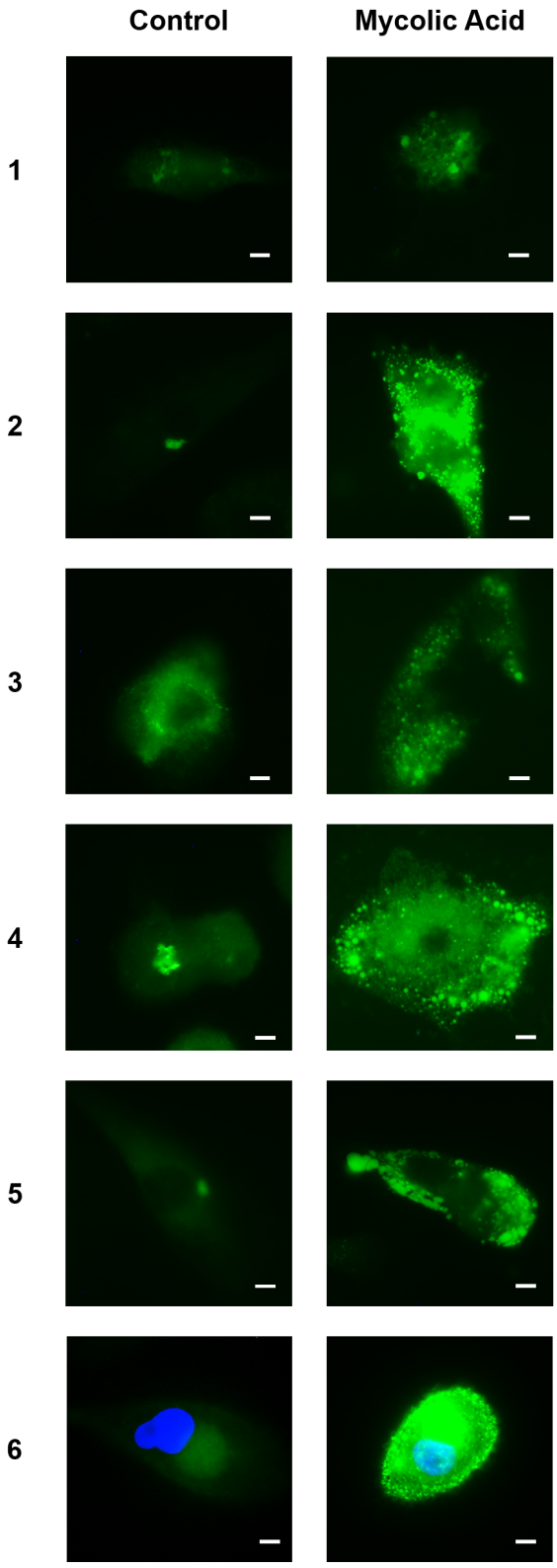

Figure 4.7: **Effect of mycolic acids on GM1 ganglioside trafficking in primary human macrophages.** 24hr treatment, 1µg/ml lipid. Images shown are representative. Macrophages obtained by differentiation of monocytes isolated from the blood of 6 independent healthy donors. Green - CtxB (GM1 ganglioside). Scale bar - 5µm.

4.3.5 Effect of Purified Glycomycolates on LysoTracker Staining Levels

We had observed that it was possible to induce NPC cellular phenotypes such as cholesterol accumulation and GM1 mistrafficking using a general mycolic acid fraction (from the cell wall of *M.bovis*) in the absence of the whole mycobacteria. To investigate the identity of the causative agent within the general fraction we assayed purified glycomycolates derived from *Mtb*. To quantify their relative efficacies we looked at the changes in LysoTracker staining in RAW 264.7 macrophages (in a 96-well plate) post 24hr incubation with the lipid. We observed that TDM from *Mtb* gave the largest increase, with LysoTracker levels being significantly higher than those in untreated macrophages (**Figure 4.8, p - 0.0166**). TMM and glucose monomycolate (GMM) (also from *Mtb*) gave smaller increases in fluorescence, with these increases falling short of statistical significance (**p - 0.1495/0.0557 respectively**). GMM from *M.smegmatis* had a minimal effect (**p - 0.3473**).

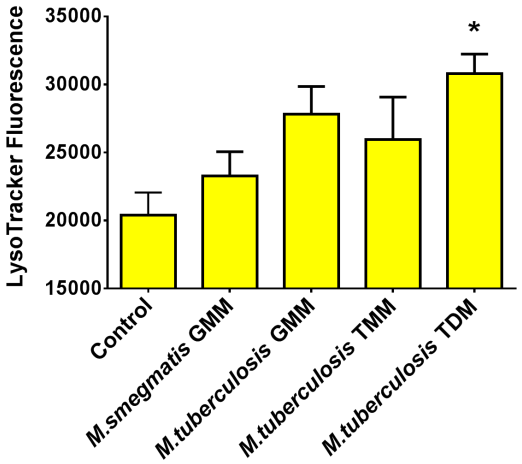

Figure 4.8: **Effect of purified glycomycolates on LysoTracker staining levels in RAW 264.7 macrophages.** 24hr treatment, 1ng/ml lipid. LysoTracker fluorescence measured via microplate reader. Mean ± SEM of 4 biological replicates. * $p<0.05$ versus untreated control (via t-test).

4.3.6 Quantification of Lysosomal Calcium Levels post Treatment with TDM

One of the key cellular phenotypes in NPC is the reduction of lysosomal Ca^{2+} [20]. A reduction in lysosomal calcium release post addition of GPN was also observed in RAW 264.7 and primary human macrophages infected with BCG (**Figure 2.2/3.2 respectively**). A similar reduction in lysosomal Ca^{2+} was observed in cells incubated with TDM. This reduction was significant in both RAW 264.7 and primary human macrophages, with levels 40-60% of that in controls (**Figure 4.9B, $p<0.0001$/4.10B, $p<0.0001$ respectively**). The TDM used in this experiment (and subsequent work) was purchased from Sigma-Aldrich, and was from the cell wall of *M.bovis*.

Infection/lipid-treatment of RAW 264.7 macrophages was associated with a small but significant decrease in basal Ca^{2+} (levels prior to addition of GPN) (**Figure 4.9C, p - 0.0067 (BCG)/ 0.0002 (TDM)**). However, this decrease was too minor to account for any changes in maximal Ca^{2+} between control macrophages and those infected with BCG or treated with TDM. There were no significant differences in basal Ca^{2+} in the primary human macrophages (**Figure 4.10**).

4.3.7 Effect of TDM on Cholesterol Distribution

TDM was able to induce the accumulation of free cholesterol in both wild-type RAW 264.7 and primary human macrophages (**Figure 4.11/4.12 respectively**). A 24hr treatment with 50ng/ml TDM appears sufficient for induction of significant cholesterol accumulation. For the human cells this phenotype induction was observed in macrophages derived from three independent healthy donors.

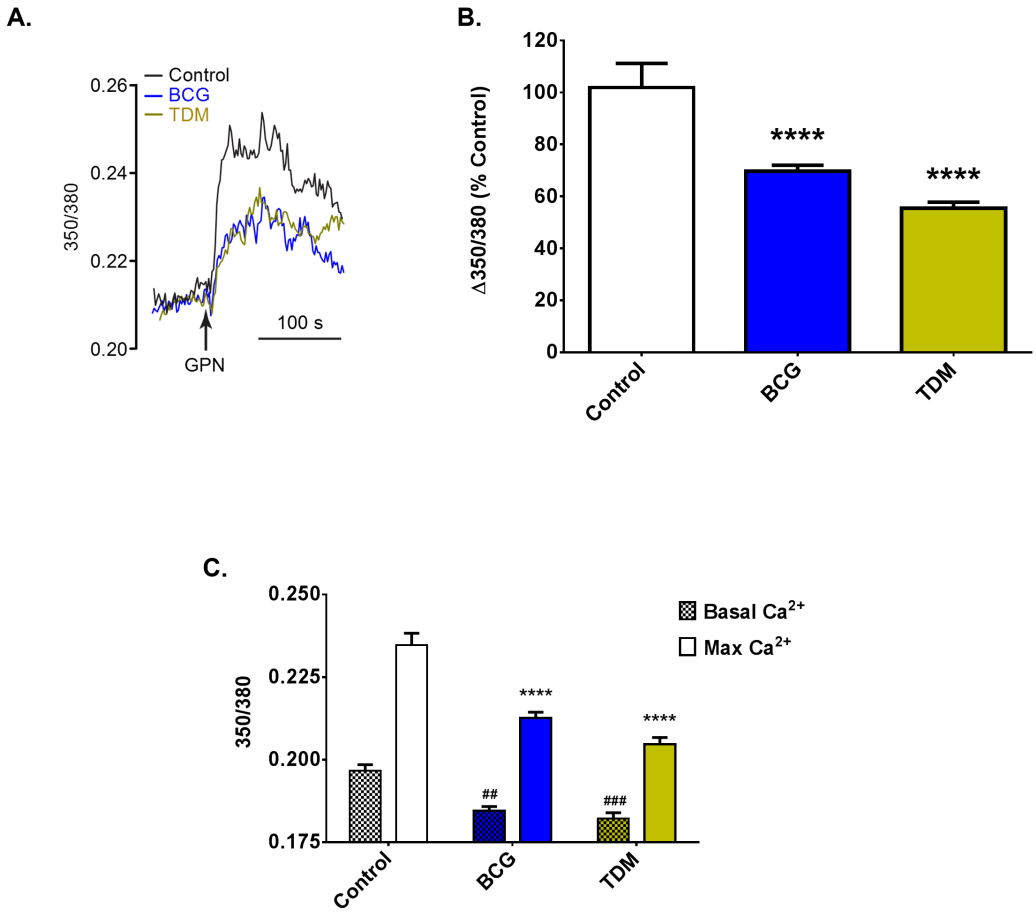

Figure 4.9: **Effect of mycobacterial infection/ TDM treatment on lysosomal Ca^{2+} levels in RAW 264.7 macrophages, as quantified by GPN-induced release of lysosomal Ca^{2+}.** 24hr infection (MOI 12.5)/ lipid treatment (50ng/ml). **A.)** Ca^{2+} responses from representative single fura-2 loaded RAW 264.7 macrophages upon addition of GPN (point of addition indicated by arrow). At the end of each run all cells responded to 1 µM ionomycin. **B.)** Maximal Ca^{2+} responses upon addition of GPN as determined by the difference between basal and maximum fura-2 ratio (Δ350/380). Changes given as percentage difference relative to Δ350/380 in uninfected/untreated controls. Mean ± SEM of n=127-252 individual cells per experimental group. **** $p<0.0001$ versus control (via 1-way ANOVA). **C.)** Basal Ca^{2+} (prior to addition of GPN) and maximum Ca^{2+} release upon lysosomal lysis. Mean ± SEM of n=127-252 individual cells per experimental group. ***/### $p<0.001$ versus control (via 1-way ANOVA).

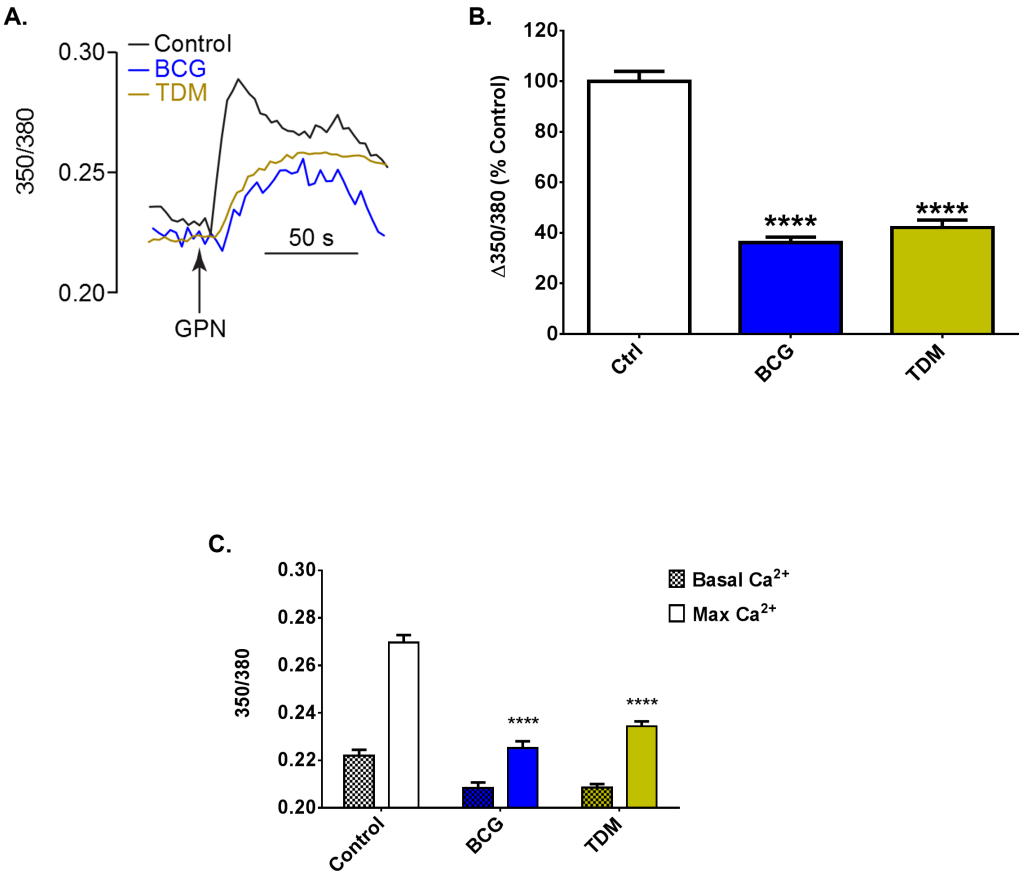

Figure 4.10: **Effect of mycobacterial infection/ TDM treatment on lysosomal Ca^{2+} levels in primary human macrophages, as quantified by GPN-induced release of lysosomal Ca^{2+}.** 24hr infection (MOI 12.5)/ lipid treatment (50ng/ml). Macrophages obtained by differentiation of monocytes isolated from blood of donor number 1. **A.)** Ca^{2+} responses from representative single fura-2 loaded primary human macrophages upon addition of GPN (point of addition indicated by arrow). At the end of each run all cells responded to 1 µM ionomycin. **B.)** Maximal Ca^{2+} responses upon addition of GPN as determined by the difference between basal and maximum fura-2 ratio (Δ350/380). Changes given as percentage difference relative to Δ350/380 in uninfected/untreated controls. Mean ± SEM of n=71-156 individual cells per experimental group. **** $p<0.0001$ versus control (via 1-way ANOVA). **C.)** Basal Ca^{2+} (prior to addition of GPN) and maximum Ca^{2+} release upon lysosomal lysis. Mean ± SEM of n=71-156 individual cells per experimental group. **** $p<0.0001$ versus control (via 1-way ANOVA).

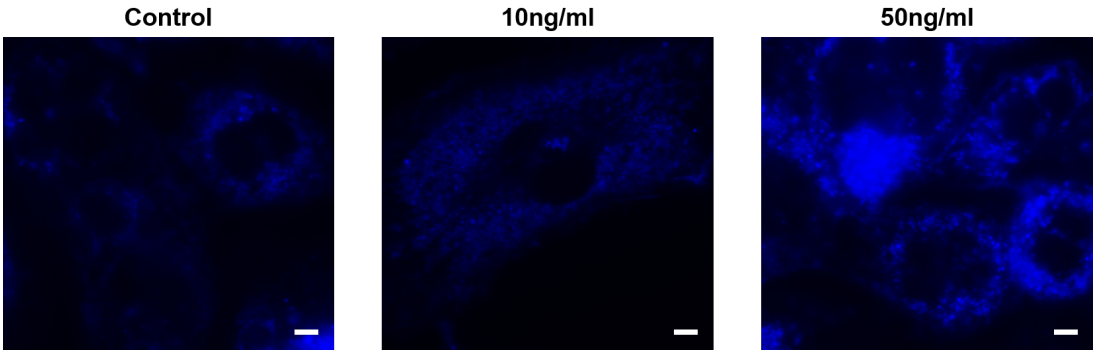

Figure 4.11: **Effect of TDM on cholesterol distribution in RAW 264.7 macrophages.** 24hr treatment. Images shown are representative. Blue - filipin (cholesterol). Scale bar - 5µm.

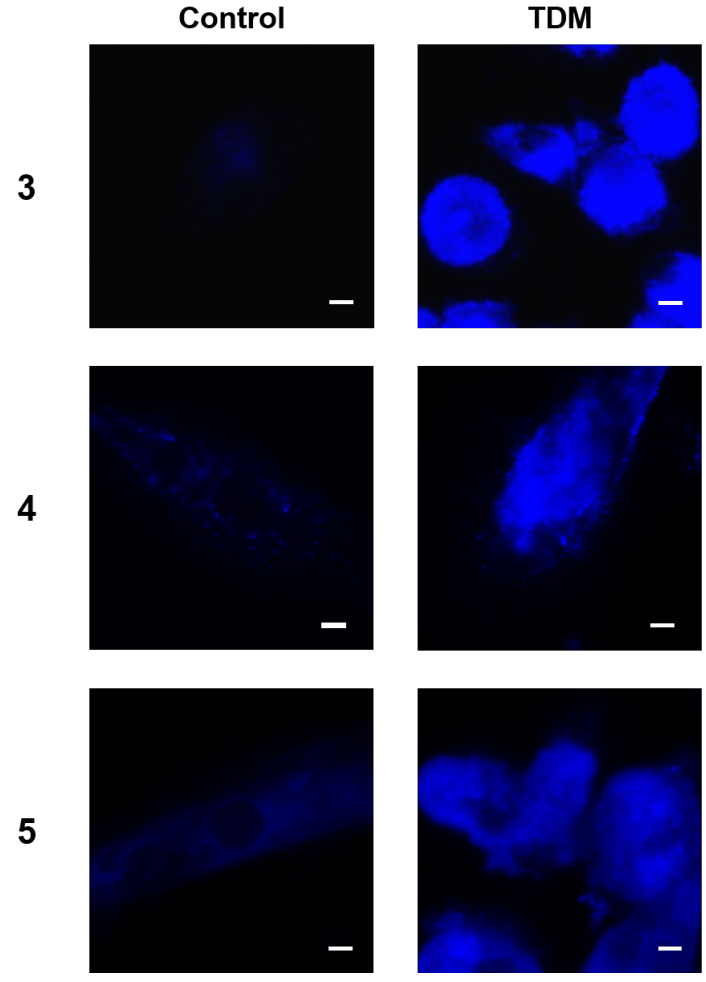

Figure 4.12: **Effect of TDM on cholesterol distribution in primary human macrophages.** 24hr treatment, 50 ng/ml. Macrophages obtained by differentiation of monocytes isolated from blood of donors number 3, 4 and 5. Images shown are representative. Blue - filipin (cholesterol). Scale bar - 5µm.

4.3.8 Effect of TDM on Trafficking of GM1 Ganglioside

Primary human macrophages treated with TDM exhibited mistrafficking of GM1 ganglioside (**Figure 4.13**) similar to that observed in cells infected with BCG or treated with a general mycolic acid fraction (**Figure 3.5/4.7 respectively)**. These experiments were replicated in primary human macrophages obtained by differentiation of monocytes isolated from the blood of 5 independent healthy donors. Cells from all donors exhibited mistrafficking of GM1 ganglioside post-TDM treatment.

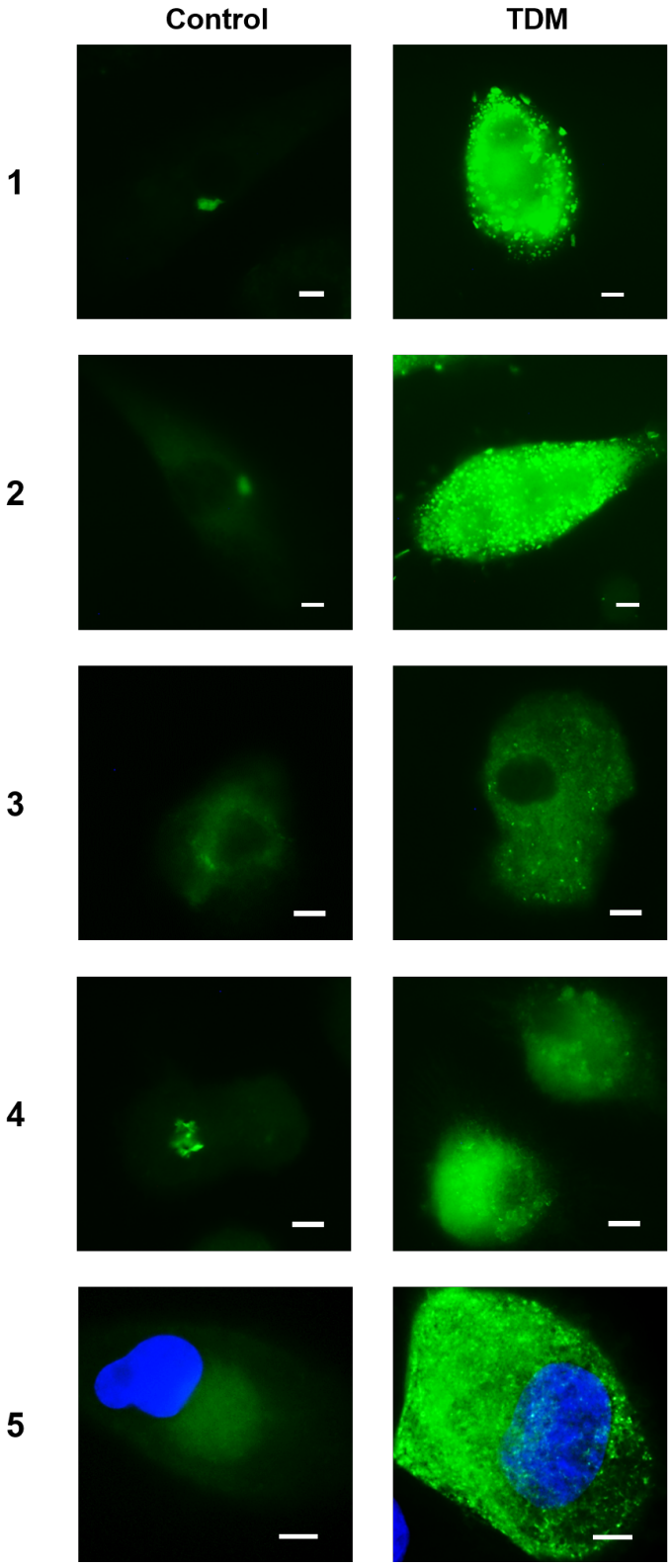

Figure 4.13: **Effect of TDM on GM1 trafficking in primary human macrophages.** 24hr treatment, 50ng/ml lipid. Macrophages obtained by differentiation of monocytes isolated from blood of donors number 1-5. Images shown are representative. Green - CtxB (GM1 ganglioside). Scale bar - 5µm.

4.3.9 Effect of Synthetic Mycolic Acids on Induction of NPC Phenotypes

LysoTracker

We wished to investigate whether there was a correlation between the presence of certain structural motifs in mycolic acids (in the absence of sugar head groups) and their ability to induce NPC disease phenotypes. We were provided with a range of synthetic mycolic acid species (27 in total). We screened these for their ability to induce NPC phenotypes in wild-type RAW 264.7 macrophages. Quantification of LysoTracker staining via fluorescence activated cell sorting (FACS) is a relatively high-throughput and quantitative method by which one can investigate induction of an NPC phenotype. Wild-type RAW 264.7 cells were incubated with 2 different concentrations of each lipid (1/100ng/ml) for 24 hours prior to analysis of LysoTracker fluorescence. These investigations were performed blinded as to the structure of the lipids.

The mycolic acids fell into 3 categories. The effects of selected lipid species are shown below (**Figure 4.14**). Some compounds (such as JRMM267C) had no apparent effect. Those lipids that induced the greatest increase in LysoTracker fluorescence included two hydroxy-mycolic acids that are present at very low-levels as intermediates in *Mtb* (JRCT50/53) and three epoxy-mycolic acids (DZ62, DZ148 and MMS130) found in environmental mycobacteria and therefore unlikely to be responsible for the inhibition of phagosome:lysosome fusion seen post-*Mtb* infection (Mark Baird, personal communication). KB9 gave the greatest increase in LysoTracker staining, with fluorescence levels 30-fold higher than in controls. It is a minor lipid species in *Mtb*. There were also a number of lipids that gave a significant decrease in LysoTracker levels. The lipid which gave the largest decrease in LysoTracker staining was JRMH140. This is believed to be a

key virulence factor in *Mtb* (Mark Baird, personal communication). A decrease in LysoTracker staining could reflect a reduction in lysosomal compartment size. However, the use of LysoTracker as a reporter of lysosomal compartment volume depends upon the acidic pH of the lysosome. LysoTracker consists of a fluorophore linked to a weak base [147]. This base is protonated at acidic pH, meaning the dye accumulates in acidic organelles. A change in lysosomal pH as a result of lipid treatment would affect the accumulation of the dye and hence levels of LysoTracker fluorescence.

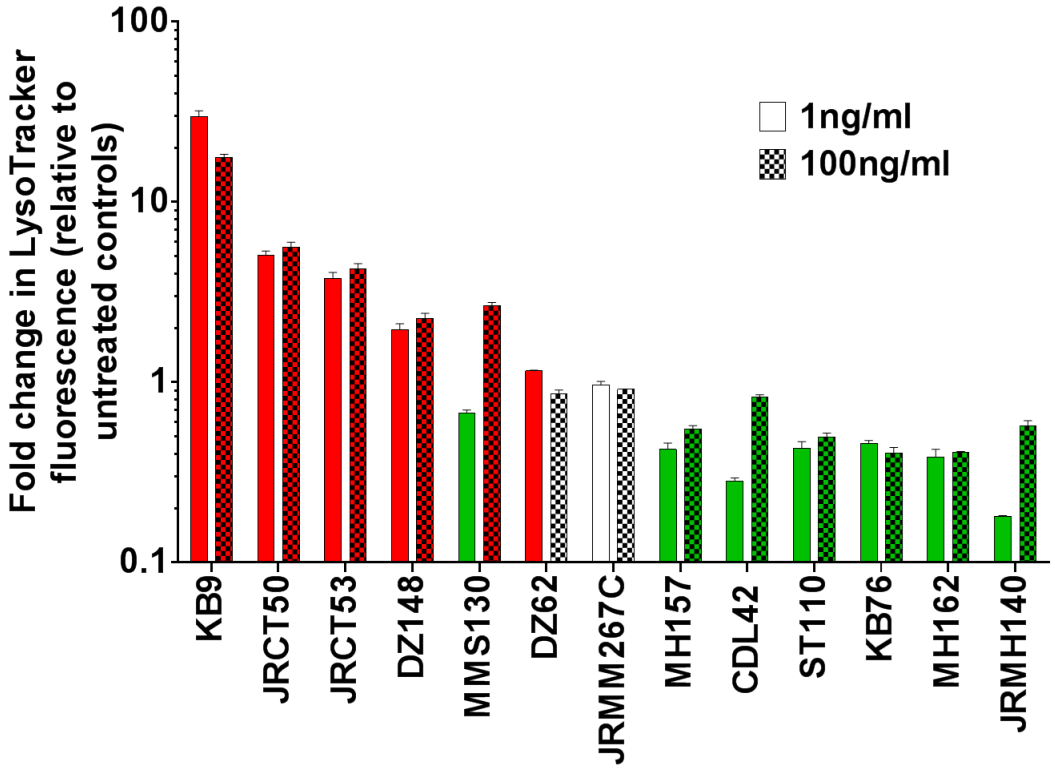

Figure 4.14: **Effect of synthetic mycolic acids on LysoTracker staining levels in RAW 264.7 macrophages (quantified via FACS).** 24 hour treatment period at indicated concentrations. LysoTracker fluorescence expressed as fold-change relative to that in untreated macrophages. Red/Green - significant increase/ decrease (respectively) in LysoTracker staining relative to untreated controls (via t-test). Mean ± SEM of 4 biological replicates.

Glycosphingolipids

A number of the synthetic mycolic acids that had an effect on LysoTracker fluorescence were investigated for their effect on GSL levels. A number of lipids were associated with significantly increased levels of the GSL LacCer (**Figure 4.15, p<0.05/0.01**). Interestingly, those lipids associated with significant increases in LacCer levels were those that gave significantly decreased LysoTracker staining (**Figure 4.14, p<0.05**).

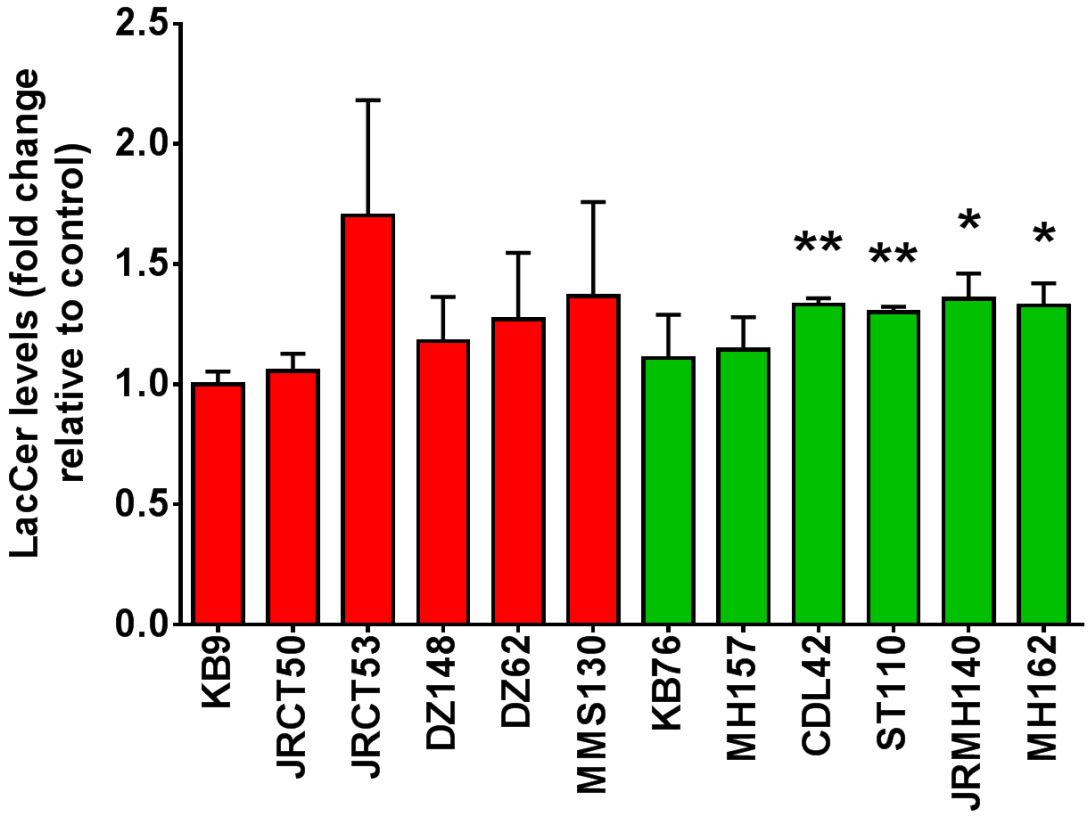

Figure 4.15: **Effect of synthetic mycolic acids on lactosylceramide levels in RAW 264.7 macrophages (quantified via HPLC).** 24hr treatment, 100ng/ml. Bars red and green to indicate a significant increase/decrease (respectively) in LysoTracker staining levels relative to untreated controls (see Fig 4.14). Mean ± SEM of 4 biological replicates. * $p<0.05$, ** $p<0.01$ versus untreated controls (via t-test).

Lipid Structures

Post-LacCer quantification we were unblinded for the lipid structures. A selection of these structures are shown (**Figure 4.16**). There were no obvious correlations between structural motifs and the effect of the lipids on LysoTracker fluorescence or LacCer levels.

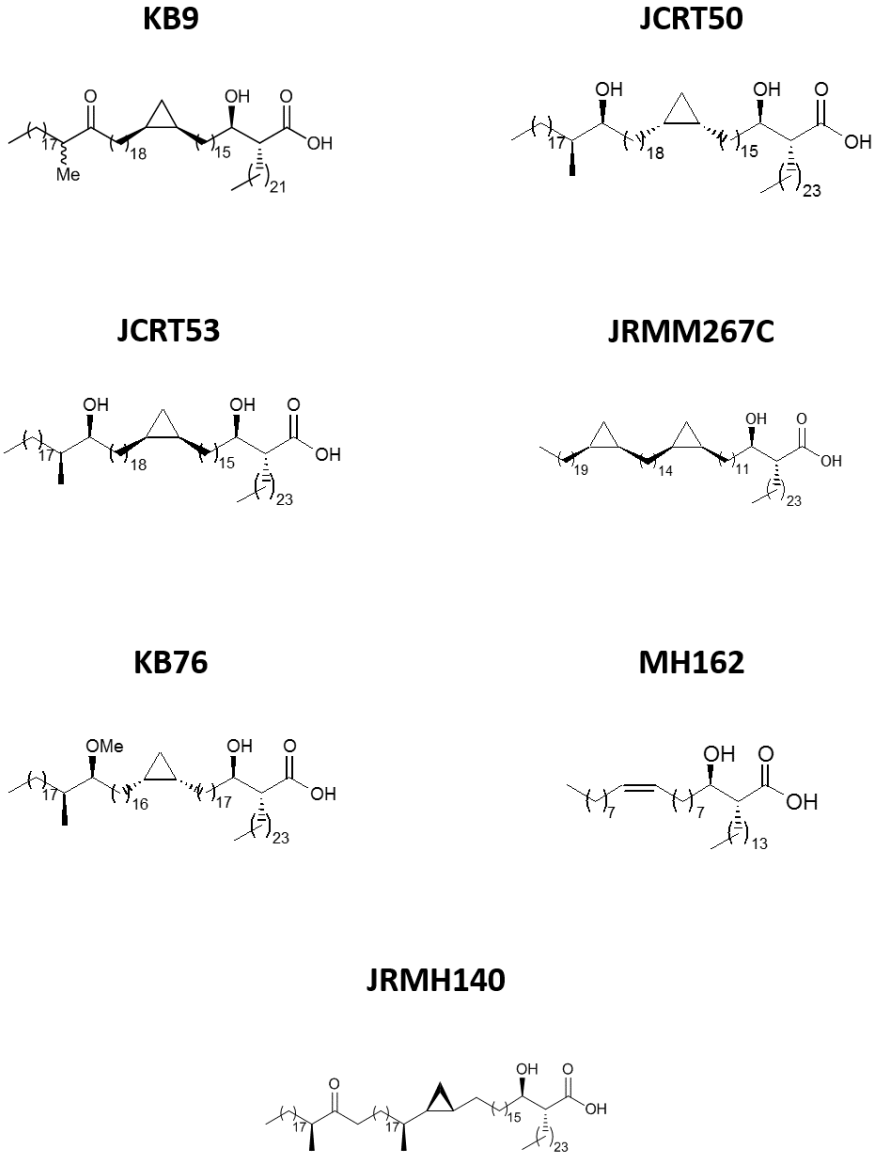

Figure 4.16: **Structure of selected synthetic mycolic acids.**

4.3.10 Induction of NPC Phenotypes by Mycolic Acid Classes

LysoTracker

A different approach to probing the structure:function relationship of mycolic acids on wild-type RAW 264.7 macrophages used synthetic versions of the 3 types of mycolic acid produced by *Mtb* - alpha, keto and methoxy (Avanti Polar Lipids) (**Figure 4.17**). As in Section 4.3.9, LysoTracker fluorescence (quantified by FACS) was used as a readout of the effect of the lipids on the NPC pathway in RAW 264.7 macrophages.

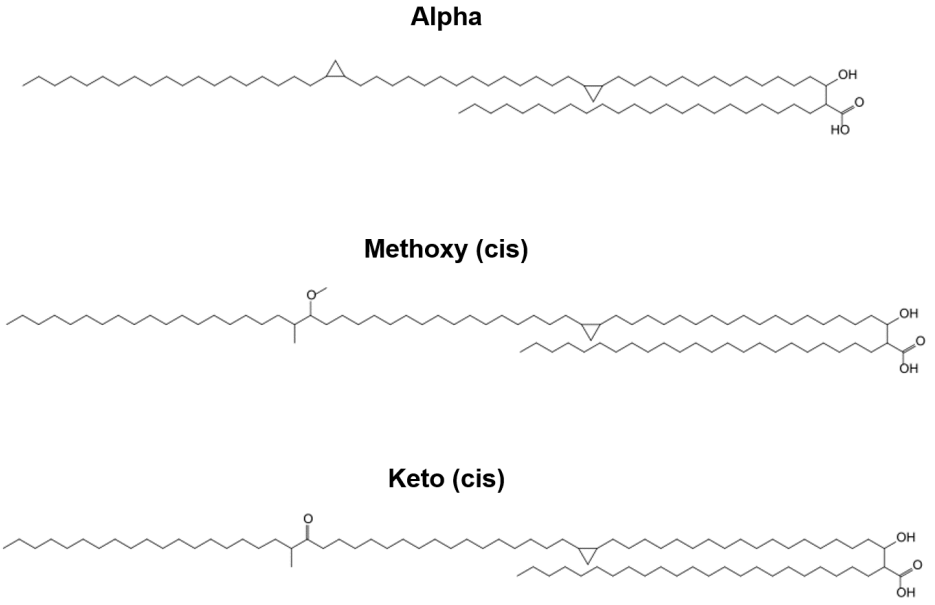

Figure 4.17: **Structure of the mycolic acids found in *Mtb*.** Adapted from [173].

The alpha mycolic acids were the most potent, with concentrations as low as 1ng/ml giving a significant increase in LysoTracker staining relative to unstained controls (**Figure 4.18, p<0.0001**). At higher concentrations (10ng/ml and above) keto mycolic acids also gave significantly increased LysoTracker levels (**Figure 4.18, p - 0.0022 (10ng/ml), 0.0020 (100ng/ml) and 0.0003**

(1000ng/ml)). No significant increase in LysoTracker staining was seen as a result of treatment with methoxy mycolic acids at any of the stated concentrations.

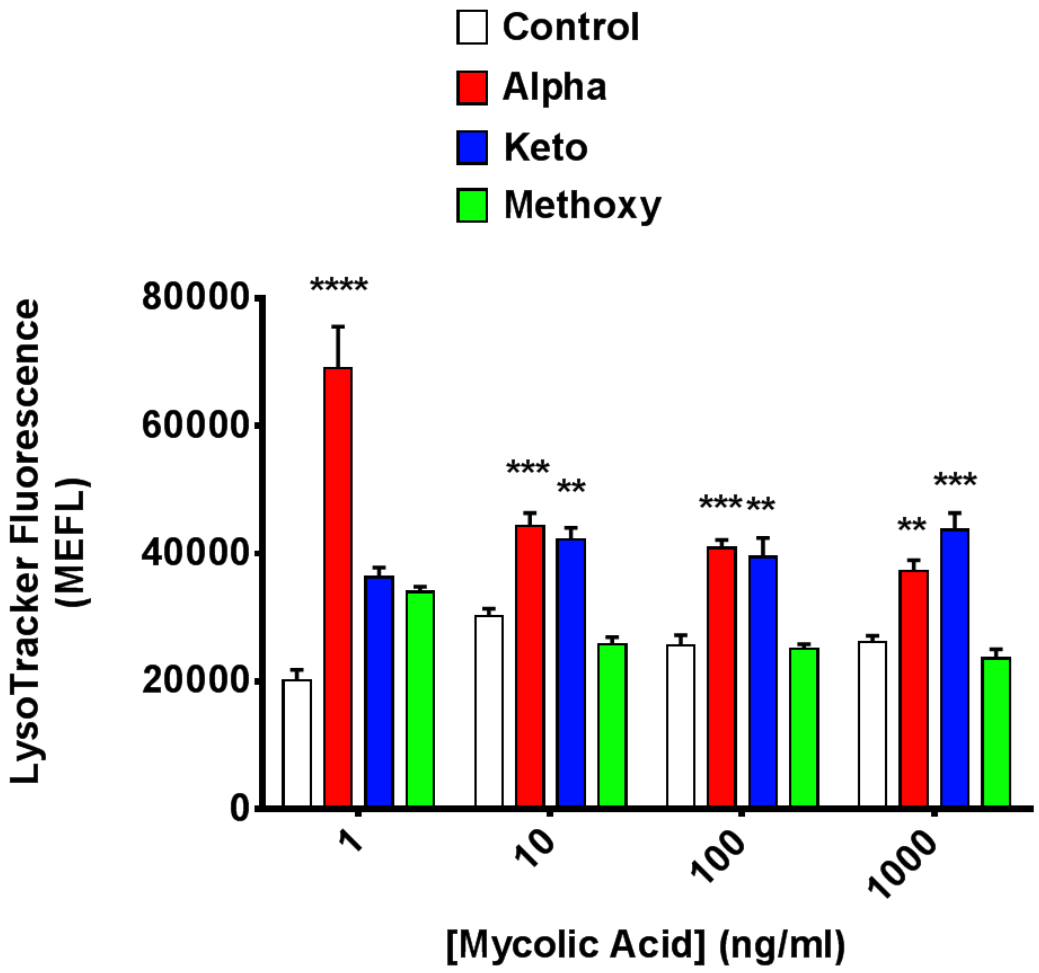

Figure 4.18: **Effect of major mycolic acid classes on LysoTracker staining levels in RAW 264.7 macrophages (quantified via FACS).** 24hr. Mean ± SEM of 4 biological replicates. ** $p<0.01$, *** $p<0.001$, **** $p<0.0001$ versus control (via 1-way ANOVA).

Filipin

Treatment of wild-type RAW 264.7 macrophages with the 3 mycolic acid types produced by *M.tuberculosis* demonstrated that each type of mycolic acids was capable of inducing cholesterol accumulation (as measured by staining with filipin) (**Figure 4.19**). By this method it is not possible to determine whether one mycolic acid type gives a more pronounced phenotype than the others.

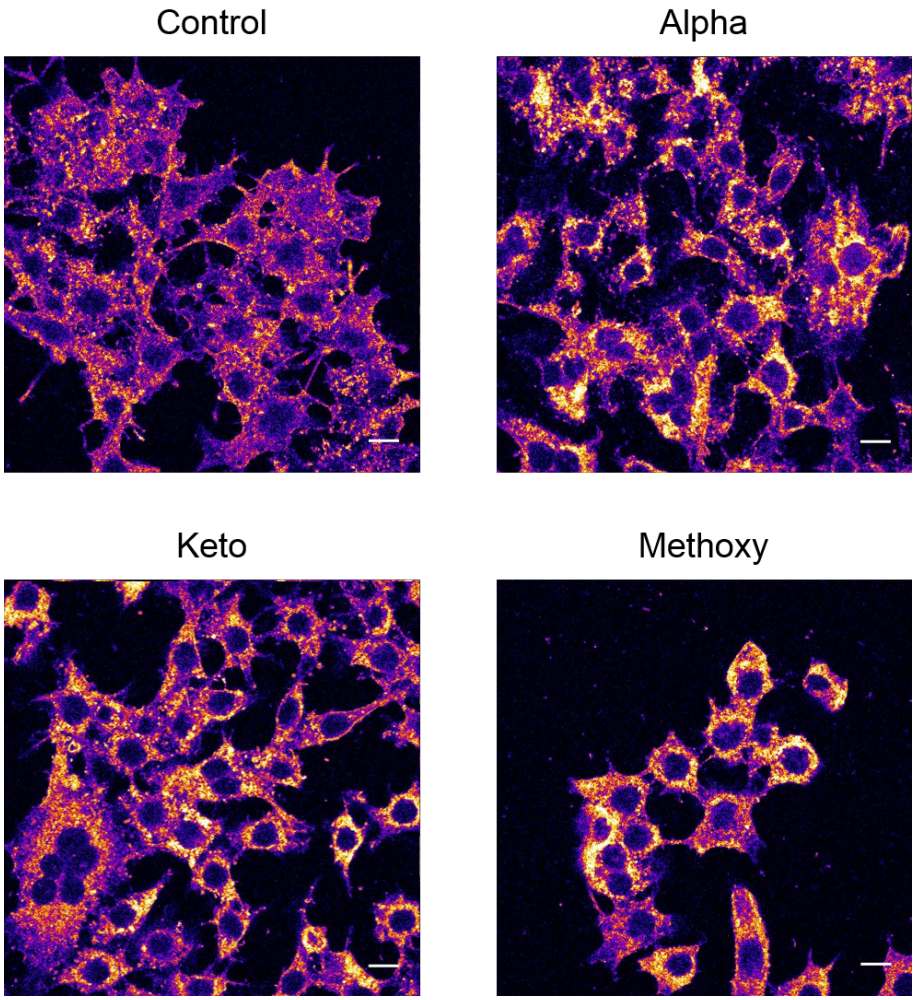

Figure 4.19: **Effect of mycolic acids on cholesterol distribution in RAW 264.7 macrophages**. Images acquired via laser scanning confocal microscopy by Doris Höeglinder at EMBL, Heidelberg. 24hr treatment, 1ng/ml lipid. Yellow - filipin (cholesterol). Scale bar - 10µm.

4.4 Discussion

In this chapter we demonstrate that the NPC cellular phenotypes observed in wild-type macrophages infected with pathogenic mycobacteria can also be induced using lipids from the mycobacterial cell wall in the absence of the mycobacteria itself. A general mycolic acid fraction containing a mixture of the mycolic acids found in the cell wall of the pathogenic mycobacteria *M.bovis* was able to induce similar storage of cholesterol (**Figure 4.4/4.5**) and mistrafficking of GM1 ganglioside (**Figure 4.7**) as seen following BCG infection. This was observed in both murine and human wild-type macrophages.

Investigations into the identity of the phenotype-inducing lipid species implicated the glycomycolate TDM as a good candidate for inhibition of the NPC pathway. Macrophages incubated with *Mtb* TDM showed significant increases in LysoTracker fluorescence, indicative of lysosomal compartment expansion (**Figure 4.8**). No such increase was associated with GMM from *M.smegmatis*. Further investigations with TDM showed that it was capable of inducing other NPC cellular phenotypes. Significantly these included a reduction in lysosomal Ca^{2+} similar to that observed in BCG infected macrophages (**Figure 4.9/4.10**). Reduced lysosomal [Ca^{2+}] is considered unique to NPC [20].

The immunological properties of TDM, and its importance to mycobacterial virulence, have been well documented. It is the most abundant lipid species in *Mtb* [183] and its presence is essential for the mycobacteria's intracellular persistence. *Mtb* in which TDM has been removed via petroleum ether extraction shows decreased intracellular viability and increased co-localisation with the late-endosome/lysosome [186]. Infection with these de-lipidated bacteria is associated with reduced production of pro-inflammatory cytokines [186]. A reduction in TDM due to mutation is also associated with increased co-localisation between the phagosome and acidic compartment [187]. TDM has been previously shown

to be capable of preventing phagosomal maturation, and inducing the formation of foam cells and caseating granulomas in the absence of intact mycobacteria [181] [182] [183].

Investigations into the relationship between mycolic acid structure and their effect on the NPC pathway are so far inconclusive. A number of synthetic mycolic acids (without sugar head groups) were investigated for their effects on LysoTracker fluorescence levels in wild-type macrophages. The lipids could be broadly divided into those that had no effect, those associated with increased LysoTracker staining (as observed in NPC cells) and those associated with a decrease in fluorescence. Whilst there were a number of lipids that gave a significant increase in LysoTracker staining (**Figure 4.14**) it is unlikely that these lipids play a role in the pathogenicity of *Mtb*, with them either possessing structures that are not found in the *Mtb* cell wall, or being present at very low levels (although the latter issue would not necessarily preclude biological relevance). There were a number of lipids that were associated with a significant increase in LacCer levels, a phenotype of both NPC and TB [119]. Interestingly, these lipids were those associated with significantly decreased levels of LysoTracker fluorescence (**Figure 4.15**). A decrease in LysoTracker fluorescence could be due to reduced acidic compartment volume. However, the accumulation of LysoTracker in the acidic compartment depends upon the acidic pH of the organelle [147]. If lysosomal pH is altered as a result of lipid treatment then this could result in reduced LysoTracker fluorescence. It will be neccessary to investigate the lysosomal pH in lipid treated cells.

We also carried out using experiments using synthetic representative versions of the 3 mycolic acid classes found in the *Mtb* cell wall (alpha, keto and methoxy). Alpha mycolic acids appeared to be the most potent, giving a significant increase in LysoTracker fluorescence at low concentrations (1ng/ml). Increased concen-

trations of keto-mycolic acids were associated with an increase in LysoTracker fluorescence (**Figure 4.18**). No significant increase in LysoTracker was observed following incubation with any concentration of methoxy-mycolic acids. However, 1ng/ml of each mycolic acid class appears sufficient to induce cholesterol accumulation in wild-type RAW 264.7 macrophages (**Figure 4.19**). Alpha mycolic acids are the most prevalent mycolic acid in *Mtb*, comprising around 70% of the total mycolic acid content [167]. Methoxy and keto mycolic acids each make up around 10-15% of the total [167].

Attempts to probe the structure-function relationship of lipids in this chapter used free mycolic acids. One future direction would be to investigate the effect of the trehalose head group on the phenotype-inducing ability of the lipid, and whether the lipids were more potent when in their glycomycolate form. As discussed in Section 4.1 there is an enormous amount of structural diversity in the cell wall lipids of mycobacteria, both in the structure of the mycolic acids themselves and the context in which they are found. Further investigation will be required to determine those lipid structures responsible for the inhibition of the NPC pathway.

Summary

Work described in this chapter supports a model in which mycobacteria inhibit the host NPC pathway via lipids shed from their cell wall, and provide a mechanistic basis for our observations in Chapters 2 and 3. We have identified TDM as a lipid species likely to play a role in phenotype induction. Attempts to probe the relationship between mycolic acid structure and phenotype-inducing ability are so far inconclusive.

5 NPC1 as a Target During Infection with Pathogenic Mycobacteria

5.1 Introduction

5.1.1 Proteins in the NPC Pathway

NPC disease is caused by mutations in the *NPC1* and *NPC2* genes, with mutations in these genes accounting for, respectively, 95% and 5% of clinical cases [6]. Whether the mutation is in the *NPC1* or *NPC2* gene (or indeed both) appears to make no difference in terms of cellular or clinical phenotypes, suggesting that NPC1 and 2 have non-redundant roles in the cell [15].

We have shown in Chapters 2-4 that infection with pathogenic mycobacteria is associated with the induction of NPC disease phenotypes in wild-type cells, supporting a model in which cellular persistence is achieved via inhibition of the NPC cellular pathway. However, this work provided no indication as to whether it is the NPC1 or NPC2 protein which is targeted during infection with pathogenic mycobacteria (or by lipids derived from their cell walls).

NPC1

There is currently no crystal structure for NPC1. The predicted structure for NPC1 consists of 13 transmembrane domains, with domains 8-13 a repeat of domains 2-7 [14]. The additional domain, domain 1, contains a hydrophilic loop. This loop is one of three in NPC1, with each protruding into the lysosomal lumen. Each of the loops exhibits a high level of glycosylation, likely to protect them from the degradative environment of the acidic compartment lumen [188]. The cytoplasmic tail contains a dileucine sequence required for the delivery of the protein to the endosomal system [189].

Domains 3-7 are designated as a sterol sensing domain due to their homology to the sterol sensing domains of 3-hydroxy-3-methylglutaryl coenzyme A reductase (HMGR) and sterol regulatory element binding protein cleavage-activating protein (SCAP) [190]. Both of these proteins are involved in cholesterol homeostasis. Binding of sterols to the purified human NPC1 protein has been previously demonstrated *in vitro* [191]. NPC1 also has homology with Patched (involved in tumour supression) [192], and with the Niemann-Pick C1-like 1 protein [193]. The latter protein is present in hepatocytes and in epithelial cells of the gastrointestinal tract where it plays a role in the absorption of cholesterol [194].

NPC1 exhibits the greatest homology with the RND permeases [14]. These are a group of prokaryotic proteins involved in the efflux of substances from the interior of the pathogen. NPC1 is more homologous to the members of this family of proteins than to any of the proteins listed above [14]. For example, the MexD protein from *Pseudomonas aeruginosa* shares the duplicated structure of NPC1, having a total of 12 TM domains, with domains 7-12 duplicates of 1-6. The two hydrophilic loops of MexD (between domains 1/2 and 7/8) are similar to the second and third hydrophilic loops of NPC1. The 1st hydrophilic loop is part

of the 13th domain of NPC1 (not present in MexD). This additional structure likely evolved after NPC1 diverged from the RND permease family [14]. NPC1 is able to act as a permease in *E.coli*, transporting acriflavine and oleic acid across the plasma membrane [14].

NPC2

A crystal structure exists for the NPC2 protein [16]. The protein is small (132 amino acids versus 1278 in NPC1) and possesses a Ig-like fold stabilised by 3 disulphide bonds. It is present in the lysosomal lumen, and is trafficked to this compartment via mannose-6-phosphate (M6P) targeting [16] [195]. The cholesterol-binding properties of NPC2 are well documented, both by crystallography and by mutational studies [196]. It is proposed to bind cholesterol in a hydrophobic cavity. In addition to cholesterol NPC2 has been demonstrated to bind the analogues cholesterol-3-*O*-sulphate, dehydroergosterol, cholestatrienol and 22-(*N*-(7-nitrobenz-2-oxa-1,3-diazol-4-yl)amino)-23,24-bisnor-5-cholen-3β-ol (NBD-cholesterol) [10] [191]. NPC2 has recently been implicated in the maturation of spermatozoa in mice, being required for the regulation of cholesterol during the maturation process [197]. *Npc2*$^{-/-}$ spermatozoa exhibited decreased fertility.

5.1.2 Does Pre-existing Dysfunction in the NPC Pathway Impair Clearance of Non-pathogenic Mycobacteria?

If pathogenic mycobacteria achieve cellular persistence by inhibition of the NPC pathway then it follows that cells with a pre-existing dysfunction in the NPC pathway may exhibit defects in the clearance of intracellular pathogens. Non-pathogenic bacteria, which would be cleared efficiently by a wild-type cell, may therefore persist. *M.smegmatis* was used in Chapters 2 and 3 as a non-pathogenic

representative of the *Mycobacterium* genus. It will be used here as an example of a mycobacteria that is readily cleared by wild-type cells.

The molecule (3-β-[2-(diethylamino)ethoxy]androst-5-en-17-one), henceforth referred to as U18666A, is a widely-used method of pharmacologically inducing NPC cellular phenotypes in wild-type cells [20] [70] [71] [198]. It is able to prevent the movement of cholesterol out of the lysosome (and the intracellular movement of cholesterol as a whole) [199]. If a functional NPC pathway is required for efficient clearance of intracellular bacteria then treatment of wild-type cells with U18666A should result in increased persistence of the non-pathogenic *M.smegmatis*. Similar persistence should be observed in cells with a mutation in the NPC pathway.

The aims of the work presented in this chapter are:

* Investigate whether the NPC pathway inhibition observed in previous chapters occurs at the level of the NPC1 or NPC2 protein.

* Investigate if a pre-existing NPC pathway dysfunction results in reduced clearance of the non-pathogenic *M.smegmatis*.

5.2 Materials and Methods

5.2.1 Cells

Murine bone marrow macrophages were isolated from wild-type, *Npc1*$^{+/-}$ and *Npc1*$^{-/-}$ mice as previously described [200]. Murine resident peritoneal macrophages were obtained via peritoneal wash of 8 week old wild-type and *Npc1*$^{-/-}$ mice. The resulting cell suspension was centrifuged (1500rpm/5min) and resuspended in RPMI supplemented with 10% FCS, 1% glutamine and 1% P/S. All mouse studies used protocols approved by UK Home Office (Animal Scientific Procedures Act, 1986). Chinese hamster ovary cells expressing variable levels of NPC1 were kindly provided by Dr. Dan Ory (St Louis, USA) and maintained in DMEM-F12 supplemented with 10% FCS, 1% P/S and 1% glutamine [201]. RAW 264.7 cells and primary human macrophages were obtained and cultured as described in Sections 2.2.1 and 3.2.3 respectively.

5.2.2 Lipids

TDM from *M.bovis* and synthetic mycolic acids were obtained as previously described (Section 4.2.2).

5.2.3 Mycobacterial Culture

Production, culture and long-term storage of mCherry-expressing mycobacteria were as detailed in Sections 2.2.1, 2.2.2, 2.2.3 and 2.2.4.

5.2.4 Infection of Host Cells

As detailed in Section 2.2.5.

5.2.5 Microscopy

As detailed in Sections 2.2.13 and 2.2.15.

5.2.6 Fixation of Cells

As detailed in Section 2.2.14.

5.2.7 Quantification of Mislocalisation of Sphingomyelin and GM1 Ganglioside

Bone marrow macrophages from wild-type and *Npc1*$^{+/-}$ mice were plated onto coverslips and approximately 18hr later treated with TDM. Post-treatment period, coverslips were assayed for mislocalisation of GM1 ganglioside and sphingomyelin. Localisation of GM1 ganglioside was carried out as detailed in Section 3.2.11. Intracellular distribution of sphingomyelin was investigated via specific binding with Lysenin (Peptanova) [202]. Pre-fixed coverslips were blocked for 8 hours at room temperature (1% BSA, 0.1% saponin in PBS). Blocking buffer was replaced with 0.5 µg/ml Lysenin in blocking buffer overnight at 4°C. Lysenin was replaced with Lysenin antiserum (Peptides International) (1:500 dilution in blocking buffer) for 1hr at room temperature. Post-PBS wash secondary Oregon Green antibody solution was added (diluted 1:200 in blocking buffer) for 30min at room temperature. Post-visualization (via microscopy), the percentage of total cells exhibiting a 'NPC-like' punctate lysosomal distribution pattern was counted.

5.2.8 Quantification of NPC1/2 Protein Levels via Western Blot

Western blot of BCG-infected RAW 264.7 macrophages was performed by Dr. Ian Williams. Western blot of *M.smegmatis*-infected macrophages was performed by Elias Adriaenssens.

Gel composition was as follows:

	Stacking Gel	**Seperating Gel**	
		NPC1	**NPC2**
mQ H_2O (ml)	10.0	13.6	10.6
Acrylamide (ml)	2.0	7.0	10.0
1.5M Tris HCl (ml)	1.44	8.0	8.0
10% Sodium Dodecyl Sulphate (µl)	144.0	307.2	307.2
10% APS (µl)	96.0	307.2	307.2
TEMED (µl)	19.2	48.0	48.0

Protein (10µg) was separated on gel at 25mA before transfer onto nitrocellulose membrane (Immoblian P) at 40mA/membrane. Membranes were blocked overnight at 4°C in Tris Buffered Saline containing 0.1% Tween-20 and 5% powdered milk, before probing with NPC1 Primary Antibody (1 in 5000 dilution) (Pierce) overnight at 4°C. Membrane was then probed with Horseradish Peroxidase-linked anti-rabbit secondary antibody (Pierce) (1 in 20000 dilution). Membranes were stripped and re-probed with anti-actin specific antibody (at 1 in 5000 dilution) to demonstrate equal protein loading into each lane.

5.2.9 Quantification of *M.smegmatis* Clearance via Microscopy

Host cells (either primary human macrophages or murine resident peritoneal macrophages) were seeded overnight on acid-washed coverslips (at around 1x10^5 cells per slip) prior to incubation with either fresh media only or media containing 2 µg/ml U18666A. After 48hrs cells were infected with mCherry-expressing *M.smegmatis* (MOI 12.5) and incubated at 37°C/5% CO_2 for 2 hours. Cells were washed, and incubated at 37°C/5% CO_2 with fresh medium. At stated time point coverslips were washed, PFA fixed, and *M.smegmatis* clearance quantified via microscopy.

5.2.10 Quantification of *M.smegmatis* Clearance via FACS

RAW 264.7 cells were seeded overnight in 6-well plates (1 x 10^6 per well) prior to incubation with either fresh media only or media containing 2 µg/ml U18666A. After 48hrs cells were infected with mCherry-expressing *M.smegmatis* (MOI 5) and incubated at 37°C/5% CO_2 for 2 hours. Cells were washed twice with media and treated with 200µg/ml amikacin (Sigma-Aldrich) (1hr, 37°C/5% CO_2) to kill extracellular mycobacteria. Post-treatment, amikacin-containing media was removed and cells were washed with 3x1ml media before addition of media with 2µg/ml amikacin and incubation at 37°C/5% CO_2. At stated time point wells were washed with 2x1ml FACS buffer (see Section 4.2.12), PFA fixed and moved to FACS tube for analysis. FACS analysis used equipment as detailed in Section 4.2.12. Levels of fluorescence were used as a readout for levels of intracellular *M.smegmatis* load. Development of this protocol is detailed in Section 5.3.6.

5.2.11 Statistical Analysis

Statistical analysis was performed using GraphPad Prism (ver 6.0). The specific test used is indicated in the figure legend.

5.3 Results

5.3.1 Quantification of Mislocalisation of Sphingomyelin and GM1 Ganglioside

Bone marrow macrophages from both wild-type and *Npc1*$^{+/-}$ mice were incubated with TDM. The effect of TDM was measured by quantifying the percentage of total observed cells showing 'NPC-like' mislocalisation (i.e. sequestration of lipid in the LE/Lys) of sphingomyelin and GM1 ganglioside. We observed that cells with 50% of wild-type NPC1 protein levels were more susceptible to the NPC phenotype-inducing effects of TDM (**Figure 5.1**). In the absence of TDM there was no significant difference in the GM1/sphingomyelin trafficking ability of wild-type and *Npc1*$^{+/-}$ macrophages (**Figure 5.1**). When cells were treated with TDM both genotypes showed an increase in the proportion of total cells mislocalising GM1 and sphingomyelin. However, lipid mislocalisation was observed in a significantly greater proportion of the *Npc1*$^{+/-}$ macrophages than the wild-type cells (**Figure 5.1 $p<0.05/0.01$**).

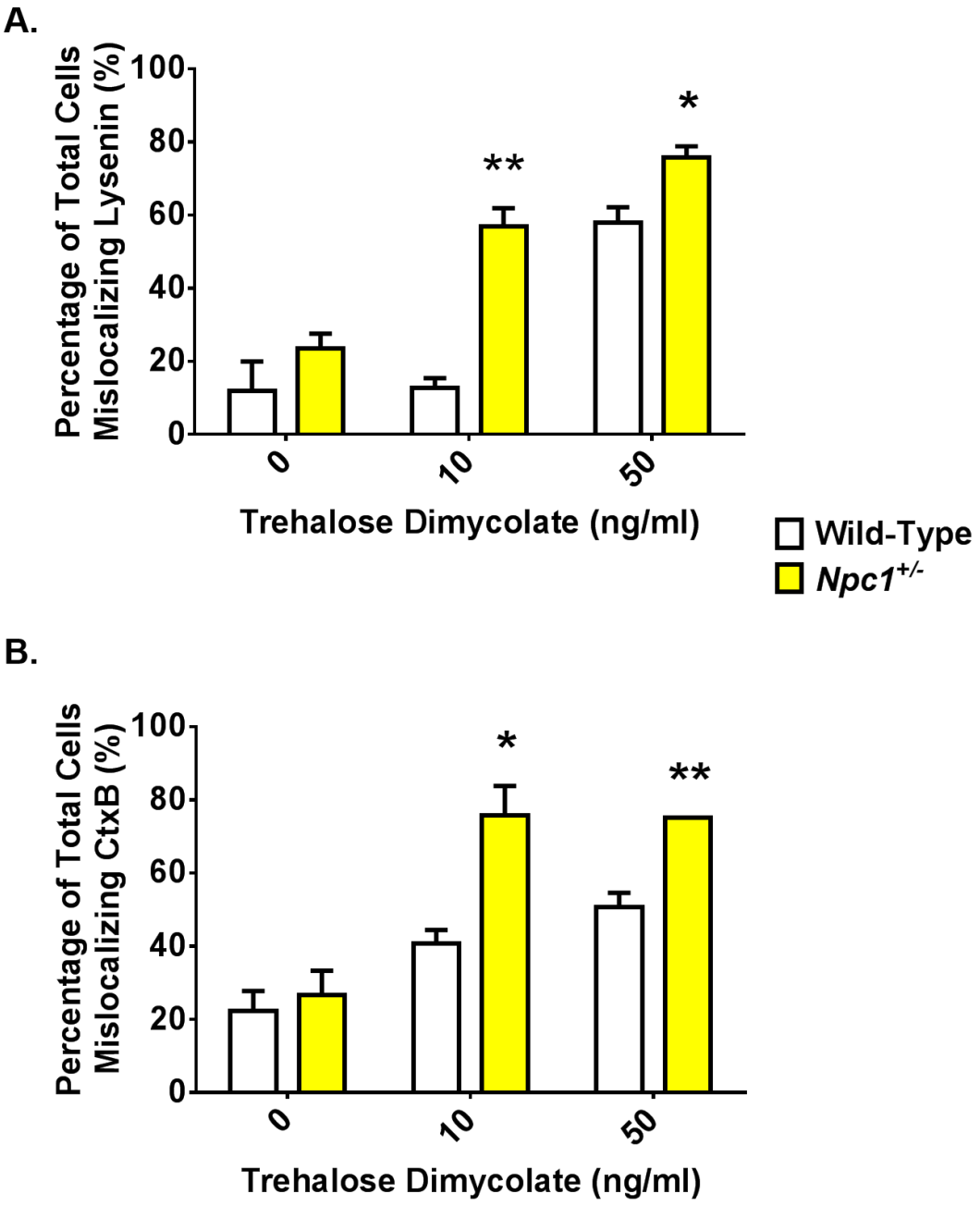

Figure 5.1: **Differential effect of TDM on lipid distribution in wild-type and *Npc1*$^{+/-}$ murine bone marrow macrophages**. 48hr lipid treatment. **A.)** Sphingomyelin mislocalisation. **B)** GM1 ganglioside mislocalisation. *- $p<0.05$, ** - $p<0.01$ versus wild-type (via t-test). Mean ± SEM of 3 fields of cells/group, >10 cells/field.

5.3.2 Resistance of NPC1-overexpressing Chinese Hamster Ovary Cells to TDM-induced GM1 Ganglioside Mislocalisation

Wild-type Chinese hamster ovary cells, and those overexpressing NPC1, were exposed to TDM. The ability of the Chinese hamster ovary cells to traffic GM1 ganglioside was subsequently investigated. In the wild-type cells incubation with TDM resulted in a punctate staining pattern, indicative of GM1 storage in the lysosome (**Figure 5.2**). As the concentration of TDM was increased the phenotype became more pronounced. This staining pattern was similar to that seen in *Npc1*$^{-/-}$ cells (**Figure 5.2**). NPC1-overexpressing cells exhibited less punctate staining in response to TDM treatment, suggesting that they retained most of their GM1 trafficking abilities (**Figure 5.2**). Cells with 5-fold wild-type levels appeared to be less resistant to phenotype induction than the 15-fold overexpressors, with slightly higher punctate staining following TDM treatment (**Figure 5.2**).

5.3.3 NPC1/2 Protein Levels post-Mycobacterial Infection

We investigated the effect of mycobacterial infection on NPC1/2 protein expression in RAW 264.7 macrophages. We observed a significant increase in NPC1 protein levels in BCG-infected macrophages relative to uninfected controls, with infected macrophages exhibiting a 5-fold increase in NPC1 (**Figure 5.3, p-0.0008**). No change was observed in NPC2 levels (**Figure 5.3**).

A preliminary experiment (n=1) looking at the effect of the non-pathogenic *M.smegmatis* on NPC1 levels in RAW 264.7 macrophages suggested that NPC1 levels are not increased as a result of *M.smegmatis* infection (**Figure 5.4**). However, this experiment will need to be repeated in order to draw firm conclusions.

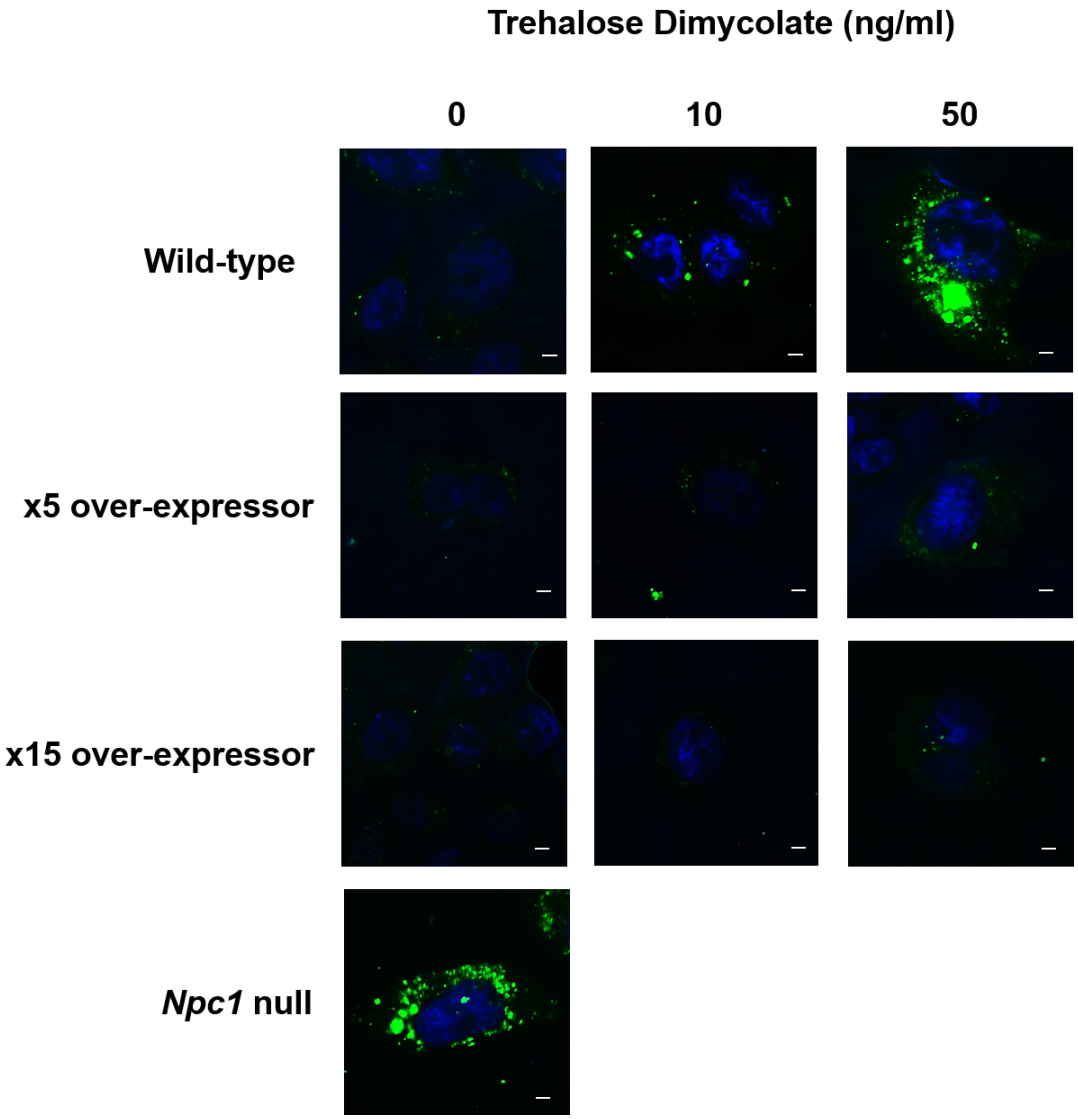

Figure 5.2: **Differential effect of TDM on GM1 trafficking in Chinese hamster ovary cells with variable NPC1 levels.** 48hr lipid treatment. Images shown are representative. Green - CtxB (GM1 ganglioside), blue - hoescht (nucleus). An untreated *Npc1*$^{-/-}$ Chinese hamster ovary cell is provided for reference. Scale bar - 5µm.

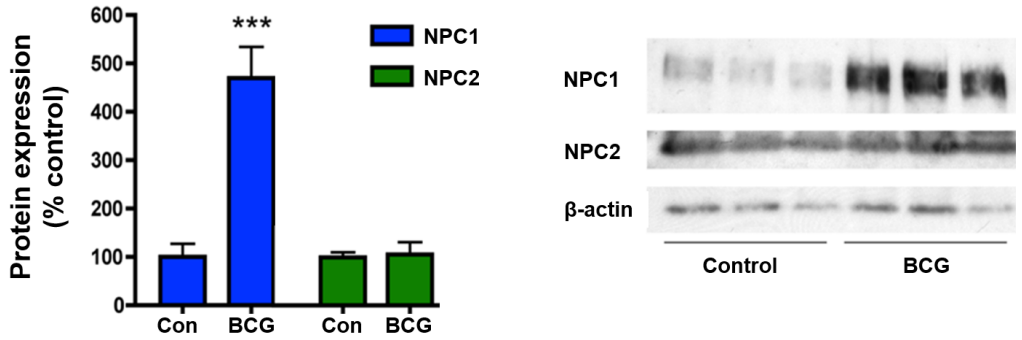

Figure 5.3: **Quantification of NPC1/NPC2 protein levels in BCG-infected RAW 264.7 macrophages.** 48hr infection, MOI 12.5. NPC1/2 protein levels in control and BCG-infected RAW 264.7 macrophages. Protein levels expressed as percentage change relative to uninfected controls. Mean ± SEM of 3 biological replicates. *** $p<0.001$ versus control (via t-test). Western blot showing protein loading (multiple lanes indicating biological replicates) β-actin controls.

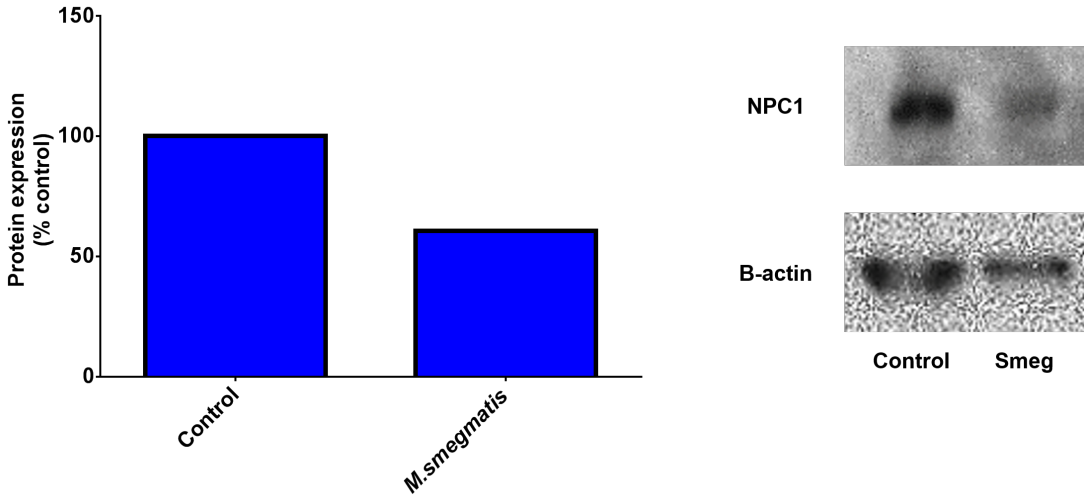

Figure 5.4: **Quantification of NPC1 protein levels in *M.smegmatis*-infected RAW 264.7 macrophages.** 48hr infection. NPC1 protein levels in control and *M.smegmatis*-infected RAW 264.7 macrophages. Protein levels expressed as percentage change relative to uninfected controls. n=1. Western blot showing protein loading β-actin controls.

5.3.4 *M.smegmatis* Clearance by Murine Resident Peritoneal Macrophages

Dysfunction of the NPC pathway in murine resident peritoneal macrophages was associated with decreased clearance of *M.smegmatis*. Four hours into the 'chase' period (following a 2hr infection with the mycobacteria) around 40% of the total wild-type macrophages exhibited intracellular *M.smegmatis* (quantified via microscopy) (**Figure 5.5**). A comparison with both *Npc1*$^{-/-}$ macrophages and wild-type macrophages in which a NPC phenotype had been pharmacologically induced (via 48hr treatment with 2 µg/ml U18666A) showed that macrophages with a functional NPC pathway had signficantly lower levels of infection (40% versus 60%) (**Figure 5.5, p - 0.0446 (WT vs WT + U18666A)/0.0211 (WT vs NPC1$^{-/-}$)**. This was indicative of enhanced mycobacterial clearance.

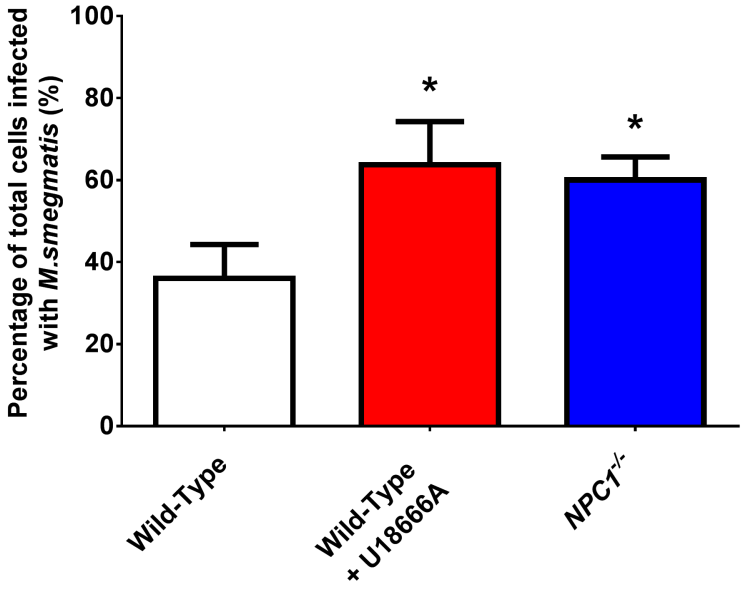

Figure 5.5: **Persistence of fluorescent *M.smegmatis* in *Npc1*$^{-/-}$ murine resident peritoneal macrophages and wild-type macrophages in presence/absence of U18666A.** Where indicated, cells were pre-treated for 48hr with 2µg/ml U18666A. 2hr infection, MOI 12.5. Cells fixed 4 hours post-infection period. Mean ± SEM of n>73 individual cells/group. * p<0.05 versus wild-type control (via t-test).

5.3.5 *M.smegmatis* Clearance by Primary Human Macrophages

Decreased clearance of *M.smegmatis* was also observed in primary human macrophages following pharmacological induction of an NPC phenotype. Cells pre-treated with U18666A (48hr, 2µg/ml) prior to infection showed a significantly higher level of infection than the untreated controls, with around 20% of control cells and 40% of U18666A-treated cells harbouring *M.smegmatis* (**Figure 5.6, p - 0.0312**).

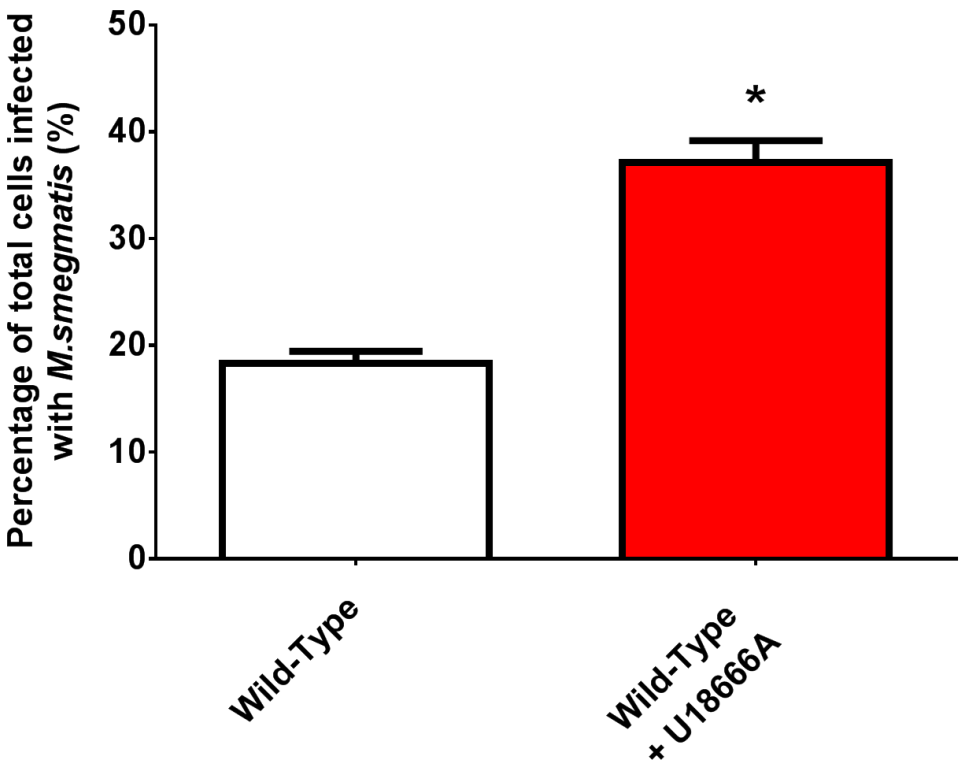

Figure 5.6: **Persistence of fluorescent *M.smegmatis* in U18666A-treated primary human macrophages.** Where indicated, cells were pre-treated for 48hr with 2µg/ml U18666A. 2hr infection, MOI 12.5. Cells fixed 18 hours post-infection period. Mean ± SEM of n>84 individual cells/group. * $p<0.05$ versus wild-type control (via t-test).

5.3.6 *M.smegmatis* Clearance by RAW 264.7 Cells as Quantified by FACS

The above investigations into the ability of macrophages to clear *M.smegmatis* were carried out by microscopy. The main drawback of this method is that it is fairly time consuming (when considered in terms of the time required to assay a relatively small number of cells (<300)). As the *M.smegmatis* used is fluorescent it should be feasible to use FACS to quantify the level of intracellular infection in a population of host cells. The development of this method is detailed below.

Choice of FACS Channel for Detection of *M.smegmatis*

The first step was to determine which FACS channel was the most appropriate for the detection of the mCherry-expressing *M.smegmatis*. We measured the fluorescence of both uninfected cells and those infected with *M.smegmatis* using a number of different channels. The data below is presented as the fold increase in fluorescence in the infected cells relative to the uninfected controls (**Figure 5.7A**). We observed that the PerCP-Cy5 channel was the most sensitive to the presence of *M.smegmatis*, with infected cells showing a 20-fold increase in fluorescence. The APC and Pacific Blue channels were also sensitive to *M.smegmatis*. Below we show FACS histograms of RAW 264.7 macrophage populations infected with *M.smegmatis* at a range of MOIs (**Figure 5.7B**). A higher MOI was associated with a higher mean level of fluorescence across the total cell population.

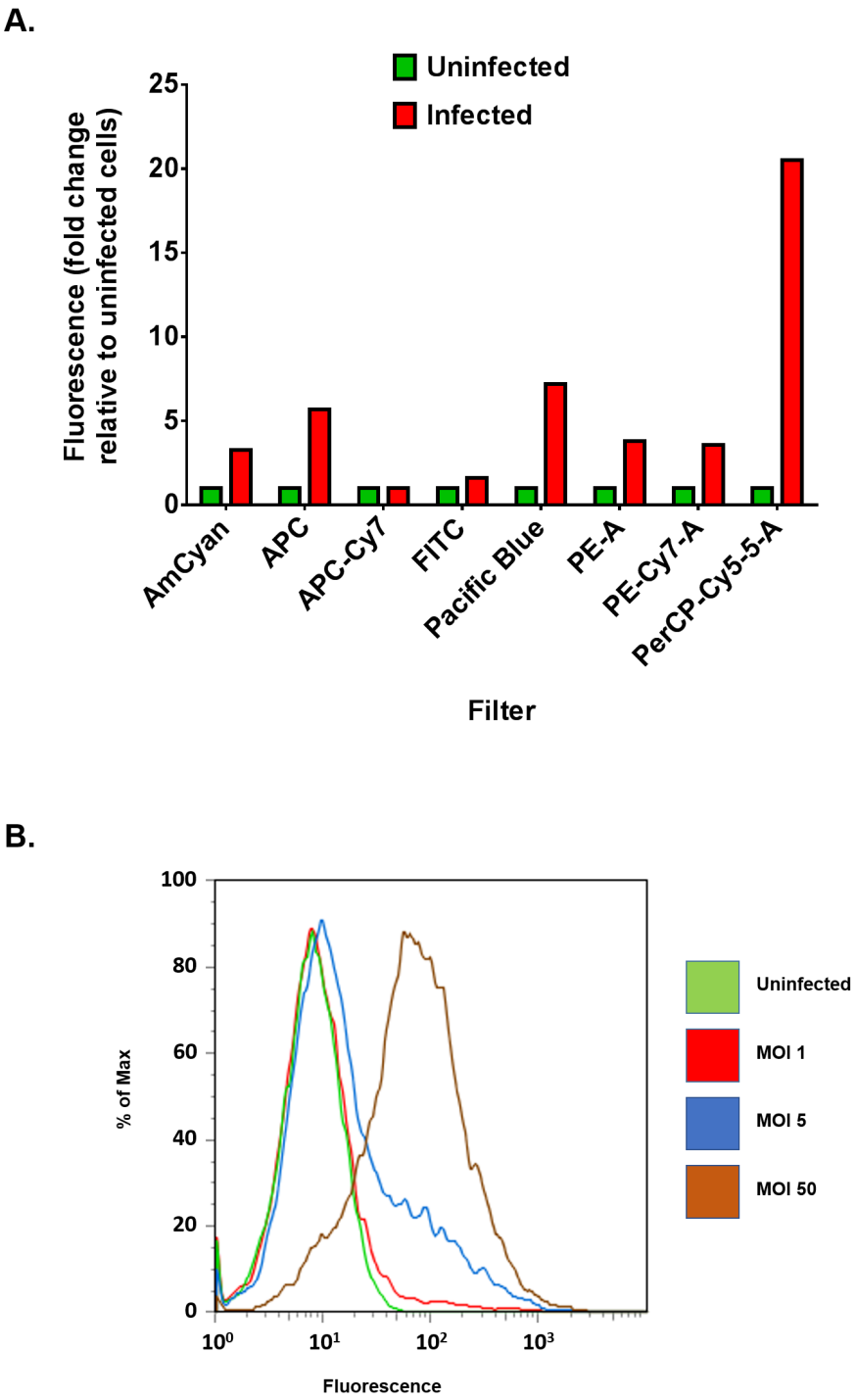

Figure 5.7: **Detection of *M.smegmatis* via FACS. A.)** Fold change in fluorescence in RAW 264.7 macrophages infected with mCherry-expressing *M.smegmatis* as measured using different FACS channels. Macrophages infected at MOI 5. Fold change relative to uninfected cells. n=1. **B.)** FACS histograms of RAW 264.7 macrophages infected with *M.smegmatis* at a range of MOIs. Measured using the PerCP-Cy5 channel.

Effect of U18666A Pre-Treatment on *M.smegmatis* Clearance by RAW 264.7 Macrophages

RAW 264.7 macrophages were pre-treated with U18666A (48hr, 2µg/ml) to induce NPC cellular phenotypes prior to infection with *M.smegmatis*. Immediately after the infection period (and subsequent washing), those cells pre-treated with U18666A had a lower mean fluorescence than the control cells (**Figure 5.8A, p - 0.0763**). This was not due to any intrinsic fluorescence of the drug. It could be indicative of the treated cells having decreased uptake of the mycobacteria. Therefore the initial mycobacterial load (at the beginning of the chase period) is greater in the wild-type cells.

Due to this initial difference in fluorescence subsequent time points were analysed in terms of fold change: the levels of mean fluorescence in that cell population relative to that at t=0. We observed that 24 hours post-wash, both control and U18666A-treated cells showed a decrease in mean fluorescence (relative to t=0) (**Figure 5.8B**). This decrease was significantly greater in the control cells (**Figure 5.8B, p - 0.0066**), suggesting that they have dealt with their initial infectious burden more efficiently than the treated cells.

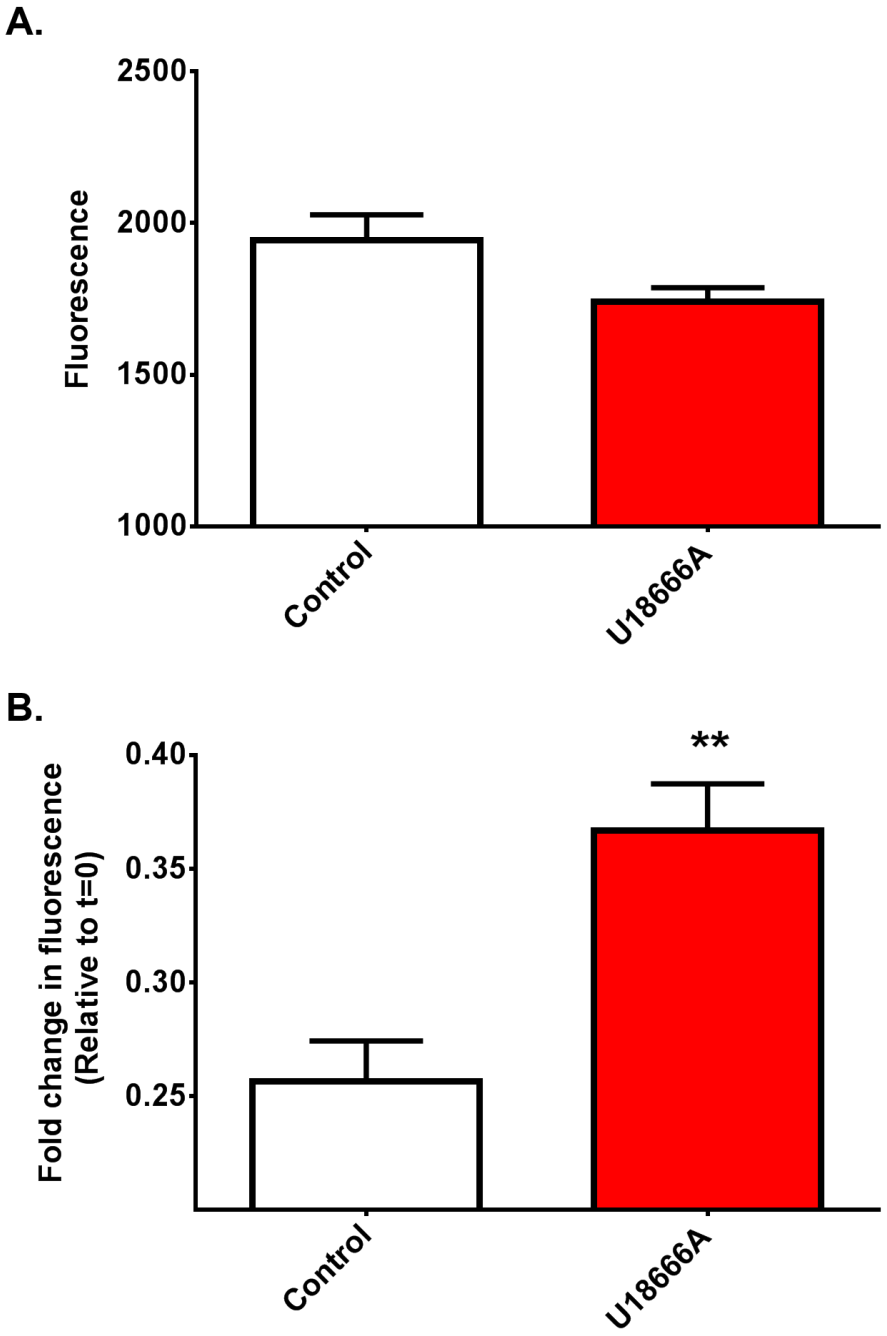

Figure 5.8: **Effect of U18666A treatment on the clearance of *M.smegmatis* from RAW 264.7 macrophages as quantified by FACS.** MOI 5. **A.)** Mean fluorescence of macrophages (with or without 48hr pre-treatment with 2µg/ml U18666A) immediately after infection with mCherry-expressing *M.smegmatis* for 2 hours. Mean ± SEM of 4 biological replicates per group. **B.)** Mean fluorescence of macrophages (with or without pre-treatment with U18666A) 24 hours post-infection period. Fold change in mean fluorescence relative to t=0. Mean ± SEM of 4 biological replicates per group. ** $p<0.01$ versus untreated *M.smegmatis*-infected controls (via t-test).

5.3.7 Interaction Between NPC1 and Synthetic Mycolic Acids

Work in this chapter has implicated the NPC1 protein as a target during mycobacterial infection. Chapter 4 supported a model in which the NPC pathway is inhibited by lipids shed from the mycobacterial cell wall. Together, this suggests that mycobacterial lipids will inhibit the NPC pathway via binding to NPC1.

There exists an assay capable of measuring ligand binding to NPC1 [191]. This assay exploits the intrinsic fluorescence of the Trp residues found in the NPC1 protein. The figure below shows the effect of U18666A and the sterols cholestatrienol and dehydroergosterol on Trp fluorescence (**Figure 5.9A**). Addition of these molecules was associated with a decrease in Trp fluorescence, indicative of binding of the ligands to NPC1. The Sharom lab kindly agreed to test the synthetic lipids used in Chapter 4 (Section 4.3.9) and investigate whether they bind to NPC1. We selected KB9 and JRMM 267C on the basis that KB9 gave a drastic increase in LysoTracker fluorescence and JRMM 267C was associated with no response (**Figure 5.9B**).

These experiments were inconclusive, with neither lipid associated with a change in Trp fluorescence (data not shown). It was posited that this was due to a concentration issue. In earlier experiments the lipids were added to intact cells (Section 4.3.9). Upon addition the lipids likely associate with the cell membrane. This means that the concentration of lipids at the cell membrane was much higher than the aqeuous concentration. In the NPC1 binding assay however, the NPC1 protein was purified and in detergent solution. The amount of NPC1 used in this experiment was much greater than in the FACS experiments, meaning the ratio of lipid:NPC1 protein was much smaller. The lack of Trp fluorescence quenching therefore does not neccesarily reflect a lack of interaction, but that the levels of lipid used would need to be greater.

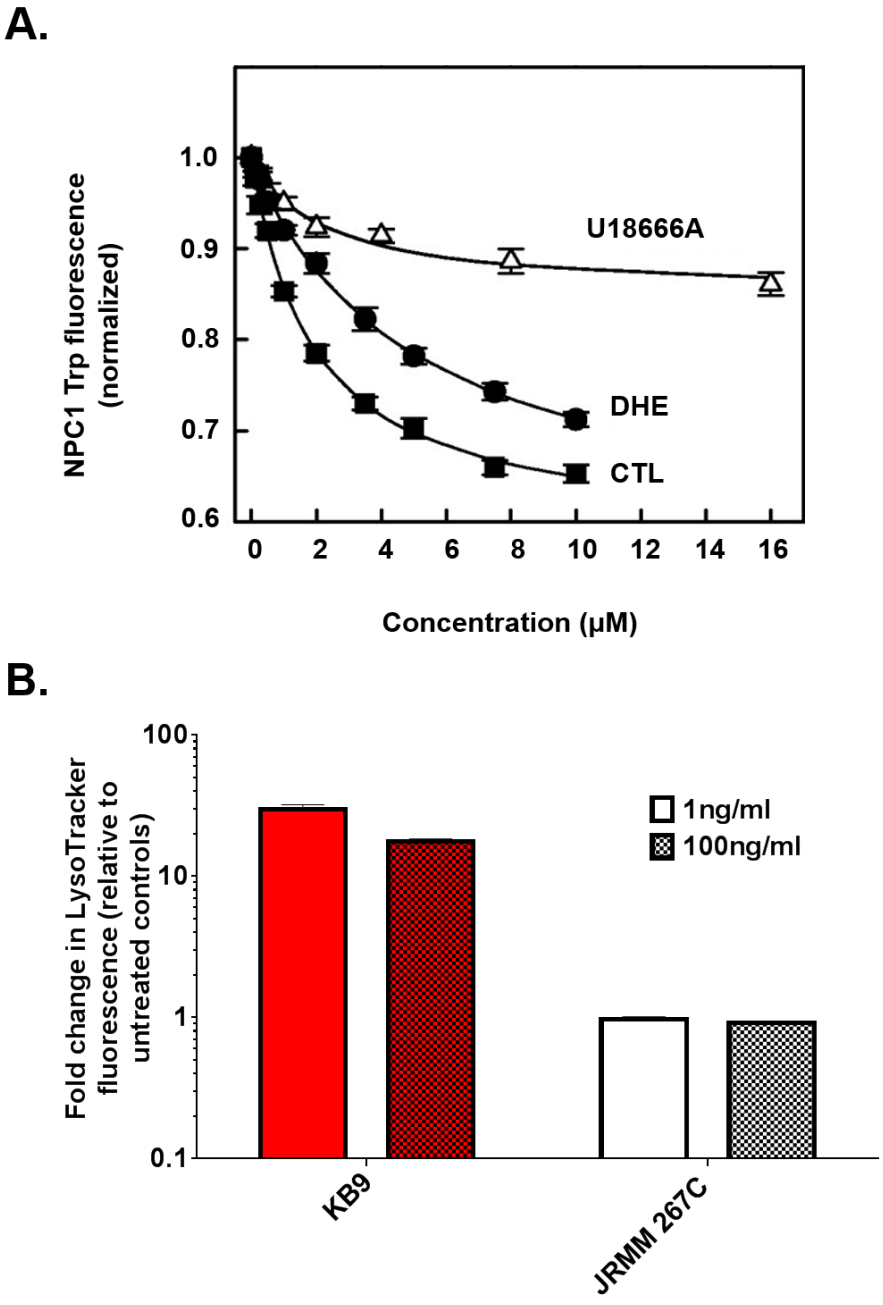

Figure 5.9: **Binding of synthetic myolic acids to NPC1 A.)** Quenching of NPC1 Trp fluorescence emission at 330 nm following excitation at 290 nm, in the presence of increasing concentrations of dehydroergosterol (DHE) (•), cholestatrienol (CTL) (■), and U18666A (△). The quenching data were fitted to an equation describing binding to a single site. Data points represent the mean ± range (n = 2). Adapted from [191] **B.)** Effect of synthetic mycolic acids on LysoTracker staining levels in RAW 264.7 macrophages. 24 hour treatment period at 1 or 100ng/ml. Values are fold-change in fluorescence relative to that in untreated macrophages. Red - significant increase in LysoTracker staining (see Fig 4.14). Mean ± SEM of 4 biological replicates.

5.4 Discussion

In this chapter we provide evidence that the NPC1 protein is targeted during mycobacterial infection, and that NPC1 inhibition is responsible for the lipid mistrafficking observed upon infection/ treatment with mycobacterial lipids. The susceptibility of a cell to TDM-induced lipid mistrafficking is inversely proportional to the amount of functional NPC1 protein the cell possesses; *Npc1*$^{+/-}$ macrophages were more sensitive than their wild-type counterparts, whilst overexpressing Chinese hamster ovary cells were resistant to the effect of TDM (**Figure 5.1/5.2 respectively**). We also observed that NPC1 levels were significantly increased in BCG-infected RAW 264.7 macrophages (**Figure 5.3**). This mirrors observations from the TB granuloma [119]. The overexpression of NPC1 may reflect an attempt by the cell to compensate for reduced protein function by increasing copy number. Preliminary experiments showed no such increase with *M.smegmatis* (**Figure 5.4**), although these experiments will need to be expanded upon.

No change in NPC2 levels were observed as a consequence of BCG infection (**Figure 5.3**). This conflicts with recent reports which showed reduced expression of *NPC2* in monocytes within the TB granuloma [203]. It was reported that NPC2 is required for the antimicrobial activity of vitamin A against *Mtb* [203]. The biological form of vitamin A (all-*trans* retinoic acid (ATRA)) was demonstrated to give a decrease in *Mtb* viability, with this effect due to the ATRA-induced reduction in cellular cholesterol. The addition of ATRA was also associated with an increase in *NPC2* mRNA. Silencing of *NPC2* abrogated the ATRA-induced cholesterol depletion. In the TB granuloma addition of ATRA was associated with a significant increase in *NPC2* mRNA [203].

One subset of the RND permease family (bacterial proteins with high homology to NPC1) are those encoded by the *mmpL* genes (mycobacterial membrane

protein large) [204]. There are 12 Mmpl proteins present in *M.tuberculosis* [204]. Mutant strains do not show altered susceptibility to anti-TB drugs, suggesting that the Mmpl proteins are not involved in the process of drug efflux. Of the 12, only Mmpl3 is essential for mycobacterial viability [204] [205]. Mmpl3 is believed to be involved in the transport of TMM out of the cell [205]. Mycolic acids are synthesized within the core of the cell before being transported and deposited in the cell wall. Experiments by Varela *et al.* suggested that the mycolic acids are transported via Mmpl3 as TMM [205]. Upon reaching the exterior of the cell the mycolic acid can be transferred either to another TMM or to arabino-galactan. This transfer is catalysed by the Ag85 complex [206] and results in the production of either TDM or mycolic acids bound to the arabino-galactan of the cell wall. If mycobacteria avoid cellular clearance by lipid-mediated inhibition of the NPC1 protein then this would provide a situation in which one branch of the RND permease family (Mmpl3) has evolved to bind and transport mycolic acids, whilst its homolog NPC1 is inhibited by the binding of these same lipids. This potential link merits further investigation.

We observed that pre-existing dysfunction in the NPC pathway rendered cells less able to clear the non-pathogenic *M.smegmatis* (**Figure 5.5/5.6/5.8**). This may have implications for NPC patients who, due to a potentially impaired ability to clear intracellular pathogens, may harbour an unusual microbiome. It would also be of value to investigate the pathogen-clearing abilities of *Npc1*$^{+/-}$ macrophages relative to wild-type, and whether a reduction in the amount of functional NPC1 affects the cell's ability to clear infection. These findings may prove to be relevant to the parents of NPC patients, as well as other carriers of the disease.

Summary

In conclusion, this chapter implicates the NPC1 protein as the target of my-

cobacterial lipid-mediated inhibition, and demonstrates that a functional NPC pathway is required for clearance of intracellular pathogens. There is an inverse correlation between levels of NPC1 protein and susceptibility to TDM-induced mistrafficking of GM1 ganglioside and sphingomyelin. A pre-existing NPC dysfunction impairs the ability of cells to clear the non-pathogenic mycobacteria *M.smegmatis*.

6 NPC Therapies in the Treatment of TB

6.1 Introduction

In light of the rise of antibiotic resistant strains of *Mtb*, and the slow rate at which novel anti-TB drugs are being brought to market, the development of novel therapies is of paramount importance [89] [90] [133] [134] [138]. Data presented in previous chapters supports a model in which pathogenic mycobacteria achieve cellular persistence via lipid-mediated inhibition of the NPC pathway. We wished to investigate whether therapies used in the treatment of NPC would be of benefit when applied to macrophages infected with pathogenic mycobacteria. An overview of therapies either currently used or under investigation for the treatment of NPC are discussed below.

Curcumin

NPC cells exhibit reduced release of lysosomal calcium [20]. This defect in calcium release is predicted to lead to downstream defects in endocytic trafficking and lysosomal fusion [207]. Curcumin (or diferuloylmethane) is derived from tumeric [208] and is able to compensate for the reduced lysosomal calcium release observed in NPC cells [20]. It is an inhibitor of the sarcoplasmic reticulum

Ca^{2+} ATPase (SERCA) [209]. The SERCA family (SERCA1-3) are responsible for the movement of Ca^{2+} from the cytosol to the lumen of the SR [210]. Inhibition of SERCA results in reduced re-uptake of cytosolic calcium, leading to an effective rise in cytosolic [Ca^{2+}]. Oral treatment of NPC with curcumin has been shown to be beneficial, with treated mice exhibiting increased lifespan, body weight and lower levels of brain GSLs [20].

Curcumin has been suggested to be of benefit in the treatment of several diseases, including cancer, depression and Alzheimer's disease [211] [212] [213] [214]. It is able to modulate several cellular pathways in addition to its effect on cellular Ca^{2+}. Proposed molecular targets for curcumin include growth factors, mediators of inflammation, adhesion molecules and proteins involved in gene expression and cell survival [213] [215] [216] [217]. The beneficial effect of curcumin in NPC cells appears related to its calcium-modulating properties: the addition of BAPTA-AM (1,2–bis(o–aminophenoxy)ethane–N,N,N',N'–tetraacetic acid) (a chelator of intracellular Ca^{2+} [218]) precludes the correction of NPC cells by curcumin treatment [20]. Curcumin was also demonstrated to have a synergistic effect when co-administered with the anti-inflammatory ibuprofen in *Npc1*$^{-/-}$ mice, suggesting that in *Npc1*$^{-/-}$ mice curcumin is not acting via an anti-inflammatory mechanism [219].

Miglustat

N-butyl-deoxynojirimycin (NB-DNJ), also called Zavesca (trade name) or miglustat (generic name), was originally developed to treat type I Gaucher disease [220]. It is an inhibitor of glucosylceramide synthase, the enzyme which catalyses the first step in the GSL biosynthetic pathway (**Fig 1.3**). Its action results in a reduction in both gluocosylceramide and the more complex glycosphingolipids. The use of miglustat in animal models of NPC showed it was able to increase

lifespan, reduce levels of GSL storage, and delay the onset of neurological dysfunction [221]. A subsequent study showed that miglustat was beneficial in NPC patients [222]. Miglustat is currently the only licenced therapy for NPC (having been approved for use virtually worldwide, although not in the USA), as well as being used in the treatment of type I Gaucher disease in cases where ERT is not feasible.

N-butyldeoxygalactonojirimycin (NB-DGJ) is a galactose analogue of miglustat. It is more selective than NB-DNJ (which in addition to glucosylceramide synthase also inhibits α-glucosidase I and II, two enzymes involved in N-glycan processing in the ER) [223] [224]. It may therefore avoid the side effects, such as diarrhea, associated with the use of miglustat.

Cyclodextrin

Cyclodextrins are a family of cyclic oligosaccharides. Due to their structure (a hydrophilic exterior and hydrophobic interior) they are often used as vehicles for drug delivery [225]. The discovery of the beneficial effects of cyclodextrin in the treatment of NPC stemmed from attempts to use HPβCD as a vehicle for the delivery of allopregnanolone to the CNS of *Npc1*$^{-/-}$ mice (which possess sub-wild type levels of this neurosteroid) [75] [226]. Mice injected with allopregnanolone solubilized in HPβCD showed delayed onset of disease symptoms and increased survival. However, it was later shown that HPβCD in isolation was responsible for these benefits, with no additional benefit gained from the addition of allopregnanolone to the injection [75]. Treatment of *Npc1*$^{-/-}$ mice was associated with decreased levels of GSL, sphingosine and cholesterol [76].

The core of cyclodextrins have a high affinity for sterols. It has been demonstrated that they will bind cholesterol, and that they are able to extract cholesterol from lipid membranes [227] [228] [229]. It was assumed that this ability to

manipulate cellular cholesterol was responsible for the beneficial effect of HPβCD in NPC. Chen *et al.* demonstrated that HPβCD will stimulate the exocytosis of components of the endosome/lysosome [230]. This exocytosis is a calcium dependent process.

A recent report demonstrated that treatment with HPβCD activates autophagic cellular pathways, with this activation mediated via transcription factor EB (TFEB) [231]. TFEB regulates the expression of genes that encode lysosomal proteins, proteins involved in the processing of lysosomal proteins, and components of the autophagy pathway. Treatment with HPβCD activates TFEB with the subsequent increased expression of genes involved in autophagy. This increased expression is associated with the clearance of autophagic material.

Therefore the aim of the work presented in this chapter is:

* Evaluate whether therapies for NPC are beneficial in the clearance of pathogenic mycobacteria from infected macrophages.

6.2 Materials and Methods

6.2.1 Cells

RAW 264.7 cells and primary human macrophages were obtained and cultured as described in 2.2.1 and 3.2.3 respectively.

6.2.2 Mycobacterial Culture

Production, culture and long-term storage of mCherry-expressing mycobacteria were as detailed in Sections 2.2.1, 2.2.2, 2.2.3 and 2.2.4.

6.2.3 Correction of U18666A-induced Cholesterol Storage by NPC Therapies

RAW 264.7 cells grown on coverslips were treated with 2µg/ml U18666A for 24hr to induce cholesterol accumulation similar to that in NPC cells. Coverslips were washed and treated with NPC therapies diluted in RPMI. Concentrations used and length of treatment were as follows:

Therapy	**Parameters**
Curcumin (Enzo)	30 µM, 24hr
HPβCD (Sigma-Aldrich)	250 µM, 24hr
Miglustat (Actelion)	50 µM, 72hr

Post-treatment period coverslips were fixed (as detailed in Section 2.2.14) and cholesterol distribution investigated via staining with filipin (as detailed in Section 2.2.16). Microscopy was carried out as detailed in Sections 2.2.13 and 2.2.15.

6.2.4 Use of FACS to Assess Effect of NPC Therapies on BCG Clearance

Host cells were seeded overnight in 6-well plates (1 x 10^6 per well) prior to 48hr infection with mCherry-expressing BCG. Cells were washed and fresh media (containing therapeutics) was added. Unless otherwise stated, concentrations and duration of treatment were as indicated below. Cells were PFA fixed (4% PFA, 15 minutes room temperature), harvested, and levels of fluorescence (indicative of intracellular mycobacterial load) were quantified using FACS. Development of protocol is detailed below (Section 6.3.2). FACS analysis used equipment as detailed in Section 4.2.12, with 10000 cells observed per tube.

Therapy	**Parameters**
Curcumin (Enzo)	30 µM, 24hr
Tetramethylcurcumin (Sigma-Aldrich)	30 µM, 24hr
HPβCD (Sigma-Aldrich)	250 µM, 24hr
Miglustat (Actelion)	50 µM, 72hr
Curcumin/Miglustat	30 µM curcumin/50µM miglustat, 72hr
Curcumin/ HPβCD	30 µM curcumin/250µM HPβCD, 24hr

6.2.5 Assessment of the Ability of Curcumin Analogues to Modulate Cellular Ca^{2+}

Intracellular calcium levels were quantified by Dr. Lianne Davis.

The fluorescence curcumin exhibited upon incorporation into cells precluded the use of standard UV- and blue-excited Ca^{2+} dyes cells. It was therefore necessary to use the genetically encoded fluorescent Ca^{2+}-indicator protein O-GECO1 (Addgene plasmid 46025, provided by Robert Campbell [232]). RAW 264.7 macrophages were transfected with 2µg O-GECO1 using jetPRIME (Source

Bioscience) and used 24hr after transfection. Cells were then incubated with or without 30µM curcuminoids in tissue culture medium for 1hr at 37°C and 5% CO_2. Recordings were conducted in Ca^{2+}-free medium to eliminate Ca^{2+} influx. Thus, cells were washed once in a Ca^{2+}-free medium containing (mM): 121 NaCl, 5.4 KCl, 0.8 $MgCl_2$, 6 $NaHCO_3$, 25 HEPES, 10 Glucose and supplemented with 1 mM EGTA and then washed twice in the same medium except with a lower EGTA concentration (100µM) and then imaged in the same. The cells were mounted on the stage of an Olympus IX71 microscope equipped with a 20x UApo/340 objective and a 12-bit Photometrics Coolsnap HQ2 CCD camera. Cells were excited at 543 nm using a Cairn monochromator; and emission collected >585 nm. Experiments were conducted at room temperature with an image collected every 2 seconds. The effect of the curcuminoids on ER Ca^{2+} store depletion was tested by subsequent addition of 2µM ionomycin which releases Ca^{2+} from the ER in control cells. At the end of each run, 10mM $CaCl_2$ was added to verify O-GECO1 expression and viability of the cells. Images were analysed on a single-cell basis using Metafluor software and Microsoft Excel. The fluorescence of high-purity curcumin itself (815 ± 35 RFU) was subtracted from the O-GECO1 signal.

6.2.6 Chelation of Intracellular Calcium

Post the 48hr infection period with BCG, and immediately prior to addition of curcumin, RAW 264.7 macrophages were treated with the intracellular calcium chelator BAPTA-AM (Sigma-Aldrich) (20µM, 30min). Cells were then washed and treated with curcumin. At stated time point cells were washed, PFA fixed and subjected to FACS analysis.

6.2.7 Assessment of the Effect of Ned-19 on *M.smegmatis* Clearance from RAW 264.7 Macrophages

RAW 264.7 macrophages were seeded overnight in 6-well plates (1 x 10^6 per well) prior to 24hr treatment with 50µM Ned-19 (IBScreen) (an inhibitor of NAADP-mediated Ca^{2+} release [233]). Cells were subsequently washed and their ability to traffic *M.smegmatis* was assessed as in Section 5.3.6.

6.2.8 Assessment of the Effect of Curcuminoids on BCG Growth in Broth

Exponentially growing BCG culture in 7H9 (20ml containing approx. 5x10^8 cells/ml) was diluted into 100ml in the presence of 30µM curcuminoids. Growth was measured spectrophotometrically via absorbance at 600nm.

6.2.9 Statistical Analysis

Statistical analysis was performed using GraphPad Prism (ver 6.0). The specific test used is indicated in the figure legend.

6.3 Results

6.3.1 NPC Therapies Correct U18666A-induced Cholesterol Storage

Treatment of wild-type RAW 264.7 macrophages with U18666A was associated with an increase in filipin staining indicative of cholesterol storage (**Figure 6.1**). Subsequent treatment with the NPC therapies curcumin, miglustat or HPβCD was able to correct this storage phenotype (at least partially), and restore the cholesterol storage pattern to that of a wild-type cell.

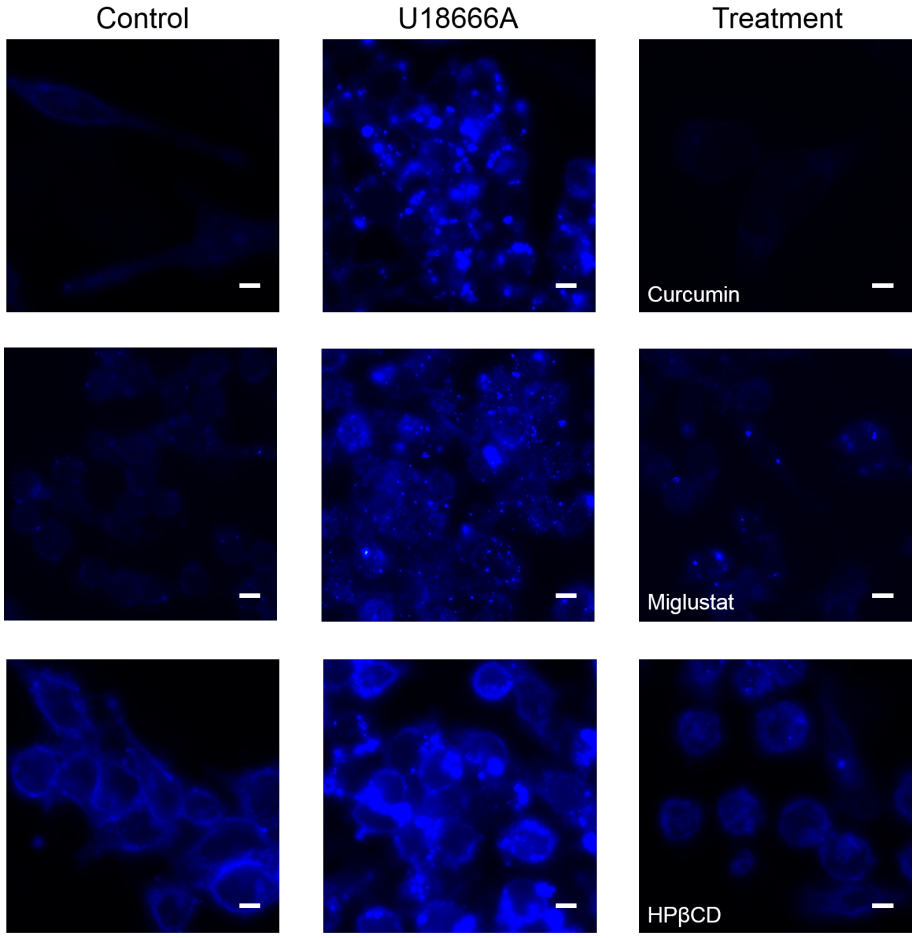

Figure 6.1: **Effect of U18666A treatment, and subsequent addition of NPC therapies, on cholesterol distribution in RAW 264.7 macrophages.** Images shown are representative. Blue - filipin (cholesterol). Scale bar - 5µm

6.3.2 The Effect of NPC Therapies on Persistence of mCherry-expressing BCG

Due to their fluorescence it should be possible to quantify the extent to which a population of host cells is infected with mCherry-expressing BCG. A similar assay (using *M.smegmatis*) was shown in Section 5.3.6.

Choice of FACS Channels

We used a number of different FACS channels to measure the fluorescence of both uninfected cells and those infected with mCherry-expressing BCG. FACS histograms showing overlays of the uninfected and infected samples for each channel are shown (**Figure 6.3**). The largest fold-change in fluorescence between the uninfected and infected samples was seen using the APC channel (**Figure 6.2**).

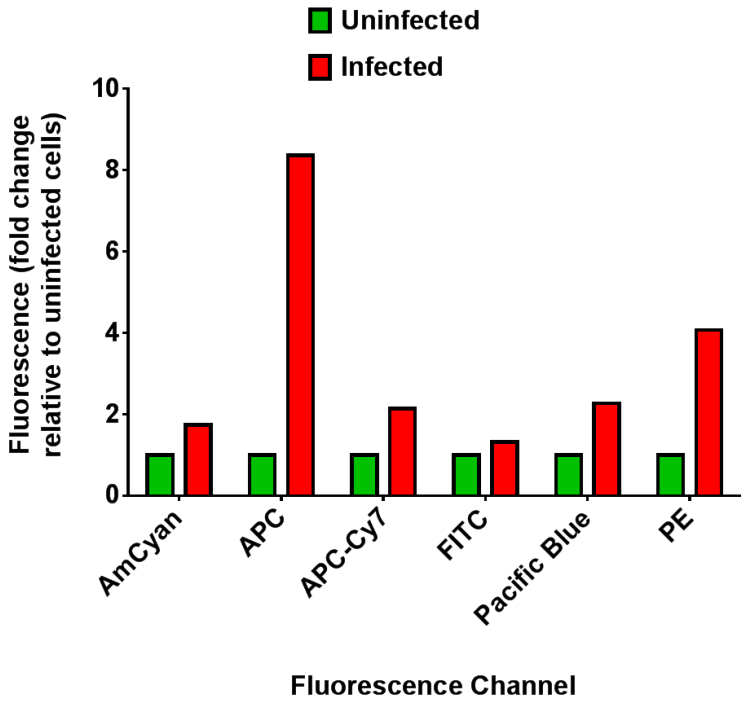

Figure 6.2: **Fold change in fluorescence in RAW 264.7 macrophages infected with mCherry-expressing BCG as measured using different FACS channels.** Fold change relative to uninfected cells. n=1.

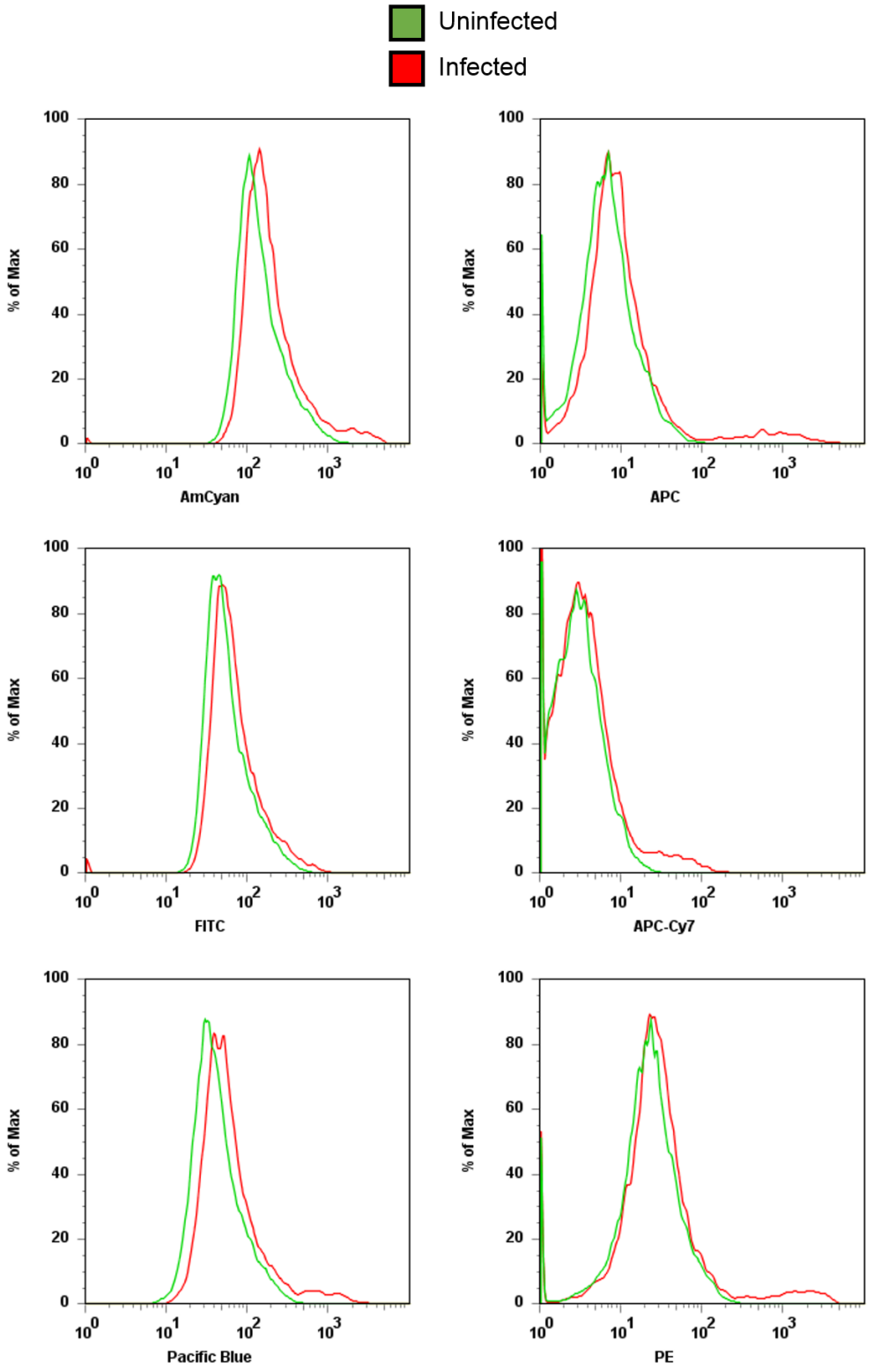

Figure 6.3: **Histograms from FACS analysis of RAW 264.7 macrophages in the presence or absence of BCG infection.** Histograms obtained using a number of different FACS channels. Comparison of fluorescence in uninfected cells (green) and those infected with mCherry-expressing BCG (red).

Proof of Principle and Methods of Analysis

Shown below are FACS plots from populations of RAW 264.7 macrophages infected with mCherry-expressing BCG at a lower (20) and higher (100) MOI (**Figure 6.4A**). There are two possible approaches to analysing this data. One option is to attempt to differentiate between uninfected and infected cells, dividing into a 'low APC' and 'high APC' population. One can thereby obtain a value for the percentage of total cells harbouring fluorescent BCG (**Figure 6.4B**). However, as Figure 6.4A shows, there is overlap between uninfected cells with high intrinsic fluorescence and infected cells with a small infectious load. A clear division between the two populations is therefore not possible. The point at which the populations are divided is arbitrary, and its placement introduces an element of subjectivity to the analysis.

A more objective means by which the data can be analysed involves looking at the mean APC fluorescence across the entire population. There is a positive correlation between mean fluorescence and the MOI used (**Figure 6.4C**).

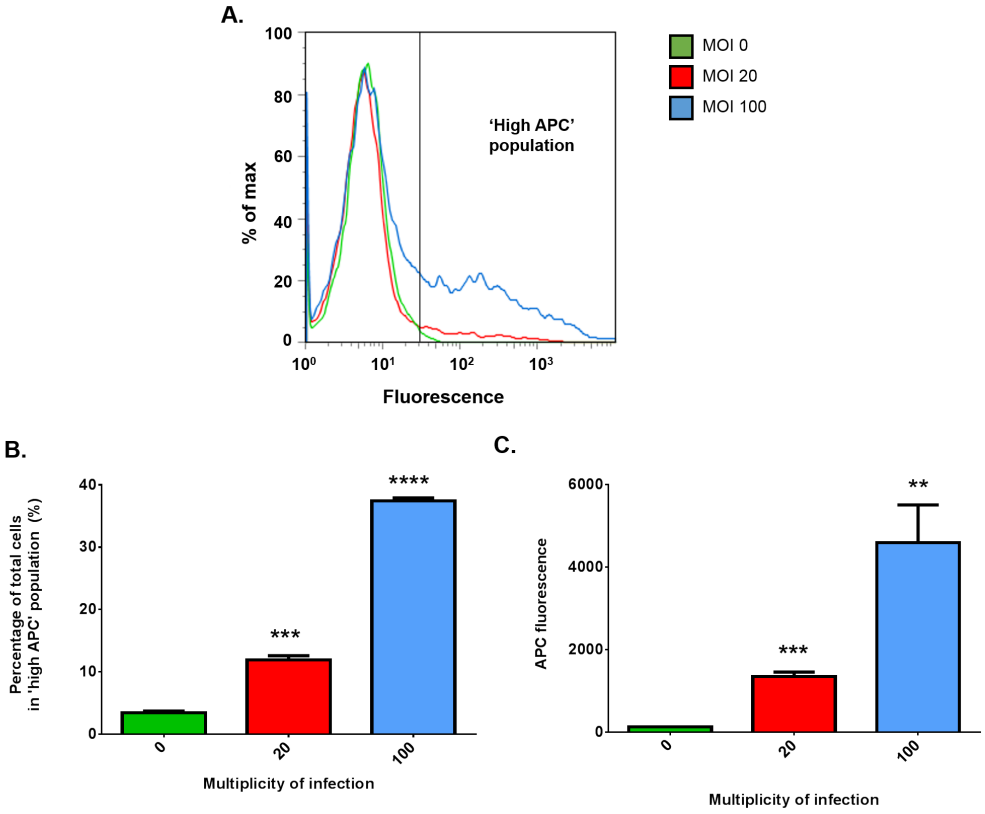

Figure 6.4: **Relationship between MOI and fluorescence of RAW 264.7 macrophages, as quantified using FACS. A.)** FACS histograms (in APC channel) of RAW 264.7 macrophages cells infected at MOI 0 (green), 20 (red) and 100 (blue). **B.)** Percentage of total cells in the 'high fluorescence' population. Mean ± SEM of 2 biological replicates. *** $p<0.001$, **** $p<0.0001$ versus uninfected control (via t-test). **C.)** Mean fluorescence (in APC channel) of RAW 264.7 macrophages infected at variable MOIs. Mean ± SEM of 2 biological replicates. ** $p<0.01$, *** $p<0.001$ versus uninfected control (via t-test).

6.3.3 Clearance of BCG from Infected Cells by NPC Therapies

Infected RAW 264.7 macrophages treated with curcumin had significantly lower levels of fluorescence (relative to untreated infected controls) indicative of increased levels of mycobacterial clearance (**Figure 6.5A/B, p - 0.0132/0.0423 respectively**). No such decrease was observed in cells treated with miglustat or HPβCD over the timecourse of the experiment. Concentrations and duration of treatment were previously shown sufficient to correct NPC phenotype induction by U18666A (**Figure 6.1**). The combination of curcumin and miglustat showed a synergistic effect, with a small but significant decrease in fluorescence relative to cells treated with curcumin only (**Figure 6.5A, p - 0.0453**). No such combinatorial effect was observed when curcumin and HPβCD were administered simultaneously. The concentration of therapies used and the duration of treatment was able to correct U18666A-induced cholesterol accumulation in RAW 264.7 macrophages (see Section 6.3.1).

6.3.4 Effect of NPC Therapies on Mycobacterial Clearance from Human Cells

As with RAW 264.7 macrophages, infected primary human cells showed significantly decreased fluorescence following treatment with curcumin (**Figure 6.6, $p<0.0131$**). This decrease (relative to untreated infected cells) was significant 48 hours post-treatment.

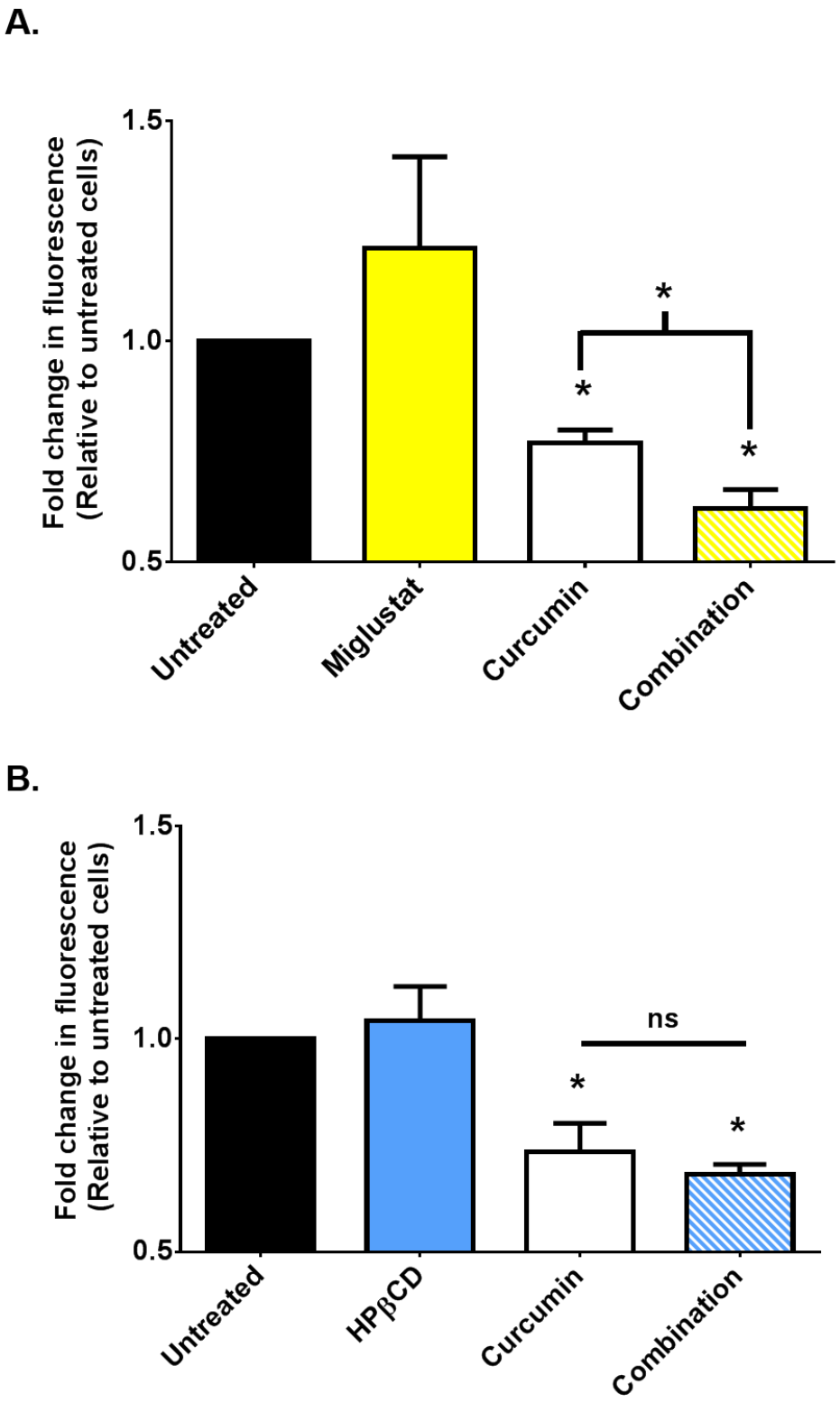

Figure 6.5: **Effect of NPC therapies on BCG clearance from RAW 264.7 macrophages.** 48hr infection (MOI 12.5) followed by incubation with therapies. Duration and concentration of therapies used as indicated in Section 6.3.1. Fold change in mean fluorescence relative to untreated BCG-infected macrophages. Mean ± SEM of 4 biological replicates. * $p<0.05$ versus untreated BCG-infected control (via t-test).

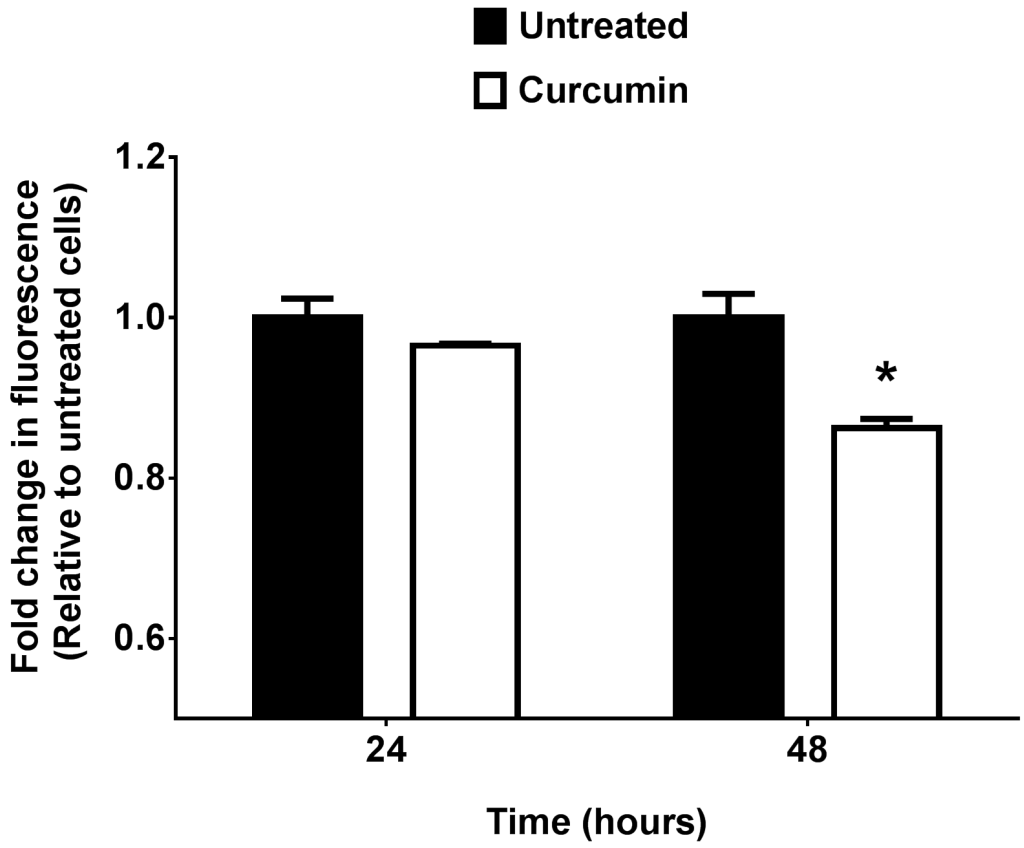

Figure 6.6: **Effect of curcumin on BCG clearance from primary human macrophages.** 48hr infection (MOI 12.5) followed by treatment with 30 µM curcumin. Fold change in mean fluorescence relative to untreated infected macrophages. Mean ± SEM of 4 biological replicates. * $p<0.05$ versus untreated BCG-infected controls (via t-test).

6.3.5 The Calcium Modulating Properties of Curcumin are Responsible for its Efficacy in Clearing BCG from Infected Cells

The effect of curcumin on mycobacterial clearance appears to be linked to its ability to modulate intracellular Ca^{2+}. We assayed both curcumin and tetramethylcurcumin for their effect on mycobacterial clearance. We observed that whereas curcumin gave a significant decrease in fluorescence (indicative of clearance of fluorescent BCG from infected cells) (**Figure 6.7, p - 0.0242 (24hrs)/**

0.0173 (48hrs)) no such decrease was associated with tetramethylcurcumin (**Figure 6.7, p - 0.4098 (24hrs)/0.4741 (48hrs)**).

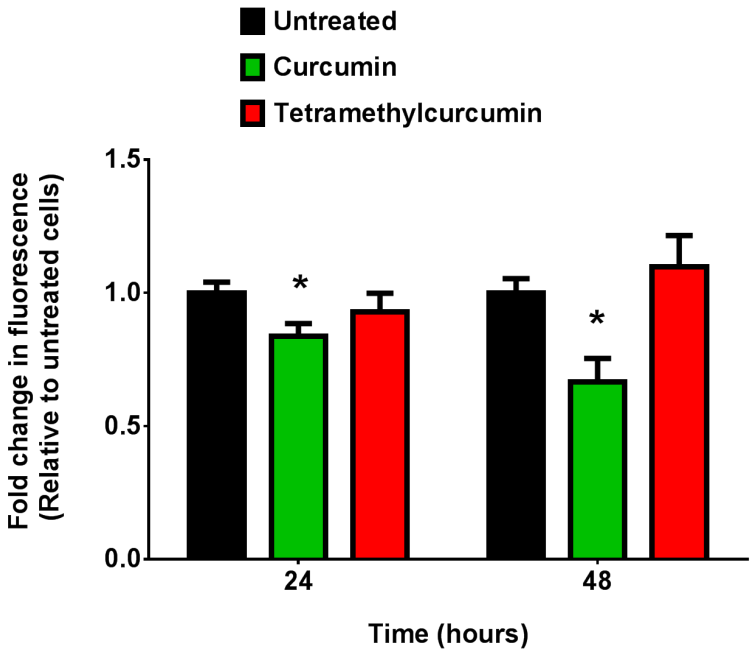

Figure 6.7: **Differential ability of curcuminoids to clear BCG from infected RAW 264.7 macrophages.** 48hr infection (MOI 12.5) followed by treatment with 30 µM curcuminoids. Fold change in mean fluorescence relative to untreated infected macrophages. Mean ± SEM of 4 biological replicates. * $p<0.05$ versus untreated BCG-infected controls (via test).

The ability of curcuminoids to clear BCG correlates with their ability to mobilise ER calcium. To investigate this we looked at the effect of the curcuminoids on Ca^{2+} homeostasis (**Fig 6.8**). This could not be carried out using the standard Ca^{2+} dyes such as fura-2 and fluo-3 (UV/Blue-excited) due to the fluorescence of curcumin upon its incorporation into cells. Curcumin has a broad excitation spectra (**Figure 6.8A**). It was therefore necessary to transfect the RAW 264.7 macrophages with O-GECO1 (encoding a fluorescent Ca^{2+}-indicator protein [232]).

Addition of curcumin was associated with a significant increase in resting cytosolic Ca^{2+}, reflecting the mobilisation of ER Ca^{2+} into the cytosol (**Figure**

6.8B, p<0.0001). No such increase was observed in cells treated with tetramethylcurcumin. Cells pre-treated with curcumin showed a drastically decreased Ca^{2+} response upon the addition of ionomycin (which releases ER Ca^{2+}). Representative single-cell Ca^{2+} traces are shown (**Figure 6.8C**). The maximum Ca^{2+} responses upon addition of ionomycin were significantly decreased in cells pre-treated with curcumin (but not tetramethylcurcumin) (**Figure 6.8D, p<0.0001**).

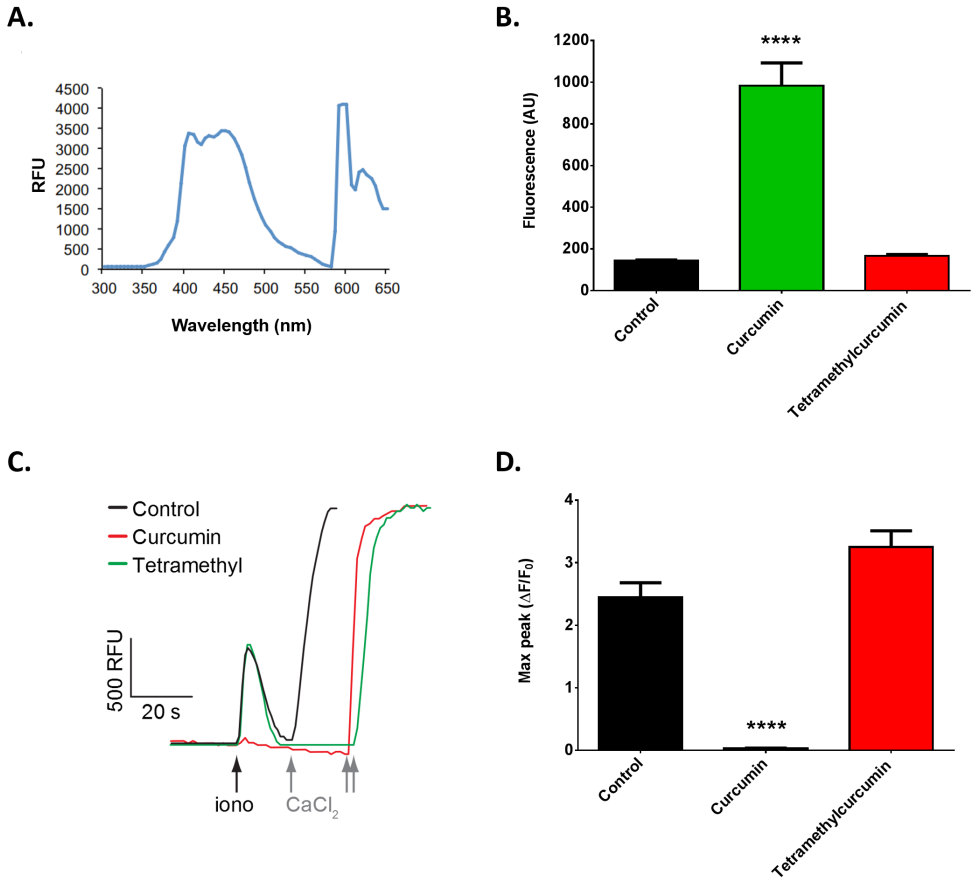

Figure 6.8: **Differential ability of curcuminoids to mobilise ER calcium.** RAW 264.7 macrophages used here were transfected with the Ca^{2+} reporter O-GECO1. **A.)** Absorbtion spectra of curcumin. **B.)** Resting Ca^{2+} in RAW 264.7 macrophages post treatment with curcuminoids. Mean ± SEM of n=42-125 individual cells per group. **** $p<0.0001$ versus untreated control (via 1-way ANOVA). **C.)** Representative single-cell Ca^{2+} traces of RAW 264.7 macrophages (pre-treated with curcuminoids) upon addition of ionomycin. Traces are normalised to basal calcium shown in **B**. **D.)** Maximum Ca^{2+} responses ($\Delta F/ F_0$) upon addition of ionomycin. Mean ± SEM of n= 42-105 individual cells per group. **** $p<0.0001$ versus untreated control (via 1-way ANOVA).

6.3.6 Clearance of BCG by Curcumin is Abrogated by Chelation of Cellular Calcium

Incubation of BCG-infected cells with the cell permeant Ca^{2+}-chelator BAPTA-AM abrogates the mycobacteria-clearing properties of curcumin. Whereas infected macrophages showed significantly decreased fluorescence upon treatment with curcumin (**Figure 6.9, p - 0.0016**), cells treated with BAPTA prior to the addition of therapy actually showed significantly increased levels of fluorescence relative to the untreated infected controls (**Figure 6.9, p<0.0001**). This may indicate that the Ca^{2+} defect induced by BCG infection is not severe enough to stop mycobacterial clearance completely, so that in untreated infected cells there remains a small amount of clearance, and that the addition of BAPTA-AM has served to completely abolish that small amount of clearance.

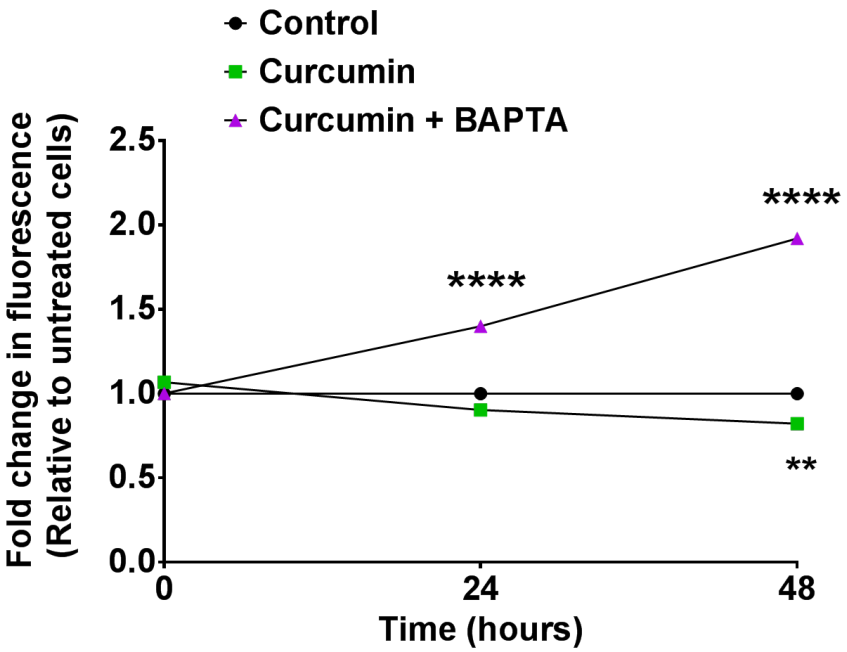

Figure 6.9: **Chelation of cytosolic calcium abrogates the beneficial effect of curcumin.** Fold change in mean fluorescence relative to untreated infected controls. Mean ± SEM of 4 biological replicates. ** p<0.01, **** p<0.0001 versus untreated infected controls (via 1-way ANOVA).

6.3.7 Effect of Ned-19 on *M.smegmatis* Clearance from Infected RAW 264.7 Macrophages

Ned-19 is an inhibitor of NAADP-mediated Ca^{2+} release [233]. A preliminary experiment suggested that RAW 264.7 macrophages pre-treated with Ned-19 (24hr, 50µM) may be less able to clear intracellular *M.smegmatis* (**Figure 6.10**). Treated cells showed a smaller fold change (relative to t=0) than the untreated controls. Note however, that this difference is not significant (p-0.13).

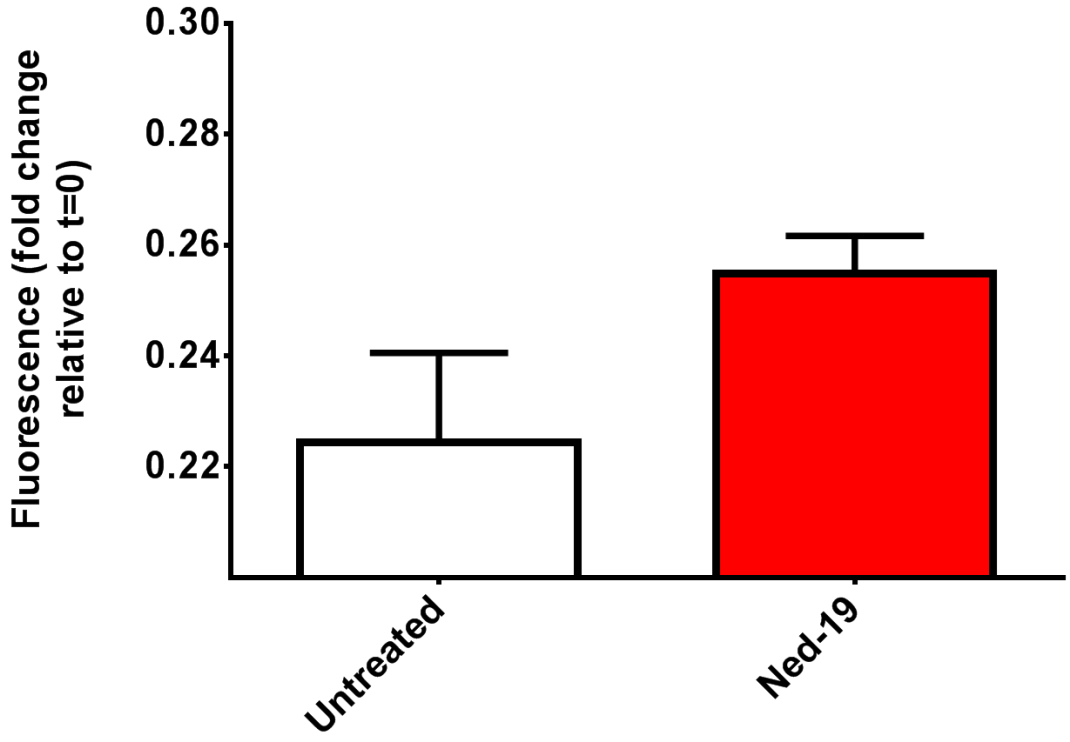

Figure 6.10: **Effect of Ned-19 treatment on *M.smegmatis* clearance from infected RAW 264.7 macrophages.** Fold change in mean fluorescence relative to t=0. Mean ± SEM of 4 biological replicates.

6.3.8 Effect of NPC Therapies on BCG Growth in Broth

Curcuminoids have been previously demonstrated to possess anti-mycobacterial properties in host-cell free systems [234]. We observed that the addition of

curcumin resulted in significantly decreased growth of BCG in broth (**Figure 6.11A**). However, the kinetics of this direct anti-mycobacterial effect are too slow (with a reduction in growth not occurring until after 3 days) to account for the relatively rapid action of curcumin observed in this chapter. No change in growth rate was associated with tetramethylcurcmin or NB-DNJ/GJ (**Figure 6.11A/B respectively**).

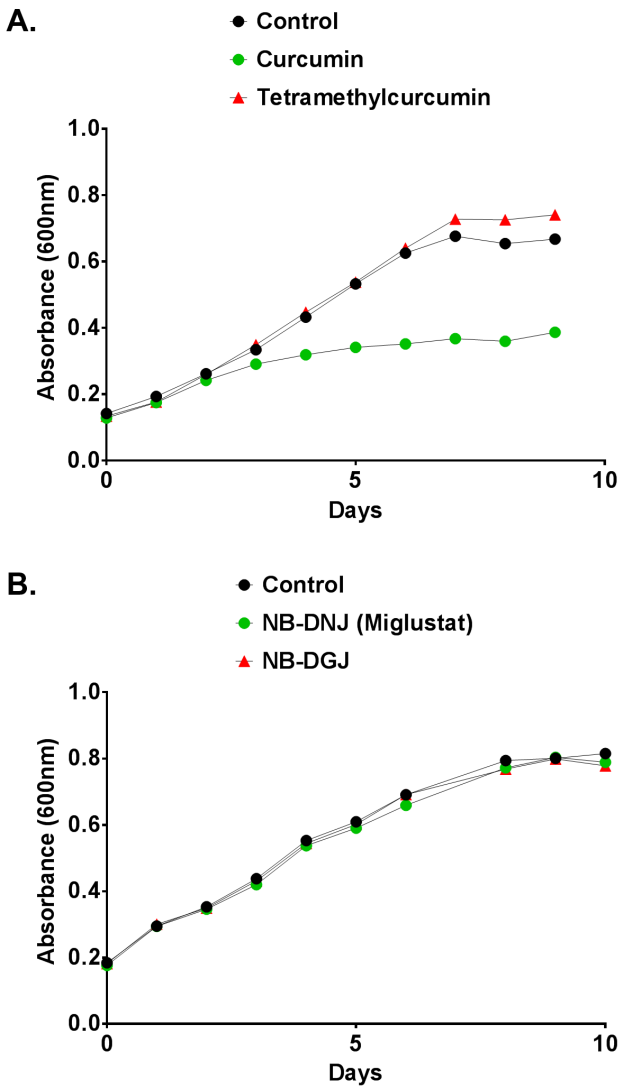

Figure 6.11: **Effect of NPC therapies on BCG growth in broth.** Mycobacteria grown in the presence of **A.)** 30µM Curcuminoids and **B.)** 50µM NB-DNJ/GJ. Mean ± SEM of 3 biological replicates. Where not visible error bars are contained within the symbols.

6.4 Discussion

In this chapter we demonstrate that treatment of infected macrophages with curcumin is associated with a decrease in fluorescence indicative of clearance of fluorescent mycobacteria. These findings applied to both mouse and human macrophages (**Figure 6.5/6.6 respectively**). No decrease in fluorescence was observed when infected macrophages were treated with miglustat only. Intriguingly, miglustat was seen to be synergistic with curcumin, with combination treatment giving a small, but significant improvement relative to curcumin alone. It would be worthwhile to investigate the effect of miglustat over longer time scales than used in this experiment (>72 hours) to determine whether this would result in an observable effect. HPβCD showed no benefit when used in infected cells, either in isolation or when used in combination with curcumin (**Figure 6.5**). This is in agreement with a proposed model of HPβCD action in which the compound gives a reduction in cellular cholesterol via stimulating exocytosis of the endosome/lysosome [230]. Mycobacteria residing in the phagosome would be unaffected by this exocytosis.

As with NPC cells, the beneficial effects of curcumin appear to be related to the calcium modulating properties of the compound [20] [219]. The ability of curcuminoids to promote the clearance of mycobacteria correlated with their ability to modulate the ER Ca^{2+} stores (**Figure 6.7/6.8**). Chelation of cellular Ca^{2+} precluded any benefit from the subsequent addition of curcumin (**Figure 6.9**), indicating that it is the ability of curcumin to compensate for reduced lysosomal $[Ca^{2+}]$ that is responsible for the mycobacteria clearance observed here. The importance of lysosomal Ca^{2+} was reinforced by experiments indicating that pre-treatment of RAW 264.7 macrophages with Ned-19 (an NAADP antagonist [233]) may render cells less able to traffic the non-pathogenic *M.smegmatis* (**Figure 6.10**). This complemented experiments in chapter 5 in which NPC

pathway dysfunction (due to mutation or pharmacological inhibition) was associated with reduced *M.smegmatis* clearance (**Figure 5.5/5.6/5.8**).

It has been previously reported that curcumin has direct anti-mycobacterial properties, inhibiting growth of *Mtb* in a host-cell free model [234]. This supports observations made in this chapter that curcumin is associated with reduced growth of BCG when added to culture media (**Figure 6.11**). However, this effect on mycobacterial growth is not apparent until after 3 days. It is therefore not rapid enough to account for the observed effect of curcumin in infected macrophages. The ability of curcumin to clear pathogenic mycobacteria from infected macrophages has been previously reported, although had been attributed to the ability of curcumin to induce apoptosis [235] [236]. In this chapter we provide evidence that it is the calcium-modulating properties of the compound that are responsible for its efficacy, which serve to compensate for the effects of NPC pathway inhibition occurring upon infection with pathogenic mycobacteria.

The increased prevalence of strains of *M.tuberculosis* that are resistant to existing antibiotics means that the development of new therapies is of paramount importance [89]. Therapies which target interactions between the mycobacterium and the host cell, as opposed to the mycobacterium directly, would be less subject to the development of resistance. Curcumin therefore potentially holds tremendous value for the future treatment of TB. The next step will be to determine whether curcumin is effective in animal models of *Mtb*/BCG infection prior to the commencement of potential clinical trials.

Summary

In conclusion, work in this chapter demonstrates that curcumin, in addition to being able to correct NPC cells, is also able to promote the clearance of pathogenic mycobacteria from infected host cells. The mycobacteria-clearing

properties of the compound are dependent on its ability to increase cytosolic $[Ca^{2+}]$.

7 Conclusion

In conclusion, the work presented in this thesis serves to support a model in which pathogenic mycobacteria prevent phagosome:lysosome fusion, and therefore achieved cellular persistence, via inhibition of the host cell NPC pathway. This inhibition is mediated through lipids shed by the mycobacteria and trafficked to the endocytic systems of both the infected host cell and uninfected bystander cells, wherein it may bind to and inhibit the NPC1 protein (**Figure 7.1**). The subsequent induction of NPC cellular phenotypes, particularly the reduced lysosomal calcium levels and defects in intracellular trafficking, provide an intracellular environment conducive to the long-term survival of mycobacteria.

This work provides a mechanistic framework which is able to account from numerous previous observations, including the accumulation of host cholesterol and LacCer in TB granulomas [99] [119] [121], the ability of *Mtb* TDM to induce granuloma formation in the absence of mycobacteria [181] [182] [183], the inhibition of phagosome:lysosome fusion in infected macrophages [80], the proposed importance of calcium to intracellular mycobacterial trafficking [103], and preliminary reports associating treatment with curcumin with a reduction in intracellular mycobacterial persistence [235] [236]. We have also provided evidence that a functional NPC pathway is required for the clearance of internalized microorganisms. This finding may hold important implications for NPC patients, who due to NPC pathway dysfunction may harbour an unusual microbiome.

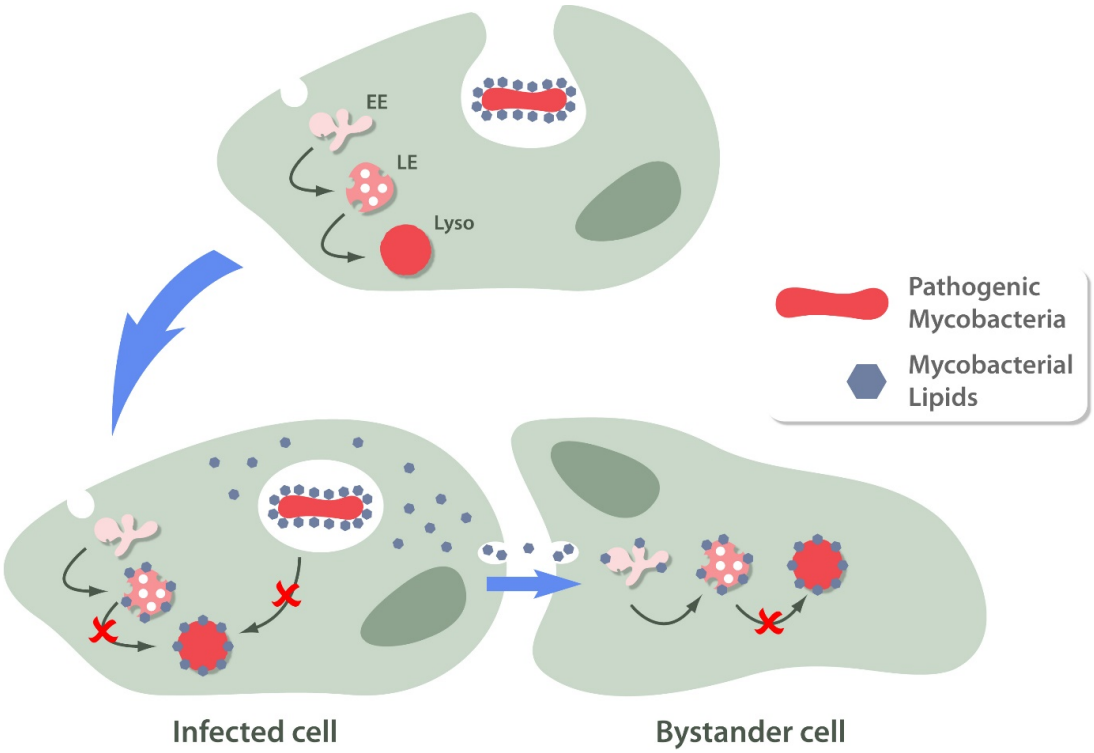

Figure 7.1: **Schematic showing lipid-mediated inhibition of the NPC pathway by pathogenic mycobacteria.** Mycobacteria residing in the phagosome shed cell wall lipids, which reach the endocytic system of the host cell. Upon reaching the late endosome/lysosome they bind to and inhibit the NPC1 protein, leading to a dysfunctional NPC pathway and a subsequent reduction in phagosome:lysosome fusion. Shed lipids also reach neighbouring uninfected cells. EE - early endosome, LE - late endosome, Lyso - lysosome. With thanks to Dr. Ant Morgan.

Perhaps the most exciting consequence of the above model is the promise it holds for the development of a new approach for the treatment of TB. Currently, anti-TB therapies directly target the mycobacteria. The current short-course treatment for TB consists of combinatorial therapy (using as many as four different antibiotics) for 6 months [89]. For latent TB the standard treatment regimen is up to 9 months with isoniazid alone (to prevent the latent infection from progressing to an active form). The increasing prevalence of *Mtb* strains resistant to treatment is well documented [89]. The rise of antibiotic resistance bacteria, and the associated reduction in therapeutic options, will provide one of the great healthcare challenges of the 21st century. The development of new therapies is therefore of paramount importance. By targeting the interaction between the pathogen and the host cell (instead of targeting the pathogen directly) we reduce the risk of the pathogen developing resistance to treatment. We have shown here that curcumin is associated with increased clearance of mycobacteria from infected cells, and that the beneficial effects of the compound are due to its ability to modulate cellular calcium levels. Demonstration of the efficacy of curcumin treatment in infected mice is therefore a priority for future work.

In recent years the NPC pathway has been reported to play a role in the functioning of several high-profile human pathogens. A functional NPC1 pathway was shown to be required for the entry of the Ebola filovirus into cells [237]. These experiments used vesicular stomatitis Indiana virus expressing recombinant glycoproteins (rVSVs) from different viruses. rVSVs bearing the Ebola glycoprotein showed reduced uptake into NPC1 patient fibroblasts, with this reduced uptake specific to the Ebola glycoprotein. rVSVs bearing other glycoproteins were not affected. A similar reduction in uptake was observed in Chinese hamster ovary NPC1 KO cells, and in wild-type kidney epithelial cells in which a NPC phenotype had been induced via U18666A [237] [238]. A functional NPC pathway

has also been demonstrated to be required for the replication of the Human immunodeficiency virus type 1 (HIV-1), with NPC dysfunction associated with the accumulation of viral proteins within the acidic compartment [239]. These observations, in conjunction with the work presented in this thesis, suggest that the NPC pathway may be implicated in the mechanisms underlying several major human diseases. One open question is whether other persistent intracellular pathogens (such as *Chlamydia* or *Toxoplasma*, both of which also induce foam cell formation) interact with the host NPC pathway [79]. This work also serves to demonstrate the importance of rare disease research. Work carried out into the underlying pathology of NPC, a condition affecting less than 0.001% of the population, may prove relevant to the treatment of several major human infectious diseases [4].

Bibliography

1. Fuller, M., Meikle, P. J. & Hopwood, J. J. in *Fabry Disease: Perspectives from 5 Years of FOS* (eds Mehta, A., Beck, M. & Sunder-Plassmann, G.) (Oxford PharmaGenesis, Oxford, 2006).

2. Platt, F. M. Sphingolipid lysosomal storage disorders. *Nature* **510,** 68–75 (2014).

3. Micsenyi, M. C. & Walkley, S. U. in *Lysosomal Storage Disorders: A Practical Guide* (eds Mehta, A. & Winchester, B.) (Wiley-Blackwell, Oxford, 2012).

4. Vanier, M. T. Niemann-Pick disease type C. *Orphanet Journal of Rare Diseases* **5,** 16 (2010).

5. Vanier, M. T. Phenotypic and genetic heterogeneity in Niemann-Pick disease type C: current knowledge and practical implications. *Wiener klinische Wochenschrift* **109,** 68–73 (1997).

6. Patterson, M. C. *et al.* Recommendations for the diagnosis and management of Niemann-Pick disease type C: an update. *Molecular genetics and metabolism* **106,** 330–344 (2012).

7. Shachar, T. *et al.* Lysosomal storage disorders and Parkinson's disease: Gaucher disease and beyond. *Movement Disorders* **26,** 1593–1604 (2011).

8. Schuchman, E. H. The pathogenesis and treatment of acid sphingomyelinase-deficient Niemann-Pick disease. *Journal of Inherited Metabolic Disease* **30,** 654–663 (2007).

9. Babalola, J. O. *et al.* Development of an assay for the intermembrane transfer of cholesterol by Niemann-Pick C2 protein. *Biological Chemistry* **388,** 617–626 (2007).

10. Xu, S., Benoff, B., Liou, H.-L., Lobel, P. & Stock, A. M. Structural basis of sterol binding by NPC2, a lysosomal protein deficient in Niemann-Pick type C2 disease. *Journal of Biological Chemistry* **282,** 23525–23531 (2007).

11. Lloyd-Evans, E. & Platt, F. M. Lipids on trial: the search for the offending metabolite in Niemann-Pick type C disease. *Traffic* **11,** 419–428 (2010).

12. Loftus, S. K. *et al.* Murine model of Niemann-Pick C disease: mutation in a cholesterol homeostasis gene. *Science* **277,** 232–235 (1997).

13. Ioannou, Y. A. The structure and function of the Niemann-Pick C1 protein. *Molecular Genetics and Metabolism* **71,** 175–181 (2000).

14. Davies, J. P., Chen, F. W. & Ioannou, Y. A. Transmembrane molecular pump activity of Niemann-Pick C1 protein. *Science* **290,** 2295–2298 (2000).

15. Sleat, D. E. *et al.* Genetic evidence for nonredundant functional cooperativity between NPC1 and NPC2 in lipid transport. *Proceedings of the National Academy of Sciences* **101,** 5886–5891 (2004).

16. Friedland, N., Liou, H.-L., Lobel, P. & Stock, A. M. Structure of a cholesterol-binding protein deficient in Niemann-Pick type C2 disease. *Proceedings of the National Academy of Sciences* **100,** 2512–2517 (2003).

17. Vruchte, D. t. *et al.* Accumulation of glycosphingolipids in Niemann-Pick C disease disrupts endosomal transport. *Journal of Biological Chemistry* **279,** 26167–26175 (2004).

18. Crocker, A. C. & Farber, S. Niemann-Pick disease: a review of eighteen patients. *Medicine* **37,** 1–95 (1958).

19. Ko, D. C., Gordon, M. D., Jin, J. Y. & Scott, M. P. Dynamic movements of organelles containing Niemann-Pick C1 protein: NPC1 involvement in late endocytic events. *Molecular Biology of the Cell* **12,** 601–614 (2001).

20. Lloyd-Evans, E. *et al.* Niemann-Pick disease type C1 is a sphingosine storage disease that causes deregulation of lysosomal calcium. *Nature Medicine* **14,** 1247–1255 (2008).

21. Eskelinen, E.-L. *et al.* Disturbed cholesterol traffic but normal proteolytic function in LAMP-1/LAMP-2 double-deficient fibroblasts. *Molecular Biology of the Cell* **15,** 3132–3145 (2004).

22. Butler, J., Vanier, M. & Pentchev, P. Niemann-Pick C disease: cystine and lipids accumulate in the murine model of this lysosomal cholesterol lipidosis. *Biochemical and Biophysical Research Communications* **196,** 154–159 (1993).

23. Goldin, E *et al.* Type C Niemann-Pick disease: a murine model of the lysosomal cholesterol lipidosis accumulates sphingosine and sphinganine in liver. *Biochimica et biophysica acta* **1127,** 303–311 (1992).

24. Cruz, J. C. & Chang, T.-Y. Fate of endogenously synthesized cholesterol in Niemann-Pick Type C1 cells. *Journal of Biological Chemistry* **275,** 41309–41316 (2000).

25. Pentchev, P. G. *et al.* A defect in cholesterol esterification in Niemann-Pick disease (type C) patients. *Proceedings of the National Academy of Sciences* **82,** 8247–8251 (1985).

26. Urano, Y. *et al.* Transport of LDL-derived cholesterol from the NPC1 compartment to the ER involves the trans-Golgi network and the SNARE protein complex. *Proceedings of the National Academy of Sciences* **105,** 16513–16518 (2008).

27. Wennekes, T. *et al.* Glycosphingolipids — nature, function, and pharmacological modulation. *Angewandte Chemie International Edition* **48,** 8848–8869 (2009).

28. Park, J.-W., Park, W.-J. & Futerman, A. H. Ceramide synthases as potential targets for therapeutic intervention in human diseases. *Biochimica et Biophysica Acta* **1841,** 671–681 (2014).

29. Simpson, M. A. *et al.* Infantile-onset symptomatic epilepsy syndrome caused by a homozygous loss-of-function mutation of GM3 synthase. *Nature Genetics* **36,** 1225–1229 (2004).

30. Harlalka, G. V. *et al.* Mutations in *B4GALNT1* (GM2 synthase) underlie a new disorder of ganglioside biosynthesis. *Brain* **136,** 3618–3624 (2013).

31. Tettamanti, G, Bassi, R, Viani, P & Riboni, L. Salvage pathways in glycosphingolipid metabolism. *Biochimie* **85,** 423–437 (2003).

32. Bersano, A. *et al.* Neurological features of Fabry disease: clinical, pathophysiological aspects and therapy. *Acta Neurologica Scandinavica* **126,** 77–97 (2012).

33. Vanier, M. T. Lipid changes in Niemann-Pick disease type C brain: personal experience and review of the literature. *Neurochemical Research* **24,** 481–489 (1999).

34. Blom, T., Somerharju, P. & Ikonen, E. Synthesis and biosynthetic trafficking of membrane lipids. *Cold Spring Harbor Perspectives in Biology* **3,** a004713 (2011).

35. Milhas, D., Clarke, C. J. & Hannun, Y. A. Sphingomyelin metabolism at the plasma membrane: implications for bioactive sphingolipids. *FEBS Letters* **584,** 1887–1894 (2010).

36. Tamura, H. *et al.* Niemann-Pick type C disease: Novel *NPC1* mutations and characterization of the concomitant acid sphingomyelinase deficiency. *Molecular Genetics and Metabolism* **87,** 113–121 (2006).

37. Abi-Mosleh, L., Infante, R. E., Radhakrishnan, A., Goldstein, J. L. & Brown, M. S. Cyclodextrin overcomes deficient lysosome-to-endoplasmic reticulum transport of cholesterol in Niemann-Pick type C cells. *Proceedings of the National Academy of Sciences* **106,** 19316–19321 (2009).

38. Kågedal, K, Zhao, M, Svensson, I & Brunk, U. T. Sphingosine-induced apoptosis is dependent on lysosomal proteases. *Biochemical Journal* **359,** 335–343 (2001).

39. Lloyd-Evans, E., Waller-Evans, H., Peterneva, K. & Platt, F. M. Endolysosomal calcium regulation and disease. *Biochemical Society Transactions* **38,** 1458–1464 (2010).

40. Mekahli, D., Bultynck, G., Parys, J. B., De Smedt, H. & Missiaen, L. Endoplasmic-reticulum calcium depletion and disease. *Cold Spring Harbor Perspectives in Biology* **3,** a004317 (2011).

41. Calcraft, P. J. *et al.* NAADP mobilizes calcium from acidic organelles through two-pore channels. *Nature* **459,** 596–600 (2009).

42. Pfeffer, S. R. Transport-vesicle targeting: tethers before SNAREs. *Nature Cell Biology* **1,** E17–E22 (1999).

43. Wang, J. *et al.* Calcium sensitive ring-like oligomers formed by synaptotagmin. *Proceedings of the National Academy of Sciences* **111,** 13966–13971 (2014).

44. Kusner, D. J. & Barton, J. A. ATP stimulates human macrophages to kill intracellular virulent *Mycobacterium tuberculosis* via calcium-dependent phagosome-lysosome fusion. *The Journal of Immunology* **167,** 3308–3315 (2001).

45. Huynh, K. K., Gershenzon, E. & Grinstein, S. Cholesterol accumulation by macrophages impairs phagosome maturation. *Journal of Biological Chemistry* **283,** 35745–35755 (2008).

46. Morgan, A. J., Platt, F. M., Lloyd-Evans, E. & Galione, A. Molecular mechanisms of endolysosomal Ca^{2+} signalling in health and disease. *Biochemical Journal* **439,** 349–374 (2011).

47. Kinnear, N. P., Boittin, F.-X., Thomas, J. M., Galione, A. & Evans, A. M. Lysosome-Sarcoplasmic reticulum junctions: a trigger zone for calcium signaling by nicotinic acid adenine dinucleotide phosphate and endothelin-1. *Journal of Biological Chemistry* **279,** 54319–54326 (2004).

48. Jeyakumar, M., Dwek, R. A., Butters, T. D. & Platt, F. M. Storage solutions: treating lysosomal disorders of the brain. *Nature Reviews Neuroscience* **6,** 713–725 (2005).

49. Doherty, G. J. & McMahon, H. T. Mechanisms of endocytosis. *Annual Review of Biochemistry* **78,** 857–902 (2009).

50. Jovic, M., Sharma, M., Rahajeng, J. & Caplan, S. The early endosome: a busy sorting station for proteins at the crossroads. *Histology and histopathology* **25,** 99–112 (2010).

51. Herbst, J. J., Opresko, L. K., Walsh, B. J., Lauffenburger, D. A. & Wiley, H. S. Regulation of postendocytic trafficking of the epidermal growth factor receptor through endosomal retention. *Journal of Biological Chemistry* **269,** 12865–12873 (1994).

52. Mu, F. T. *et al.* EEA1, an early endosome-associated protein. *Journal of Biological Chemistry* **270,** 13503–13511 (1995).

53. Grosshans, B. L., Ortiz, D. & Novick, P. Rabs and their effectors: achieving specificity in membrane traffic. *Proceedings of the National Academy of Sciences* **103,** 11821–11827 (2006).

54. Piper, R. C. & Luzio, J. P. Late endosomes: sorting and partitioning in multivesicular bodies. *Traffic* **2,** 612–621 (2001).

55. Griffiths, G., Matteoni, R., Back, R. & Hoflack, B. Characterization of the cation-independent mannose 6-phosphate receptor-enriched prelysosomal compartment in NRK cells. *Journal of Cell Science* **95,** 441–461 (1990).

56. Rodman, J. S. & Wandinger-Ness, A. Rab GTPases coordinate endocytosis. *Journal of Cell Science* **113,** 183–192 (2000).

57. Harrison, R. E., Bucci, C., Vieira, O. V., Schroer, T. A. & Grinstein, S. Phagosomes fuse with late endosomes and/or lysosomes by extension of membrane protrusions along microtubules: role of Rab7 and RILP. *Molecular and Cellular Biology* **23,** 6494–6506 (2003).

58. Lombardi, D *et al.* Rab9 functions in transport between late endosomes and the trans Golgi network. *The EMBO Journal* **12,** 677–682 (1993).

59. Luzio, J. P., Pryor, P. R. & Bright, N. A. Lysosomes: fusion and function. *Nature Reviews Molecular Cell Biology* **8,** 622–632 (2007).

60. Eskelinen, E.-L. Roles of LAMP-1 and LAMP-2 in lysosome biogenesis and autophagy. *Molecular Aspects of Medicine* **27,** 495–502 (2006).

61. Appelqvist, H., Wäster, P., Kågedal, K. & Öllinger, K. The lysosome: from waste bag to potential therapeutic target. *Journal of Molecular Cell Biology* **5,** 214–226 (2013).

62. Mindell, J. A. Lysosomal acidification mechanisms. *Annual Review of Physiology* **74,** 69–86 (2012).

63. Chen, Y. A. & Scheller, R. H. SNARE-mediated membrane fusion. *Nature Reviews Molecular Cell Biology* **2,** 98–106 (2001).

64. Narita, K. *et al.* Protein transduction of Rab9 in Niemann-Pick C cells reduces cholesterol storage. *The FASEB Journal* **19,** 1558–60 (2005).

65. Charman, M., Kennedy, B. E., Osborne, N. & Karten, B. MLN64 mediates egress of cholesterol from endosomes to mitochondria in the absence of functional Niemann-Pick Type C1 protein. *Journal of Lipid Research* **51,** 1023–1034 (2010).

66. Erickson, R. P., Garver, W. S., Camargo, F., Hossian, G. S. & Heidenreich, R. A. Pharmacological and genetic modifications of somatic cholesterol do not substantially alter the course of CNS disease in Niemann-Pick C mice. *Journal of Inherited Metabolic Disease* **23,** 54–62 (2000).

67. Somers, K. L. *et al.* Effects of dietary cholesterol restriction in a feline model of Niemann-Pick type C disease. *Journal of Inherited Metabolic Disease* **24,** 427–436 (2001).

68. Patterson, M. C. *et al.* The effect of cholesterol-lowering agents on hepatic and plasma cholesterol in Niemann-Pick disease type C. *Neurology* **43,** 61–64 (1993).

69. Infante, R. E. *et al.* Purified NPC1 Protein II. Localization of sterol binding to a 240-amino acid soluble luminal loop. *Journal of Biological Chemistry* **283,** 1064–1075 (2008).

70. Mohammadi, A. *et al.* Golgi localization and phosphorylation of oxysterol binding protein in Niemann-Pick C and U18666A-treated cells. *Journal of Lipid Research* **42,** 1062–1071 (2001).

71. Pol, A. *et al.* A caveolin dominant negative mutant associates with lipid bodies and induces intracellular cholesterol imbalance. *The Journal of Cell Biology* **152,** 1057–1070 (2001).

72. Zeidan, Y. H. & Hannun, Y. A. Activation of acid sphingomyelinase by protein kinase Cδ-mediated phosphorylation. *Journal of Biological Chemistry* **282,** 11549–11561 (2007).

73. Rodriguez-Lafrasse, C *et al.* Modulation of protein kinase C by endogenous sphingosine: inhibition of phorbol dibutyrate binding in Niemann-Pick C fibroblasts. *Biochemical Journal* **325,** 787–791 (1997).

74. Péret-Almeida, L., Cherubino, A. P. F., Alves, R. J., Dufossé, L. & Glória, M. B. A. Separation and determination of the physico-chemical characteristics of curcumin, demethoxycurcumin and bisdemethoxycurcumin. *Food Research International* **38,** 1039–1044 (2005).

75. Griffin, L. D., Gong, W., Verot, L. & Mellon, S. H. Niemann-Pick type C disease involves disrupted neurosteroidogenesis and responds to allopregnanolone. *Nature Medicine* **10,** 704–711 (2004).

76. Davidson, C. D. *et al.* Chronic cyclodextrin treatment of murine Niemann-Pick C disease ameliorates neuronal cholesterol and glycosphingolipid storage and disease progression. *PLoS ONE* **4,** e6951 (2009).

77. Peake, K. B. & Vance, J. E. Normalization of cholesterol homeostasis by 2-Hydroxypropyl-β-cyclodextrin in neurons and glia from Niemann-Pick C1 (NPC1)-deficient mice. *Journal of Biological Chemistry* **287,** 9290–9298 (2012).

78. Pontikis, C. C., Davidson, C. D., Walkley, S. U., Platt, F. M. & Begley, D. J. Cyclodextrin alleviates neuronal storage of cholesterol in Niemann-Pick C disease without evidence of detectable blood-brain barrier permeability. *Journal of Inherited Metabolic Disease* **36,** 491–498 (2013).

79. Russell, D. G., Cardona, P.-J., Kim, M.-J., Allain, S. & Altare, F. Foamy macrophages and the progression of the human TB granuloma. *Nature Immunology* **10,** 943–948 (2009).

80. Tjelle, T. E., Lovdal, T. & Berg, T. Phagosome dynamics and function. *BioEssays* **22,** 255–263 (2000).

81. Djelouadji, Z., Raoult, D., Daffé, M. & Drancourt, M. A single-step sequencing method for the identification of *Mycobacterium tuberculosis* complex species. *PLoS Neglected Tropical Diseases* **2,** e253 (2008).

82. Golden, M. P. & Vikram, H. R. Extrapulmonary tuberculosis: an overview. *American Family Physician* **72,** 1761–1768 (2005).

83. Gutierrez, M. C. *et al.* Ancient origin and gene mosaicism of the progenitor of *Mycobacterium tuberculosis*. *PLoS Pathog* **1,** e5 (2005).

84. Brosch, R. *et al.* A new evolutionary scenario for the *Mycobacterium tuberculosis* complex. *Proceedings of the National Academy of Sciences* **99,** 3684–3689 (2002).

85. Donoghue, H. D. Human tuberculosis - an ancient disease, as elucidated by ancient microbial biomolecules. *Microbes and Infection* **11,** 1156–1162 (2009).

86. *The Old Testament (Deutoronomy 28:22)* (Holy Bible, New International Version, 2011).

87. Herodotus. *The Histories (Book VII, chapter 88)* (Harvard University Press, 1920).

88. Chalke, H. D. The impact of tuberculosis on history, literature and art. *Medical History* **6,** 301–318 (1962).

89. *WHO | Global Tuberculosis Report 2013*

90. *Health Protection Agency | Tuberculosis in the UK: 2013 report*

91. Cambau, E. & Drancourt, M. Steps towards the discovery of *Mycobacterium tuberculosis* by Robert Koch, 1882. *Clinical Microbiology and Infection* **20,** 196–201 (2014).

92. Klann, A. G., Belanger, A. E., Abanes-De Mello, A., Lee, J. Y. & Hatfull, G. F. Characterization of the *dnaG* locus in *Mycobacterium smegmatis* reveals linkage of DNA replication and cell division. *Journal of Bacteriology* **180,** 65–72 (1998).

93. Brennan, P. J. & Nikaido, H. The envelope of mycobacteria. *Annual Review of Biochemistry* **64,** 29–63 (1995).

94. Rajni, Rao, N. & Meena, L. S. Biosynthesis and virulent behavior of lipids produced by *Mycobacterium tuberculosis*: LAM and cord factor: an overview. *Biotechnology Research International* **2011,** e274693 (2010).

95. Trifiro, S, Bourgault, A. M., Lebel, F & René, P. Ghost mycobacteria on gram stain. *Journal of Clinical Microbiology* **28,** 146–147 (1990).

96. Hett, E. C. & Rubin, E. J. Bacterial growth and cell division: a mycobacterial perspective. *Microbiology and Molecular Biology Reviews* **72,** 126–156 (2008).

97. Chen, P. *et al.* A highly efficient Ziehl-Neelsen stain: identifying *de novo* intracellular *Mycobacterium tuberculosis* and improving detection of extracellular *M. tuberculosis* in cerebrospinal fluid. *Journal of Clinical Microbiology* **50,** 1166–1170 (2012).

98. Radhakrishnan, V. V., Sehgal, S. & Mathai, A. Correlation between culture of *Mycobacterium tuberculosis* and detection of mycobacterial antigens in cerebrospinal fluid of patients with tuberculous meningitis. *Journal of Medical Microbiology* **33,** 223–226 (1990).

99. Vieira, O., Botelho, R. & Grinstein, S. Phagosome maturation: aging gracefully. *Biochemical Journal* **366,** 689–704 (2002).

100. Desjardins, M., Huber, L. A., Parton, R. G. & Griffiths, G. Biogenesis of phagolysosomes proceeds through a sequential series of interactions with the endocytic apparatus. *The Journal of Cell Biology* **124,** 677–688 (1994).

101. Sun-Wada, G.-H., Tabata, H., Kawamura, N., Aoyama, M. & Wada, Y. Direct recruitment of H^+-ATPase from lysosomes for phagosomal acidification. *Journal of Cell Science* **122,** 2504–2513 (2009).

102. Nunes, P. & Demaurex, N. The role of calcium signaling in phagocytosis. *Journal of Leukocyte Biology* **88,** 57–68 (2010).

103. Majeed, M., Perskvist, N., Ernst, J. D., Orselius, K. & Stendahl, O. Roles of calcium and annexins in phagocytosis and elimination of an attenuated strain of *Mycobacterium tuberculosis* in human neutrophils. *Microbial Pathogenesis* **24,** 309–320 (1998).

104. Zimmerli, S. *et al.* Phagosome-lysosome fusion is a calcium-independent event in macrophages. *The Journal of Cell Biology* **132,** 49–61 (1996).

105. Fällman, M., Deleuil, F. & McGee, K. Resistance to phagocytosis by *Yersinia*. *International Journal of Medical Microbiology* **291,** 501–509 (2001).

106. Isberg, R. R. & Van Nhieu, G. T. The mechanism of phagocytic uptake promoted by invasin-integrin interaction. *Trends in Cell Biology* **5,** 120–124 (1995).

107. High, N, Mounier, J, Prevost, M. C. & Sansonetti, P. J. IpaB of *Shigella flexneri* causes entry into epithelial cells and escape from the phagocytic vacuole. *The EMBO Journal* **11,** 1991–1999 (1992).

108. Smith, G. A. *et al.* The two distinct phospholipases C of *Listeria monocytogenes* have overlapping roles in escape from a vacuole and cell-to-Cell spread. *Infection and Immunity* **63,** 4231–4237 (1995).

109. Voth, D. E. & Heinzen, R. A. Lounging in a lysosome: the intracellular lifestyle of *Coxiella burnetii*. *Cellular Microbiology* **9,** 829–840 (2007).

110. Rohde, K., Yates, R. M., Purdy, G. E. & Russell, D. G. *Mycobacterium tuberculosis* and the environment within the phagosome. *Immunological Reviews* **219,** 37–54 (2007).

111. Armstrong, J. A. & Hart, P. D. Response of cultured macrophages to *Mycobacterium tuberculosis*, with observations on fusion of lysosomes with phagosomes. *The Journal of Experimental Medicine* **134,** 713–740 (1971).

112. Wong, D., Bach, H., Sun, J., Hmama, Z. & Av-Gay, Y. *Mycobacterium tuberculosis* protein tyrosine phosphatase (PtpA) excludes host vacuolar-H^+-ATPase to inhibit phagosome acidification. *Proceedings of the National Academy of Sciences* **108,** 19371–19376 (2011).

113. Sharbati-Tehrani, S. *et al.* Porins limit the intracellular persistence of *Mycobacterium smegmatis*. *Microbiology* **151,** 2403–2410 (2005).

114. Malik, Z. A., Denning, G. M. & Kusner, D. J. Inhibition of Ca^{2+} signaling by *Mycobacterium tuberculosis* is associated with reduced phagosome-lysosome fusion and increased survival within human macrophages. *The Journal of Experimental Medicine* **191,** 287–302 (2000).

115. Comstock, G. W., Livesay, V. T. & Woolpert, S. F. The prognosis of a positive tuberculin reaction in childhood and adolescence. *American Journal of Epidemiology* **99,** 131–138 (1974).

116. Tsai, M. C. *et al.* Characterization of the tuberculous granuloma in murine and human lungs: cellular composition and relative tissue oxygen tension. *Cellular Microbiology* **8,** 218–232 (2006).

117. Fuller, C. L., Flynn, J. L. & Reinhart, T. A. In situ study of abundant expression of proinflammatory chemokines and cytokines in pulmonary granulomas that develop in cynomolgus macaques experimentally infected with *Mycobacterium tuberculosis*. *Infection and Immunity* **71,** 7023–7034 (2003).

118. Rhoades, E. R., Cooper, A. M. & Orme, I. M. Chemokine response in mice infected with *Mycobacterium tuberculosis*. *Infection and Immunity* **63,** 3871–3877 (1995).

119. Kim, M.-J. *et al.* Caseation of human tuberculosis granulomas correlates with elevated host lipid metabolism. *EMBO Molecular Medicine* **2,** 258–274 (2010).

120. Gill, W. P. *et al.* A replication clock for *Mycobacterium tuberculosis*. *Nature Medicine* **15,** 211–214 (2009).

121. Peyron, P. *et al.* Foamy macrophages from tuberculous patients' granulomas constitute a nutrient-rich reservoir for *M. tuberculosis* persistence. *PLoS Pathog* **4,** e1000204 (2008).

122. Sharma, S. K., Mohanan, S. & Sharma, A. Relevance of Latent TB Infection in Areas of High TB Prevalence. *CHEST* **142,** 761–773 (2012).

123. Pandey, A. K. & Sassetti, C. M. Mycobacterial persistence requires the utilization of host cholesterol. *Proceedings of the National Academy of Sciences* **105,** 4376–4380 (2008).

124. McKinney, J. D. *et al.* Persistence of *Mycobacterium tuberculosis* in macrophages and mice requires the glyoxylate shunt enzyme isocitrate lyase. *Nature* **406,** 735–738 (2000).

125. Norbis, L., Miotto, P., Alagna, R. & Cirillo, D. M. Tuberculosis: lights and shadows in the current diagnostic landscape. *New Microbiologica* **36,** 111–120 (2013).

126. Nayak, S. & Acharjya, B. Mantoux test and its interpretation. *Indian Dermatology Online Journal* **3,** 2–6 (2012).

127. Bass, J. B. *et al.* Treatment of tuberculosis and tuberculosis infection in adults and children. *American Journal of Respiratory and Critical Care Medicine* **149,** 1359–1374 (1994).

128. Blomberg, B., Spinaci, S., Fourie, B. & Laing, R. The rationale for recommending fixed-dose combination tablets for treatment of tuberculosis. *Bulletin of the World Health Organization* **79,** 61–68 (2001).

129. Menzies, D., Al Jahdali, H. & Al Otaibi, B. Recent developments in treatment of latent tuberculosis infection. *The Indian Journal of Medical Research* **133,** 257–266 (2011).

130. Kolattukudy, P. E., Fernandes, N. D., Azad, A. K., Fitzmaurice, A. M. & Sirakova, T. D. Biochemistry and molecular genetics of cell-wall lipid biosynthesis in mycobacteria. *Molecular Microbiology* **24,** 263–270 (1997).

131. Niederweis, M. Mycobacterial porins - new channel proteins in unique outer membranes. *Molecular Microbiology* **49,** 1167–1177 (2003).

132. Gandhi, N. R. *et al.* Multidrug-resistant and extensively drug-resistant tuberculosis: a threat to global control of tuberculosis. *Lancet* **375,** 1830–1843 (2010).

133. Velayati, A. A. *et al.* Emergence of new forms of totally drug-resistant tuberculosis bacilli: super extensively drug-resistant tuberculosis or totally drug-resistant strains in Iran. *CHEST* **136,** 420–425 (2009).

134. Udwadia, Z. F., Amale, R. A., Ajbani, K. K. & Rodrigues, C. Totally drug-resistant tuberculosis in India. *Clinical Infectious Diseases* **54,** 579–581 (2012).

135. McShane, H. Tuberculosis vaccines: beyond Bacille Calmette–Guérin. *Philosophical Transactions of the Royal Society B: Biological Sciences* **366,** 2782–2789 (2011).

136. Brewer, T. F. Preventing tuberculosis with Bacillus Calmette-Guérin vaccine: a meta-analysis of the literature. *Clinical Infectious Diseases* **31,** S64–S67 (2000).

137. Kaufmann, S. H. E. Tuberculosis vaccines: Time to think about the next generation. *Seminars in Immunology* **25,** 172–181 (2013).

138. Kakkar, A. K. & Dahiya, N. Bedaquiline for the treatment of resistant tuberculosis: promises and pitfalls. *Tuberculosis* **94,** 357–362 (2014).

139. Garnier, T. *et al.* The complete genome sequence of *Mycobacterium bovis*. *Proceedings of the National Academy of Sciences* **100,** 7877–7882 (2003).

140. Talbot, E. A., Perkins, M. D., Silva, S. F. M. & Frothingham, R. Disseminated Bacille Calmette-Guérin disease after vaccination: case report and review. *Clinical Infectious Diseases* **24,** 1139–1146 (1997).

141. Brown-Elliott, B. A. & Wallace, R. J. Clinical and taxonomic status of pathogenic nonpigmented or late-pigmenting rapidly growing mycobacteria. *Clinical Microbiology Reviews* **15,** 716–746 (2002).

142. Pierre-Audigier, C. *et al.* Fatal disseminated *Mycobacterium smegmatis* infection in a child with inherited interferon γ receptor deficiency. *Clinical Infectious Diseases* **24,** 982–984 (May 1997).

143. He, X., Dagan, A., Gatt, S. & Schuchman, E. H. Simultaneous quantitative analysis of ceramide and sphingosine in mouse blood by naphthalene-2,3-dicarboxyaldehyde derivatization after hydrolysis with ceramidase. *Analytical Biochemistry* **340,** 113–122 (2005).

144. Bach, G., Chen, C.-S. & Pagano, R. E. Elevated lysosomal pH in Mucolipidosis type IV cells. *Clinica Chimica Acta* **280,** 173–179 (1999).

145. Neville, D. C. A. *et al.* Analysis of fluorescently labeled glycosphingolipid-derived oligosaccharides following ceramide glycanase digestion and anthranilic acid labeling. *Analytical Biochemistry* **331,** 275–282 (2004).

146. Berg, T. O., Stromhaug, E, Lovdal, T, Seglen, O & Berg, T. Use of glycyl-L-phenylalanine 2-naphthylamide, a lysosome-disrupting cathepsin C substrate, to distinguish between lysosomes and prelysosomal endocytic vacuoles. *Biochemical Journal* **300,** 229–236 (1994).

147. Te Vruchte, D. *et al.* Relative acidic compartment volume as a lysosomal storage disorder–associated biomarker. *Journal of Clinical Investigation* **124,** 1320–1328 (2014).

148. Hostetter, J., Steadham, E., Haynes, J., Bailey, T. & Cheville, N. Phagosomal maturation and intracellular survival of *Mycobacterium avium* subspecies paratuberculosis in J774 cells. *Comparative Immunology, Microbiology and Infectious Diseases* **26,** 269–283 (2003).

149. Orme, I. M. The mouse as a useful model of tuberculosis. *Tuberculosis* **83,** 112–115 (2003).

150. Apt, A. & Kramnik, I. Man and mouse TB: contradictions and solutions. *Tuberculosis (Edinb)* **89,** 195–198 (2009).

151. Via, L. E. *et al.* Tuberculous granulomas Are hypoxic in guinea pigs, rabbits, and nonhuman primates. *Infection and Immunity* **76,** 2333–2340 (2008).

152. Gomez, J. E. & McKinney, J. D. *M. tuberculosis* persistence, latency, and drug tolerance. *Tuberculosis* **84,** 29–44 (2004).

153. Flynn, J. L. & Chan, J. Immunology of tuberculosis. *Annual Review of Immunology* **19,** 93–129 (2001).

154. Rhoades, E. R., Frank, A. A. & Orme, I. M. Progression of chronic pulmonary tuberculosis in mice aerogenically infected with virulent *Mycobacterium tuberculosis*. *Tubercle and Lung Disease* **78,** 57–66 (1997).

155. Kramnik, I., Dietrich, W. F., Demant, P. & Bloom, B. R. Genetic control of resistance to experimental infection with virulent *Mycobacterium tuberculosis*. *Proceedings of the National Academy of Sciences* **97,** 8560–8565 (2000).

156. Harper, J. *et al.* Mouse model of necrotic tuberculosis granulomas develops hypoxic lesions. *The Journal of Infectious Diseases* **205,** 595–602 (2012).

157. Blank, N. *et al.* Cholera toxin binds to lipid rafts but has a limited specificity for ganglioside GM1. *Immunology and Cell Biology* **85,** 378–382 (2007).

158. Beatty, W. L. *et al.* Trafficking and release of mycobacterial lipids from infected macrophages. *Traffic* **1,** 235–247 (2000).

159. Brennan, P. J. Structure, function, and biogenesis of the cell wall of *Mycobacterium tuberculosis*. *Tuberculosis* **83,** 91–97 (2003).

160. McNeil, M., Wallner, S. J., Hunter, S. W. & Brennan, P. J. Demonstration that the galactosyl and arabinosyl residues in the cell-wall arabinogalactan of *Mycobacterium leprae* and *Mycobacterium tuberculosis* are furanoid. *Carbohydrate Research* **166,** 299–308 (1987).

161. McNeil, M., Daffe, M. & Brennan, P. J. Evidence for the nature of the link between the arabinogalactan and peptidoglycan of mycobacterial cell walls. *Journal of Biological Chemistry* **265,** 18200–18206 (1990).

162. Verschoor, J. A., Baird, M. S. & Grooten, J. Towards understanding the functional diversity of cell wall mycolic acids of *Mycobacterium tuberculosis*. *Progress in Lipid Research* **51,** 325–339 (2012).

163. Gebhardt, H. *et al.* The key role of the mycolic acid content in the functionality of the cell wall permeability barrier in *Corynebacterineae*. *Microbiology* **153,** 1424–1434 (2007).

164. Sutcliffe, I. C. Cell envelope composition and organisation in the genus *Rhodococcus*. **74,** 49–58 (1998).

165. Nishiuchi, Y., Baba, T., Hotta, H. H. & Yano, I. Mycolic acid analysis in *Nocardia* species: The mycolic acid compositions of *Nocardia asteroides*, *N. farcinica*, and *N. nova*. *Journal of Microbiological Methods* **37,** 111–122 (1999).

166. Watanabe, M., Aoyagi, Y., Ridell, M. & Minnikin, D. E. Separation and characterization of individual mycolic acids in representative mycobacteria. *Microbiology* **147,** 1825–1837 (2001).

167. Takayama, K., Wang, C. & Besra, G. S. Pathway to synthesis and processing of mycolic acids in *Mycobacterium tuberculosis*. *Clinical Microbiology Reviews* **18,** 81–101 (2005).

168. Alibaud, L. *et al.* Temperature-dependent regulation of mycolic acid cyclopropanation in saprophytic mycobacteria: role of the *Mycobacterium smegmatis* 1351 gene in cis-cyclopropanation of α-mycolates. *Journal of Biological Chemistry* **285,** 21698–21707 (2010).

169. Behr, M. A., Schroeder, B. G., Brinkman, J. N., Slayden, R. A. & Barry, C. E. A point mutation in the *mma3* gene is responsible for impaired methoxymycolic acid production in *Mycobacterium bovis* BCG strains obtained after 1927. *Journal of Bacteriology* **182,** 3394–3399 (2000).

170. Minnikin, D. E. *et al.* Mycolic acid patterns of four vaccine Strains of *Mycobacterium bovis* BCG. *Journal of General Microbiology* **129,** 889–891 (1983).

171. Barkan, D., Hedhli, D., Yan, H.-G., Huygen, K. & Glickman, M. S. *Mycobacterium tuberculosis* lacking all mycolic acid cyclopropanation is viable but highly attenuated and hyperinflammatory in mice. *Infection and Immunity* **80,** 1958–1968 (2012).

172. Barkan, D., Rao, V., Sukenick, G. D. & Glickman, M. S. Redundant function of *cmaA2* and *mmaA2* in *Mycobacterium tuberculosis cis* cyclopropanation of oxygenated mycolates. *Journal of Bacteriology* **192,** 3661–3668 (2010).

173. Glickman, M. S., Cahill, S. M. & Jacobs, W. R. The *Mycobacterium tuberculosis cmaA2* gene encodes a mycolic acid *trans*-cyclopropane synthetase. *Journal of Biological Chemistry* **276,** 2228–2233 (2001).

174. Dao, D. N. *et al.* Mycolic acid modification by the *mmaA4* gene of *M. tuberculosis* modulates IL-12 production. *PLoS Pathogens* **4,** e100081 (2008).

175. Glickman, M. S., Cox, J. S. & Jacobs Jr., W. R. A novel mycolic acid cyclopropane synthetase is required for cording, persistence, and virulence of *Mycobacterium tuberculosis*. *Molecular Cell* **5,** 717–727 (2000).

176. Corrales, R. M. *et al.* Phosphorylation of mycobacterial PcaA inhibits mycolic acid cyclopropanation: consequences for intracellular survival and for phagosome maturation block. *Journal of Biological Chemistry* **287,** 26187–26199 (2012).

177. Ryll, R., Kumazawa, Y. & Yano, I. Immunological properties of trehalose dimycolate (cord factor) and other mycolic acid-containing glycolipids–a review. *Microbiology and Immunology* **45,** 801–811 (2001).

178. Woodruff, P. J. *et al.* Trehalose Is required for growth of *Mycobacterium smegmatis*. *Journal of Biological Chemistry* **279,** 28835–28843 (2004).

179. Fujita, Y., Naka, T., Doi, T. & Yano, I. Direct molecular mass determination of trehalose monomycolate from 11 species of mycobacteria by MALDI-TOF mass spectrometry. *Microbiology* **151,** 1443–1452 (2005).

180. Fujita, Y., Naka, T., McNeil, M. R. & Yano, I. Intact molecular characterization of cord factor (trehalose 6,6'-dimycolate) from nine species of mycobacteria by MALDI-TOF mass spectrometry. *Microbiology* **151,** 3403–3416 (2005).

181. Lang, R. Recognition of the mycobacterial cord factor by Mincle: relevance for granuloma formation and resistance to tuberculosis. *Frontiers in Immunology* **4** (2013).

182. Axelrod, S. *et al.* Delay of phagosome maturation by a mycobacterial lipid is reversed by nitric oxide. *Cellular Microbiology* **10,** 1530–1545 (2008).

183. Hunter, R. L., Olsen, M., Jagannath, C. & Actor, J. K. Trehalose 6,6'-dimycolate and lipid in the pathogenesis of caseating granulomas of tuberculosis in mice. *The American Journal of Pathology* **168,** 1249–1261 (2006).

184. Rao, V., Fujiwara, N., Porcelli, S. A. & Glickman, M. S. *Mycobacterium tuberculosis* controls host innate immune activation through cyclopropane modification of a glycolipid effector molecule. *The Journal of Experimental Medicine* **201,** 535–543 (2005).

185. Tatituri, R. V. V. *et al.* Inactivation of *Corynebacterium glutamicum* NCgl0452 and the role of MgtA in the biosynthesis of a novel mannosylated glycolipid involved in lipomannan biosynthesis. *Journal of Biological Chemistry* **282,** 4561–4572 (2007).

186. Indrigo, J., Hunter, R. L. & Actor, J. K. Cord factor trehalose 6,6'-dimycolate (TDM) mediates trafficking events during mycobacterial infection of murine macrophages. *Microbiology* **149,** 2049–2059 (2003).

187. Katti, M. K. *et al.* The *ΔfbpA* mutant derived from *Mycobacterium tuberculosis* H37Rv has an enhanced susceptibility to intracellular antimicrobial oxidative mechanisms, undergoes limited phagosome maturation and activates macrophages and dendritic cells. *Cellular Microbiology* **10,** 1286–1303 (2008).

188. Scott, C. & Ioannou, Y. A. The NPC1 protein: structure implies function. *Biochimica et Biophysica Acta* **1685,** 8–13 (2004).

189. Watari, H. *et al.* Niemann-Pick C1 protein: obligatory roles for N-terminal domains and lysosomal targeting in cholesterol mobilization. *Proceedings of the National Academy of Sciences* **96,** 805–810 (1999).

190. Carstea, E. D. *et al.* Niemann-Pick C1 disease gene: homology to mediators of cholesterol homeostasis. *Science* **277,** 228–231 (1997).

191. Liu, R., Lu, P., Chu, J. W. K. & Sharom, F. J. Characterization of fluorescent sterol binding to purified human NPC1. *Journal of Biological Chemistry* **284,** 1840–1852 (2009).

192. Stone, D. M. *et al.* The tumour-suppressor gene patched encodes a candidate receptor for Sonic hedgehog. *Nature* **384,** 129–134 (1996).

193. Davies, J. P., Levy, B. & Ioannou, Y. A. Evidence for a Niemann-Pick C (NPC) gene family: identification and characterization of NPC1L1. *Genomics* **65,** 137–145 (2000).

194. Temel, R. E. *et al.* Hepatic Niemann-Pick C1-like 1 regulates biliary cholesterol concentration and is a target of ezetimibe. *Journal of Clinical Investigation* **117,** 1968–1978 (2007).

195. Willenborg, M. *et al.* Mannose 6-phosphate receptors, Niemann-Pick C2 protein, and lysosomal cholesterol accumulation. *Journal of Lipid Research* **46,** 2559–2569 (2005).

196. Ko, D. C., Binkley, J., Sidow, A. & Scott, M. P. The integrity of a cholesterol-binding pocket in Niemann–Pick C2 protein is necessary to control lysosome cholesterol levels. *Proceedings of the National Academy of Sciences* **100,** 2518–2525 (2003).

197. Busso, D. *et al.* Spermatozoa from mice deficient in Niemann-Pick disease type C2 (NPC2) protein have defective cholesterol content and reduced *in vitro* fertilising ability. *Reproduction, Fertility and Development* **26,** 609–621 (2014).

198. Iftakhar-E-Khuda, I *et al.* Novel mechanism of U18666A-induced tumour necrosis factor-α production in RAW 264.7 macrophage cells. *Clinical and Experimental Immunology* **155,** 552–558 (2009).

199. Cenedella, R. J. Cholesterol synthesis inhibitor U18666A and the role of sterol metabolism and trafficking in numerous pathophysiological processes. *Lipids* **44,** 477–487 (2009).

200. Elliot-Smith, E. *et al.* Beneficial effects of substrate reduction therapy in a mouse model of GM1 gangliosidosis. *Molecular Genetics and Metabolism* **94,** 204–211 (2008).

201. Millard, E. E., Srivastava, K., Traub, L. M., Schaffer, J. E. & Ory, D. S. Niemann-Pick Type C1 (NPC1) overexpression alters cellular cholesterol homeostasis. *Journal of Biological Chemistry* **275,** 38445–38451 (2000).

202. Yamaji, A. *et al.* Lysenin, a novel sphingomyelin-specific binding protein. *Journal of Biological Chemistry* **273,** 5300–5306 (1998).

203. Wheelwright, M. *et al.* All-*trans* retinoic acid–triggered antimicrobial activity against *Mycobacterium tuberculosis* is dependent on NPC2. *The Journal of Immunology* **192,** 2280–2290 (2014).

204. Domenech, P., Reed, M. B. & Barry, C. E. Contribution of the *Mycobacterium tuberculosis* MmpL protein family to virulence and drug resistance. *Infection and Immunity* **73,** 3492–3501 (2005).

205. Varela, C. *et al. MmpL* genes are associated with mycolic acid metabolism in mycobacteria and corynebacteria. *Chemistry & Biology* **19,** 498–506 (2012).

206. Puech, V. *et al.* Evidence for a partial redundancy of the fibronectin-binding proteins for the transfer of mycoloyl residues onto the cell wall

arabinogalactan termini of *Mycobacterium tuberculosis*. *Molecular Microbiology* **44,** 1109–1122 (2002).

207. Piper, R. C. & Luzio, J. P. CUPpling calcium to lysosomal biogenesis. *Trends in Cell Biology* **14,** 471–473 (2004).

208. Gescher, A., Pastorino, U., Plummer, S. M. & Manson, M. M. Suppression of tumour development by substances derived from the diet - mechanisms and clinical implications. *British Journal of Clinical Pharmacology* **45,** 1–12 (1998).

209. Bilmen, J. G., Khan, S. Z., Javed, M.-u.-H. & Michelangeli, F. Inhibition of the SERCA Ca^{2+} pumps by curcumin. *European Journal of Biochemistry* **268,** 6318–6327 (2001).

210. Periasamy, M. & Kalyanasundaram, A. SERCA pump isoforms: their role in calcium transport and disease. *Muscle & Nerve* **35,** 430–442 (2007).

211. Jiao, Y. *et al.* Curcumin, a cancer chemopreventive and chemotherapeutic agent, is a biologically active iron chelator. *Blood* **113,** 462–469 (2009).

212. Keiloff, G. J. *et al.* New agents for cancer chemoprevention. *Journal of Cellular Biochemistry* **63,** 1–28 (1996).

213. Lopresti, A. L., Hood, S. D. & Drummond, P. D. Multiple antidepressant potential modes of action of curcumin: a review of its anti-inflammatory, monoaminergic, antioxidant, immune-modulating and neuroprotective effects. *Journal of Psychopharmacology* **26,** 1512–1524 (2012).

214. Zhao, L. N., Chiu, S.-W., Benoit, J., Chew, L. Y. & Mu, Y. The effect of curcumin on the stability of Aβ dimers. *The Journal of Physical Chemistry* **116,** 7428–7435 (2012).

215. Hatcher, H., Planalp, R., Cho, J., Torti, F. M. & Torti, S. V. Curcumin: from ancient medicine to current clinical trials. *Cellular and Molecular Life Sciences* **65,** 1631–1652 (2008).

216. Basnet, P. & Skalko-Basnet, N. Curcumin: an anti-inflammatory molecule from a curry spice on the path to cancer treatment. *Molecules* **16,** 4567–4598 (2011).

217. Belcaro, G. *et al.* Efficacy and safety of Meriva, a curcumin-phosphatidylcholine complex, during extended administration in osteoarthritis patients. *Alternative Medicine Review: A Journal of Clinical Therapeutic* **15,** 337–344 (2010).

218. Tang, Q. *et al.* The membrane permeable calcium chelator BAPTA-AM directly blocks human ether a-go-go-related gene potassium channels stably expressed in HEK 293 cells. *Biochemical Pharmacology* **74,** 1596–1607 (2007).

219. Williams, I. M. *et al.* Improved neuroprotection using miglustat, curcumin and ibuprofen as a triple combination therapy in Niemann-Pick disease type C1 mice. *Neurobiology of Disease* **67,** 9–17 (2014).

220. Platt, F. M., Neises, G. R., Dwek, R. A. & Butters, T. D. *N*-butyldeoxynojirimycin is a novel inhibitor of glycolipid biosynthesis. *Journal of Biological Chemistry* **269,** 8362–8365 (1994).

221. Zervas, M., Somers, K. L., Thrall, M. A. & Walkley, S. U. Critical role for glycosphingolipids in Niemann-Pick disease type C. *Current Biology* **11,** 1283–1287 (2001).

222. Patterson, M. C., Vecchio, D., Prady, H., Abel, L. & Wraith, J. E. Miglustat for treatment of Niemann-Pick C disease: a randomised controlled study. *The Lancet Neurology* **6,** 765–772 (2007).

223. Andersson, U., Butters, T. D., Dwek, R. A. & Platt, F. M. *N*-butyldeoxygalactonojirimycin: a more selective inhibitor of glycosphingolipid biosynthesis than *N*-butyldeoxynojirimycin, *in vitro* and *in vivo*. *Biochemical Pharmacology* **59,** 821–829 (2000).

224. Platt, F. M., Neises, G. R., Karlsson, G. B., Dwek, R. A. & Butters, T. D. *N*-Butyldeoxygalactonojirimycin inhibits glycolipid biosynthesis but does not affect *N*-linked oligosaccharide processing. *Journal of Biological Chemistry* **269,** 27108–27114 (1994).

225. Tiwari, G., Tiwari, R. & Rai, A. K. Cyclodextrins in delivery systems: Applications. *Journal of Pharmacy and Bioallied Sciences* **2,** 72–79 (2010).

226. Liu, B., Li, H., Repa, J. J., Turley, S. D. & Dietschy, J. M. Genetic variations and treatments that affect the lifespan of the NPC1 mouse. *Journal of Lipid Research* **49,** 663–669 (2008).

227. Atger, V. M. *et al.* Cyclodextrins as catalysts for the removal of cholesterol from macrophage foam cells. **99,** 773–780 (1997).

228. Christian, A. E., Haynes, M. P., Phillips, M. C. & Rothblat, G. H. Use of cyclodextrins for manipulating cellular cholesterol content. *Journal of Lipid Research* **38,** 2264–2272 (1997).

229. Giocondi, M.-C., Milhiet, P. E., Dosset, P. & Grimellec, C. L. Use of cyclodextrin for AFM monitoring of model raft formation. *Biophysical Journal* **86,** 861–869 (2004).

230. Chen, F. W., Li, C. & Ioannou, Y. A. Cyclodextrin induces calcium-dependent lysosomal exocytosis. *PLoS ONE* **5,** e15054 (2010).

231. 2-Hydroxypropyl-β-cyclodextrin promotes transcription factor EB-mediated activation of autophagy: implications for therapy.

232. Wu, J. *et al.* Improved orange and red Ca^{2+} indicators and photophysical considerations for optogenetic applications. *ACS Chemical Neuroscience* **4,** 963–972 (2013).

233. Naylor, E. *et al.* Identification of a chemical probe for NAADP by virtual screening. *Nature Chemical Biology* **5,** 220–226 (2009).

234. Leal, P. F. *et al.* Functional properties of spice extracts obtained via supercritical fluid extraction. *Journal of Agricultural and Food Chemistry* **51,** 2520–2525 (2003).

235. Gupta, P. K., Kulkarni, S. & Rajan, R. Inhibition of intracellular survival of multi drug resistant clinical isolates of *Mycobacterium tuberculosis* in macrophages by curcumin. *The Open Antimicrobial Journal* **4,** 1–5 (2013).

236. Chan, E. D., Oberley-Deegan, R. E., McGibney, M., Ovrutsky, A. & Bai, X. in *Tuberculosis and non-tuberculosis mycobacterium: treatment outcome studies and case reports* (American Thoracic Society, 2010).

237. Carette, J. E. *et al.* Ebola virus entry requires the cholesterol transporter Niemann-Pick C1. *Nature* **477,** 340–343 (2011).

238. Côté, M. *et al.* Small molecule inhibitors reveal Niemann-Pick C1 is essential for Ebola virus infection. *Nature* **477,** 344–348 (2011).

239. Tang, Y., Leao, I. C., Coleman, E. M., Broughton, R. S. & Hildreth, J. E. K. Deficiency of Niemann-Pick type C-1 protein impairs release of human immunodeficiency virus type 1 and results in Gag accumulation in late endosomal/lysosomal compartments. *Journal of Virology* **83,** 7982–7995 (2009).